Characterization of NDNF neurons in the mouse basolateral amygdala and in the primary motor cortex of a Huntington's disease model

Dissertation

der Graduate School of Systemic Neurosciences der Ludwig-Maximilians-Universität München

Prepared at the Max Planck Institute for Biological Intelligence

Submitted by

Ylenia Mastrodicasa

Munich, 2024

Supervisor:

Prof. Dr. Ruediger Klein

Max Planck Institute for Biological Intelligence

Department of Molecules – Signaling – Development

Project Subgroup: Circuit dynamics and behavior

First Reviewer: Prof. Dr. Ruediger Klein

Second Reviewer: Prof. Dr. Laura Busse

External Reviewer: Prof. Dr. Inga Neumann

Date of Submission: 27.11.2024
Date of Defense: 29.04.2025

TABLE OF CONTENTS

LIST OF ABBREVIATIONS

Abbreviation	Definition
2PE	2-phenylethanol
4MT	4-methylthiazoline
5-HT	5-hydroxytryptamine
5-HT3R	5-hydroxytryptamine 3 serotonin receptor
AAA	Anterior amygdala area
AAC	Axoaxonic cells
AAd	Anterior amygdala area, dorsal
AAV	Adeno-associated virus
AAv	Anterior amygdala area, ventral division
AAV-DIO-eGFP	Adeno-associated virus double-floxed inverse orientation enhanced green fluorescent protein
AC	Auditory cortex
ACC	Accommodating
ACo	Anterior cortical nucleus
AD	Alzheimer’s disease
AHP	Afterhyperpolarization
ANOVA	Analysis of variance
AP	Action potential
Arch	Archaerhodopsin
BA	Basal amygdala
BF	Basal forebrain
BLA	Basolateral amygdala
BLAa	Basolateral amygdala, anterior

BLAp	Basolateral amygdala, posterior
BMA	Basomedial nucleus
BNST	Bed Nucleus of the Stria Terminalis
BS	Burst-spiking
Ca^{2+}	Calcium ion
CAG	Cytosine-adenine-guanine
CaMKII	Ca^{2+}/calmodulin-dependent protein kinase II
CB	Calbindin
CB1	Cannabinoid receptor 1
CCK	Cholecystokinin
CCKL	Large multipolar CCK neurons
CeA	Central amygdala
CeC	Capsular Area of central amygdala
CeL	Central lateral amygdala
CeM	Central medial amygdala
CFC	Contextual fear conditioning
cFos	Cellular proto-oncogene Fos
ChR1 / ChR2	Channelrhodopsin-1 / channelrhodopsin-2
Cl^-	Chloride anion
CoA	Cortical amygdala
CPNs	Cortico-pyramidal neurons
CR	Calretinin
Cre	Cre recombinase
CS	Conditioned stimulus
dgCre	Destabilized EGFP/Cre fusion gene

DGLα	Diacylglycerol lipase alpha
DRN	Dorsal raphe nucleus
E/I	Excitation/inhibition
EC	Entorhinal cortex
EGFP	Enhanced green fluorescent protein
EPM	Elevated plus maze
FACS	Fluorescence-activated cell sorting
Flpo	Flp recombinase
FOV	Field of view
FS	Fast-spiking
GABA	Gamma-aminobutyric acid
$GABA_AR$	Gaba type a receptor
$GABA_BR$	Gaba type b receptor
GABAR	Gaba receptor
Gabbr2	$GABA_BR$ subunit 2
Gabrb2	$GABA_AR$ subunit beta2
Gabrg2	$GABA_AR$ subunit gamma2
GAD	Glutamate decarboxylase
Gad1	Glutamate decarboxylase 1
Gad2	Glutamate decarboxylase 2
GCaMP	Genetically encoded calcium indicator protein
GECIs	Genetically encoded calcium indicators
GRIN	Gradient index
HCR	Hairpin chain reaction
HD	Huntington’s disease

HPC	Hippocampus
HTT	Huntingtin gene
IB	Inclusion bodies
IHC	Immunohistochemistry
IL	Infralimbic cortex
INs	Interneurons
IPSCs	Inhibitory postsynaptic currents
IRES2	Internal ribosome entry site 2
IS	Irregular-spiking
ISI	Interneuron-selective interneurons
L1	Layer 1 (Neocortex)
LA	Lateral amygdala
Lamp5	Lysosome-associated membrane protein 5
LC	Locus coeruleus
LTP	Long-term potentiation
Lypd1	Ly6/PLAUR domain containing 1
M1	Primary motor cortex
mDlx	Modified Distal-less Homeobox Promoter
MDm	Medial dorsal thalamic nucleus
MeA	Medial amygdala
MePD	Medial amygdala, posterodorsal
MePV	Medial amygdala, posteroventral
MGN	Medial geniculate nucleus
mHTT	Mutant huntingtin gene
mPFC	Medial prefrontal cortex

MSNs	Medium spiny neurons
NAc	Nucleus accumbens
NDNF	Neuron-derived neurotrophic factor
NGFC	Neurogliaform cell
nLOT	Lateral olfactory tract nucleus
nNOS	Neuronal nitric oxide synthase
Nos1	Nitric oxide synthase 1
NpHR / Halo	*Natronomonas pharaonis* Halorhodopsin
NPY	Neuropeptide Y
NTS	Nucleus of the solitary tract
Ntsr2	Neurotensin receptor 2
OFT	Open field test
PAG	Periaqueductal grey
PBN	Parabrachial nucleus
PD	Parkinson’s disease
PEA	Peanut oil extract
PKC-δ	Protein kinase C delta
PL	Prelimbic cortex
PLCo	Posterior lateral cortical amygdala nucleus
plCoA	Posterolateral cortical amygdala
PMCo	Posterior cortical amygdala nuclei
PNs	Principal neurons / pyramidal neurons
polyQ	Polyglutamine tract
Ppp1r1b	Protein phosphatase 1 regulatory subunit 1b
PTSD	Post-traumatic stress disorder

PV / Pvalb	Parvalbumin
REG	Regular-spiking
Reln	Reelin
RNA-FISH	RNA fluorescence in situ hybridization
Rspo2	R-spondin 2
Slc17a7	Vesicular glutamate transporter 1
smFISH	Sequential multiplexed fluorescent in situ hybridization
SNL	Lateral substantia nigra
snRNA-Seq	Single-nucleus RNA sequencing
SOM	Somatostatin
SPNs	Spiny projection neurons
ST	Stuttering
Thy1	Thymus cell antigen 1
TMT	Trimethylthiazoline
UMAP	Uniform Manifold Approximation and Projection
US	Unconditioned stimulus
VGlut3	Vesicular glutamate transporter type 3
vHPC	Ventral hippocampus
VIP	Vasoactive intestinal peptide
VTA	Ventral tegmental area
Y1, Y2, Y5	Neuropeptide Y Receptor Subtypes 1, 2, and 5

ABSTRACT

The basolateral amygdala (BLA) and motor cortex (M1) are both important regions involved in the regulation of complex behaviours and both display distinct patterns of activity and cellular alterations in neurodegenerative and neuropsychiatric conditions. The BLA, is an integrative center within the amygdala, is known to regulate responses to both positive and negative stimuli by processing and modulating fear-related behaviours. While excitatory pyramidal neurons (PNs) make up most of the BLA, local inhibitory interneurons (INs) tightly control PNs activity and thus are essential in shaping BLA responses to aversive stimuli. In this study, we explore the role of neuron-derived neurotrophic factor (NDNF)-positive INs within BLA microcircuits, focusing on their activity in response to fear-related behaviours. Using *in vivo* Ca^{2+} imaging, we identified two distinct ensembles of BLA^{Ndnf} neurons which show opposite activity patterns during contextual fear conditioning and exposure to the predator odour trimethylthiazoline (TMT). Optogenetic loss-of-function studies indicate that BLA^{Ndnf} neuron activity promotes freezing behaviour in response to aversive stimuli, suggesting a functional role in mediating fear responses. Additionally, monosynaptic tracing reveals significant inputs from the cortical amygdala (CoA) to BLA^{Ndnf} neurons, emphasising their involvement in processing odour-induced fear. Parallel to this study, we examined the role of NDNF INs in the primary motor cortex (M1) within the context of Huntington's disease (HD), a hereditary neurodegenerative disorder characterized by motor, cognitive, and psychiatric symptoms linked to progressive neurodegeneration in the cortex and striatum. In the R6/2 mouse model of HD, we used single-nuclei RNA sequencing (snRNA-seq), *ex vivo* patch clamp recordings, and *in vivo* two-photon Ca^{2+} imaging to investigate how NDNF INs contribute to local circuitry dysfunction over the course of HD. Transcriptomic analysis revealed that key genes associated with NDNF IN markers are downregulated at advanced disease

stages in R6/2 mice compared to wild-type controls. Patch-clamp experiments indicated an increased action potential (AP) firing rate in NDNF INs within the M1 of R6/2 mice, while synaptic transmission appeared unaffected. Two-photon imaging during a running wheel task revealed increased Ca^{2+} activity in NDNF INs specifically at the onset of locomotion in HD mice, suggesting that these neurons may impact motor control circuits by influencing transitions between different behavioural states.

In summary, this work highlights the diverse roles that NDNF INs play in modulating neural circuitry across different brain regions and contexts, from fear processing in the BLA to motor function in the M1. In the BLA, NDNF INs influence responses to negative stimuli, potentially shaping behaviour through differential activity patterns in response to fear conditioning. In the M1, NDNF INs exhibit hyperexcitability in the context of HD, which may exacerbate cortical network dysfunction as the disease progresses. These findings emphasise the importance of local inhibitory circuits in maintaining region-specific excitatory-inhibitory balance and suggest that NDNF INs may be important in both behavioural modulation and neurodegenerative diseases.

1. INTRODUCTION

1.1 The Amygdala

1.1.1 Cytoarchitecture of the mouse Basolateral Amygdala

The amygdala is a small region of the mammalian limbic system situated deep within the temporal lobe, named for its unique almond-like shape[1]. The amygdala can be divided into four functional divisions and further subdivided into 13 nuclei, characterized by differences in their cytoarchitectural organization, cellular composition and functional connectivity[2]. The four functional subdivisions of the amygdaloid complex are the basolateral amygdala (BLA), central (CeA), medial amygdala (MeA) and the cortical amygdala (CoA) [3]. Amygdaloid nuclei are commonly described by their position on the anterior-posterior axis, with distinct structural and functional variation along that axis [4]. Starting rostrally, we find the anterior amygdala area (AAA) followed by its more ventral (AAv) and dorsal (AAd) divisions. The central amygdala is situated alongside the basomedial nucleus (BMA), the lateral olfactory tract (nLOT) and the anterior cortical nucleus (ACo) [5] (**Fig. 1A, A'**). Transitioning to a more intermediate position, the CeA divides into the medial (CeM) and lateral (CeL) nuclei, both confined by a larger capsular area (CeC) (**Fig. 1B, B'**). The BLA begins to divide into the lateral (LA) and basal (BA) regions, with the BA further divided into the anterior (BLAa) and posterior (BLAp) areas (**Fig. 1C, C'**). These regions are located adjacent to the lateral part of the CeA, the posterodorsal (MePD) and posteroventral (MePV) subnuclei of the MeA and all surrounded by intercalated nuclei. At a more caudal level, the posterior cortical amygdala nuclei (PMCo, PLCo) can be seen lying adjacent to the amygdalo-hippocampal interface (AHi), with the BLA growing smaller along the rostral-caudal axis [5] (**Fig. 1D, D'**).

The nuclei of the amygdala have been explored in great depth regarding their molecular, electrophysiological, and functional differences.

The CeA and the BLA have been previously described as the two major amygdalar centers responsible for integrating a variety of brain wide information in order to regulate overall animal behavior. In particular, the CeA and BLA are developmentally defined in different ways, based on their different embryological origins[2]. The CeA is a striatal-like structure, mainly composed of medium spiny neurons, that show considerable neurochemical heterogeneity [6], and that are mostly GABAergic. The GABAergic neurons of the CeA are primarily classified on the basis of expression of either somatostatin (SOM) or protein kinase C-δ (PKC-δ), which show mainly non-overlapping expression [7]. In contrast, the BLA has a cortical-like structure, albeit lacking the typical organization into layers that is present in the cortex. BLA neurons are primarily glutamatergic pyramidal principal neurons (PNs) and express Ca^{2+}/calmodulin-dependent protein kinase II (CaMKII) [8] . These cells represent around 80% of all BLA neurons [9,10]. Within this population, two genetically distinct subtypes were described [11]. The first subtype consists of protein phosphatase 1 regulatory subunit $1B^{+}$ ($Ppp1r1b^{+}$)-expressing parvocellular neurons, which are characterized by smaller cell bodies and are located in the BLAp. The second major subtype comprises R-spondin2^{+} ($Rspo2^{+}$)-expressing magnocellular neurons, which have larger somata and are found in the BLAa [12]. Recent studies [13] have further defined the BA and LA by the genetic markers their glutamatergic neurons express, Rspo2/Etv1 and Lypd1 respectively. The clear division of these two populations within the BLA, is suggestive of differing functional roles that the LA and BA (see chapter 1.2.1) play in overall BLA activity. A third distinct population of glutamatergic cells in the BLA is defined by expression of thymus cell antigen 1 (Thy1) [14]. Fluorescence-activated cell sorting (FACS)-based isolation of Thy1 and RNA sequencing has revealed the presence of differentially expressed genes selectively enriched in these neurons, including Rspo2 and neurotensin receptor 2 (Ntsr2) [15]. GABAergic cells account for ~ 20% of total BLA

neurons [9] (see chapter 1.1.2), consisting of interneurons that release GABA both locally or via long range projections.

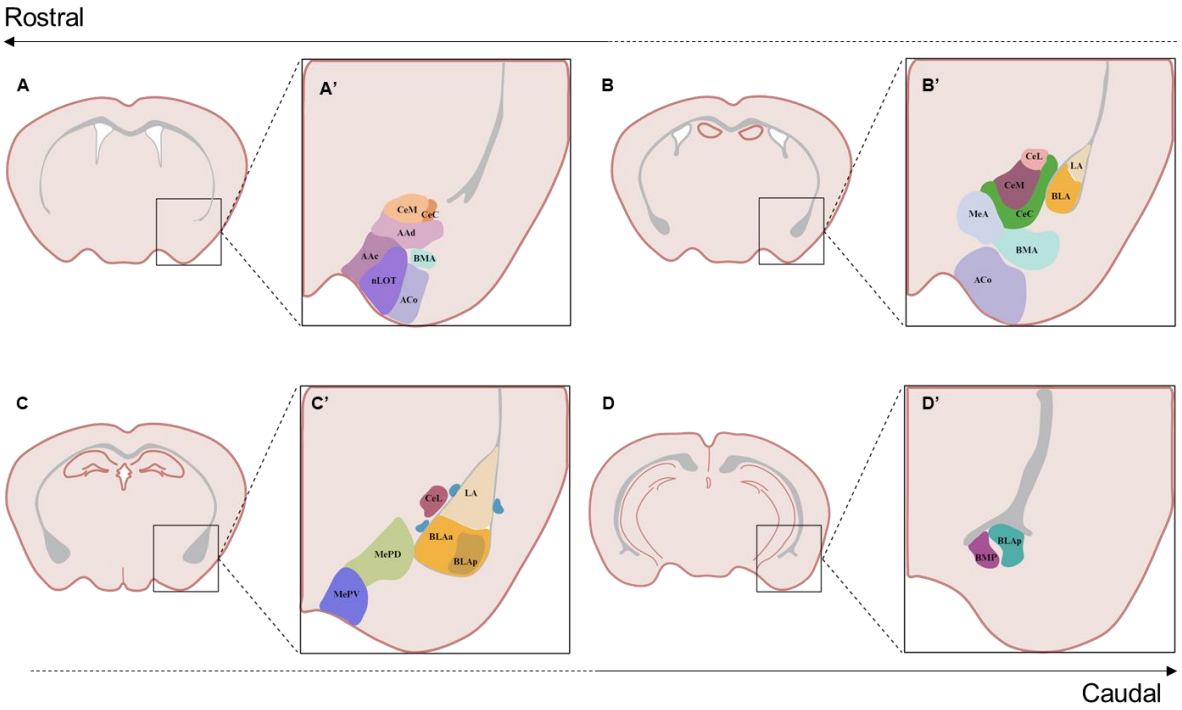

Fig. 1 - Nuclear subdivisions of the Amygdala.

(A, A') Starting rostrally the anterior amygdala area (AAA), divided in ventral (AAv, in dark pink) and dorsal (AAd, in light pink); the central amygdala complex (CeA, orange), subdivided into the medial (CeM, light orange) and capsular part (CeC, dark orange); the basomedial nucleus (BMA, light blue), the lateral olfactory tract (nLOT, purple) and the anterior cortical nucleus (ACo, light purple). **(B, B')** Moving more medially, the BLA (yellow) is forming adjacent to the CeC (green), which encloses both the CeM (dark pink) and CeL (light pink) and it is adjacent to the medial amygdala (MeA, grey) and BMA (light blue), followed by the ACo (light purple).**(C, C')** The BLA appears to be fully formed presenting its main subnuclei, the lateral part (LA, light yellow), BLA anterior (BLAa, yellow) and BLA posterior (BLAp, in dark yellow), all surrounded by the intercalated nuclei (blue). Adjacent to the BLA we find a smaller CeL (dark pink), and larger MeA divided into the posterodorsal (MePD, light green) and posteroventral (MePV, purple) nuclei. **(D, D')** Caudally, the basomedial nucleus (BMP, purple) emerges next to the BLAp (aqua). Figure is adapted from Aerts T., and Seuntjens E., (2021)[5]. Image created with BioRender.

1.1.2 Cellular diversity of the BLA

The LA and BA nuclei of the BLA, exhibit different distributions of molecular markers, suggesting that they contain differing compositions of neuronal subtypes. In the BA, neurons are primarily characterized as either parvocellular, intermediate or magnocellular neurons [16].

The parvocellular population is mainly composed of type I (large spiny neurons, soma diameter 8–17μm) and type II neurons (small multipolar cells) [17], the latter can be found together with type IV (large pyramidal cells) neurons in the intermediate division, whereas type I cells can be also located, although at a lower density, in the magnocellular division. [18]

Neurons within the BLA display a diverse array of molecular markers, including calcium-binding albumin proteins, neuropeptides, enzymes, and membrane receptors[1]. Calcium-binding albumin proteins include parvalbumin (PV), calbindin (CB) and calretinin (CR) [1]. Calretinin positive (CR^+) neurons in the LA are mainly composed of small multipolar type I cells, but medium-sized multipolar type II or pyramidal type 4 CR^+ cells are also observed. Calbindin positive (CB^+) neurons are mainly type I and II in both the LA and BA, with a moderate presence of type III cells in the BA magnocellular division [18]. In general, the majority of neurons classified by their expression of specific calcium-binding proteins are inhibitory interneurons (INs). BLA CB^+ interneurons are further subdivided into PV, somatostatin (SOM), neuropeptide Y (NPY) and cholecystokinin (CCK) expressing cells [18,19]. CR positive cells account for approximately 20% of BLA interneurons and additionally express CCK and vasoactive intestinal peptide (VIP) [18,19]. In the BLA all non-pyramidal CB^+ interneurons are PV cells [20] and can be morphologically classified as either basket or chandelier cells [21].

SOM interneurons are a heterogeneous population of non-pyramidal cells, that are also seen to express CB. These cells constitute 11-15% of all GABAergic interneurons in the BLA [9, 22] and are morphologically indistinguishable from PV cells [23].

CCK neurons are instead classified mainly by their morphology rather than by which calcium-binding protein they express, as CCK neurons are positive for both CB and CR [24]. Large multipolar CCK (CCK_L) neurons [25] co-express CB and are also characterized by expression of vesicular glutamate transporter type 3 (VGlut3), and 88% express cannabinoid receptor 1 (CB1) [19, 26]. Bipolar CCK interneurons, type S (small) [14], which are negative for CB1, co-express VIP and CR. Moreover, Mascagni F. and McDonald A.J (2007) [27] revealed that 16.1% of CCK_L neurons express the 5-HT3 serotonin receptor (5-HT3R), suggesting that CCK interneurons may act to mediate some of the neuromodulatory effects that serotonin plays in the BLA [14] (BLA functions related to anxiety and fear processes will be described in depth in the next chapters. See chapter 1.2, subsection 1.2.2).

A subpopulation of CCK type S cells in the BLAa, also express another neuropeptide, VIP [19]. VIP neurons, morphologically similar to SOM neurons [28], have been studied mainly for their unique capacity to inhibit other interneuron subclasses and so not only belonging to the CCK^+/VIP^+ subclass but also to the interneuron-selective interneurons (ISI), exerting their inhibition via their short, local axons and small cell bodies. VIP neurons also express CB1 and are also CR^+ [29].

NPY-positive interneurons are also widely found within the BLA and are mainly classified as neurogliaform cells (NGF cells). These cells are also characterized by expression of neuronal nitric oxide synthase (nNOS), SOM and CCK [9]. Approximately 15% of GABAergic neurons in the BLA express NPY. NPY-positive interneurons co-release NPY alongside GABA, which acts as an agonist at the neuropeptide Y type 1 (Y_1), type 2 (Y_2) and type 5 (Y_5) receptors [30]. A study by Bompolaki M. et al, 2024,

explored the role of NPY^+ neurons in the BLA during stress resilience and social interaction [31]. The authors investigated the role that NPY^+ neurons have in the regulation of PNs projecting to the bed nucleus of the stria terminalis (BNST), an area important for anxiety-related behaviors including social interactions (SI). The study [31] showed, that when NPY neurons provide inhibition to BLA-PNs neurons projecting to BNST, this is enough to enhance stress resilience in rats subjected to restraint tests. Moreover, the Y_1 receptor subtype is the predominant receptor in the BLA - this is thought to be responsible for NPY's regulation of anxiogenic-like effects that results from stressful stimuli [32]. For example, during SI experiments, chemogenetic activation of NPY Y_1 together with Y_5 receptors, promotes SI, thereby decreasing anxiety-like phenotypes [31] (**Fig. 2**).

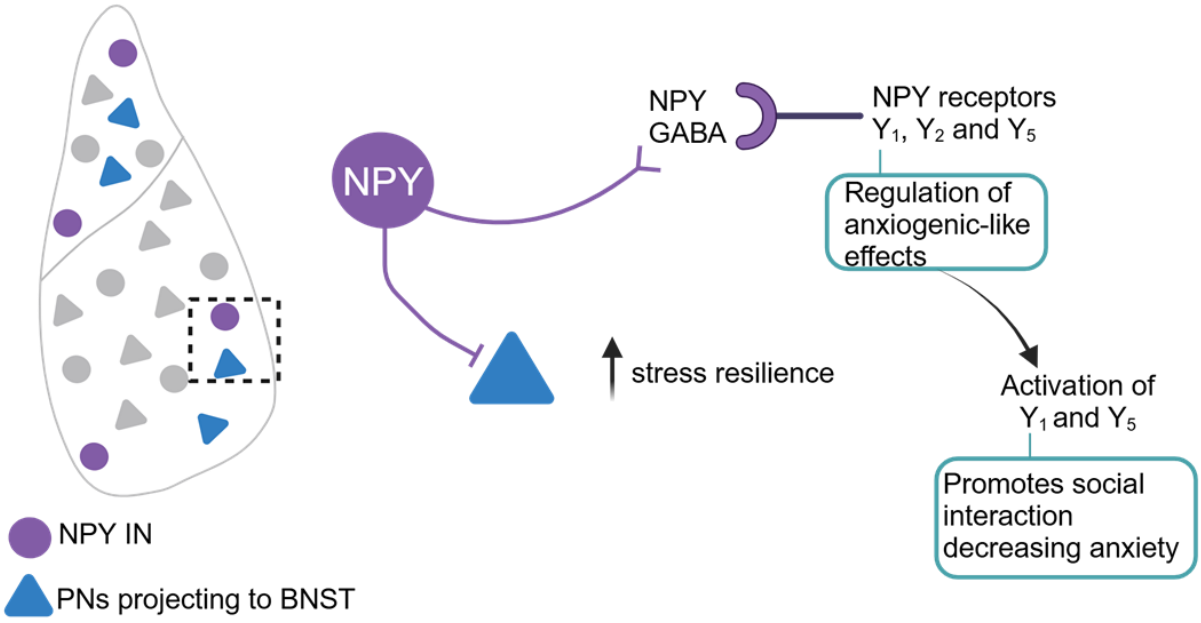

Fig. 2 – Role of NPY neurons in the regulation of anxiety related behaviors.

In the BLA, NPY neurons (purple), directly inhibit a specific population of PNs neurons, known to project to BNST and regulate downstream circuits contributing to appropriate behavioral responses (i.e. enhance stress resilience). NPY INs act via their receptors type Y1, Y2 and Y5.[30,31] Figure created with BioRender.

In addition to the expression of NPY, neuron-derived neurotrophic factor (NDNF) is another common marker of NGF cells. A 2010 study first identified NDNF as a potent neurotrophic factor uniquely expressed in neurons, with its main roles being the promotion of neuronal migration, neurite outgrowth, and neuronal survival in the hippocampus [33]. The first inducible Ndnf-IRES2-dgCre (**Fig. 3A**) knock-in Cre mouse line was generated in 2016 [34]. This mouse line is characterized by an IRES2 (internal ribosome entry site 2) sequence and a destabilized EGFP/Cre fusion gene (dgCre) inserted downstream of the translational STOP codon of the *Ndnf* gene. In the study from Tasic et al.[34], single-cell RNA sequencing of the mouse primary visual cortex revealed that $NDNF^{+}$ neurons are GABAergic and predominantly found in layer 1 (L1) of the neocortex. The development of this mouse line has enabled specific labelling of NDNF INs, allowing for ready genetic access to this population and easy detection of these cells through expression of genetically encoded fluorescent markers. This mouse line was firstly used to study the molecular, electrophysiological, and morphological characteristics of NDNF INs. Later, other mouse lines were generated, importantly a tamoxifen-inducible Cre line (Ndnf-IRES-CreERT2, used in our studies, **Fig. 3B**), as well as a Flp line, in order to allow specific targeting of these neurons [35].

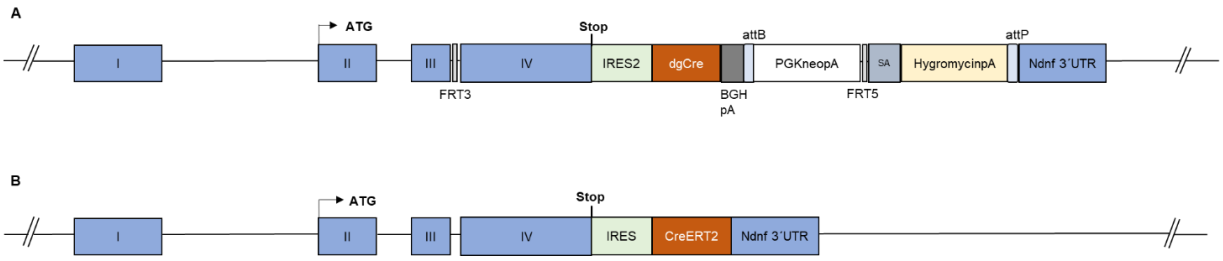

Fig. 3 – NDNF-Cre mouse line constructs.

(A) Ndnf-IRES2-dgCre-D knock-in mouse line construct, characterized by IRES2 sequence and a destabilized EGFP/Cre fusion gene (dgCre). The endogenous expression of Cre in Ndnf cells can be achieved with or without trimethoprim. (Jackson JAX:028536)[34].

(B) Ndnf-IRES-CreERT2 knock-in mouse line construct, characterized by cre/ERT2 fusion gene inserted into the 3' UTR in exon 4 of the *Ndnf* gene. Cre recombination in Ndnf cells is ensured with tamoxifen application. (Jackson, JAX:034875)[35]. Recent studies[36] suggest that this mouse line could be ideal for minimizing off-target Cre expression in non-Ndnf cells, using the tamoxifen induction strategy for more precise control. Figure created with Dr. Pilar Alcala Morales.

The first investigation of NDNF INs in the BLA was published in 2024 [36]. In the BLA, NDNF neuron-mediated inhibition is mediated by both $GABA_A$ and $GABA_B$ receptors [36]. $GABA_A$ receptors are ionotropic receptors, specifically ligand-gated chloride channels, and mediate fast inhibitory neurotransmission through rapid influx of chloride anions (Cl^-) postsynaptically, causing membrane hyperpolarization. $GABA_BR$ are metabotropic receptors, producing slower and prolonged postsynaptic inhibition via G-protein signalling and other second messengers that often trigger activation of potassium channels or inhibit calcium channel activation [37].

The unique characteristics of NDNF neuron-mediated GABAergic inhibition were further studied by Ozsvàr et al., 2024, through voltage-clamp recordings, by applying both gabazine, a $GABA_AR$ antagonist, and CGP-55845, a $GABA_BR$ antagonist, during optogenetic stimulation of NDNF INs via channelrhodopsin 2 (ChR2) expression. Optogenetically-evoked inhibitory postsynaptic currents (IPSCs) were altered by the application of both drugs, further demonstrating that both types of receptors are activated by the firing of NDNF neurons.

The ability to activate slow, extrasynaptic $GABA_B$ receptor-mediated currents is crucial for the powerful and atypical form of inhibition that NDNF INs can mediate in the BLA and elsewhere, and results from the unique properties of these cells [38] . As a result of their unique axonal morphology, they release GABA via volume transmission rather than classical synaptic transmission[39] and exert slower, more long-lasting control of pyramidal neurons (see chapter 1.1.3).

NDNF INs within the BLA were shown to express typical NGF cell genetic markers, such as NPY and Reelin (Reln) and were characterized by a small, round soma with a dense local axonal arbor [36] . The prevalence of the different interneuron classes described above is not uniform throughout the BLA. In addition to classification by protein-marker, interneurons are also subdivided into three main groups on the basis

of their axonal targeting: 1) perisomatically targeting cells, i.e. PV and CCK cells, innervate the soma and proximal dendrites; 2) dendrite-targeting, i.e. SOM and NGF cells target more distal dendritic regions; 3) ISI cells innervate other interneurons in order to provide disinhibition of PNs; 4) Axoaxonic (AAC) cells target the axon initial segment of PNs [9] (**Fig. 4A**).

Within the LA, GABAergic neuron subtypes are found in the following percentages: NGF cells comprise 14% of the total GABAergic population, SOM cells 10%, PV cells 17%, VIP cells 38%, CCK cells 7%, AAC 6% and GABAergic PNs 8% (**Fig. 4B**). Within the BA, the distribution of interneuron subtypes is slightly different, with 15% NGF cells, 15% SOM cells, 20% PV cells, 29% VIP cells, 9% CCK cells, and 5.5% each of AAC and GABAergic PN cells [9] (**Fig. 4C**). I will discuss available data pertaining to the role of GABA in the BLA, with a focus on NGF neurons and their respective markers, in the following chapter.

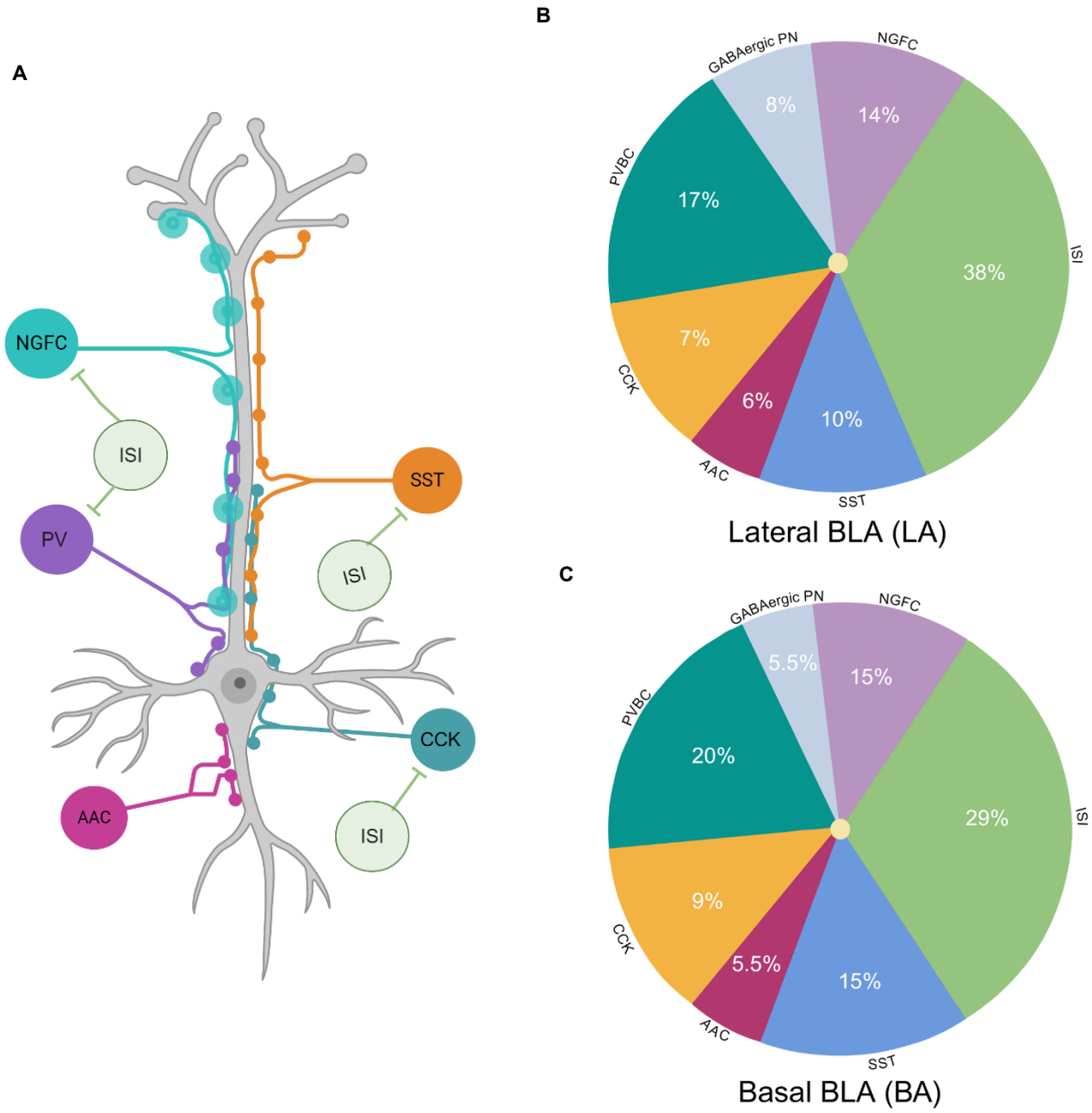

Fig. 4 - Interneurons organization in the BLA and their respective PNs targets.

(A) Characterization of different INs in the BLA based on their PNs targeting: perisomatic targeting cells, PV and CCK cells, innervate the soma and proximal dendrites; dendrite-targeting, SST and NGF cells target more distal dendritic regions; ISI, that innervate other interneurons in order to provide disinhibition to PNs; Axoaxonic (AAC) cells. **(B)** Percentages of respective Lateral BLA (LA) interneurons. **(C)** Percentages of respective Basal BLA (BA) interneurons. Modified from Norbert Hájos (2021)[9]. Image created with BioRender.

1.1.3 Differential role of NGF cells in synaptic transmission in the BLA

The excitatory pyramidal neurons of the BLA are tightly controlled by the diverse population of GABAergic neurons they are surrounded by. Disruptions of GABAergic inhibition or reductions in glutamate decarboxylase (GAD), can alter the general neuromodulation within the entire BLA. To achieve a precise labelling of NDNF INs in the BLA, Ozsvàr et al., 2024, followed a viral strategy using a Ndnf-cre mouse line, that combines AAV-DIO-eGFP with a mDlx promoter in order to target all NDNF interneurons in the BLA. This labelling enabled the authors to study the electrophysiological properties of BLA NDNF INs in detail. The authors discuss the unique synaptic properties of NDNF INs, characterized by volume transmission resulting in slow-phasic and tonic GABA release, with a further focus on atypical intrinsic properties characterized by broad action potentials (AP) and very strong afterhyperpolarization (AHP), a feature also found in NGF cells of both the hippocampus and cortex. The slow-phasic and tonic release of GABA results in extensive spill over of GABA from the synaptic space, allowing NDNF INs to activate extrasynaptic receptors [40] . This property is highly important for maintaining excitation/inhibition (E/I) balance. A decrease in the tonic inhibition that NGF cells produce may lead to a loss of E/I balance, thus resulting in overall BLA hyperexcitability and altered network dynamics. Hence, one could speculate that dysregulation of NGF cells may directly contribute to increased anxiety, emotional impairments, epilepsy, and post-traumatic stress disorder [38].

Disruptions to GABAergic transmission have also been shown to be involved in various neurodegenerative diseases, including Huntington's disease (HD) [41] , Alzheimer's disease (AD) and Parkinson's disease (PD) [42]. These conditions result in specific changes in GABAergic interneuron populations, GABAR subtypes, and inhibitory

synaptic transmission. (for a detailed analysis of GABAergic role in HD, see chapter 1.3.2). Given the unique forms of inhibition that NGF cells mediate and their prevalence within the BLA, studying their influence on anxiety-related behaviours and emotional states may provide the basis for developing more effective treatments for anxiety disorders and related conditions.

1.1.4 Intrinsic properties of interneurons in the BLA

Interneurons display unique intrinsic properties, which vary across subtypes. Characterization of intrinsic properties of BLA INs is fundamental to developing a deeper understanding of how these cells contribute to overall BLA activity. Interneurons in the BLA exert a significant inhibitory influence on the pyramidal cells they innervate and this mechanism is essential for the complex processing and integration of high-level information within the BLA, enabling the appropriate regulation of various behaviors. GABAergic cells can be divided into different categories based on their firing properties: accommodating (ACC), regular-spiking (REG), fast-spiking (FS), burst-spiking (BS), stuttering (ST) and irregular-spiking (IS)[43] (**Fig. 5**). PV-positive INs can be categorized as burst-, stuttering- [21] or fast-spiking [38]. On the other hand, SOM-INs are generally either fast-spiking or accommodating[9]. Firing pattern variability can be also observed in VIP INs, which fall into four distinct groups: ACC (or short-spiking), FS, ST [24] and IS (or low-late spiking) [29]. VIP interneurons that show high-frequency in firing rates are mainly located in the LA of the BLA [24]. Moreover, CCK neurons, interestingly, are characterized by a change in their firing properties depending on age. At postnatal day 20-30, CCK cells show ACC firing and wider action potentials [44], at older ages between postnatal days 40-48 CCK cells develop non-adapting firing properties [9, 14].

In order to fine-tune BLA activity, FS SOM-INs innervate PV and VIP neurons in the BLA, thus mediating feedforward inhibition[23] . In turn, PV and VIP neurons target SOM neurons dendrites. Interestingly, SOM interneurons, are also known to provide powerful inhibitory regulation over PNs , consequently a lack of this inhibition provides PNs disinhibition and depolarization [45].

Lastly, NPY^+ NGF cells are characterized by a regular-spiking phenotype and a pronounced afterhyperpolarization (AHP) phase [9,39]. However, some NDNF INs differ from other NGF cells, exhibiting a narrower AHP and faster repolarization phase [36].These properties are unique to NDNF INs as they are not shared with any other type of interneuron present in the BLA [46].

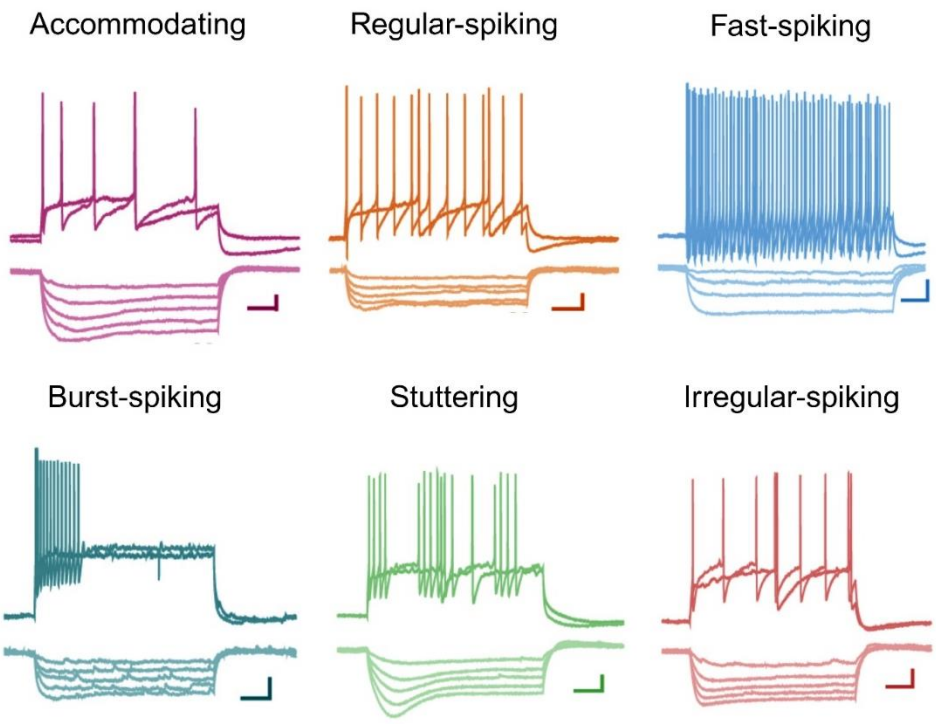

Fig. 5 – Diversity of interneurons firing properties in the BLA.
Classification of interneurons in the BLA can be done based on their different electrical properties. From left to right: accommodating cell (ACC, purple), regular-spiking cell (REG, orange), fast-spiking cell (FS, blue), burst-spiking cell (BS, teal blue), stuttering cell (ST, light green), irregular-spiking cell (IS, red). Image adapted and modified from Jai S. Polepalli, et al., 2020.[43] Image created with BioRender.

1.1.5 Neuronal circuits in the BLA: inputs and outputs

The BLA functions as a computational center, integrating diverse signals from other brain regions. The interconnections it forms between these inputs, its outputs, and other amygdala nuclei are known to be responsible for regulating specific behavioral processes. Broadly we can describe the "*inputs*" and "*outputs*" system in the BLA as follows[47]: regulatory inputs coming from the medial geniculate nucleus (MGN) and auditory cortex (AC) promote freezing; others from the medial prefrontal cortex (mPFC) promote feeding; bidirectional projections to and from the enthorinal cortex (EC) and hippocampus (HPC) regulate episodic memory and contextual fear responses[49]; thalamus, associative cortex and brainstem glutamatergic inputs provide sensory information[48]. Neuromodulation is provided by inputs coming from ventral tegmental area (VTA), dorsal raphe nucleus (DRN), locus coeruleus (LC), basal forebrain (BF)[48]. The information arising from these inputs is then integrated in the BLA and glutamatergic outputs are subsequentially sent to nucleus accumbens (NAc), promoting anxiety and reward behaviors, to EC, promoting freezing, to centrolateral and centromedial amygdala nuclei, inhibiting anxiety and promoting freezing[47], to mPFC, promoting anxiety and freezing, ventral hippocampus (vHPC), promoting anxiety and inhibiting social behavior, the BNST, inhibiting anxiety and regulating fear responses, and to prelimbic cortex (PL) which prevents reinstatement in relation to cue-reward associations[47]. It is important to note that the BLA glutamatergic outputs extensively target not only the CeL or CeM, but project to the entire CeA and MeA. These outputs are then sent to other brain areas such as the hypothalamus, the basal forebrain (BF, controlling motor behavior), parabrachial nucleus (PBN, feeding control), periaqueductal grey (PAG, pain and freezing), VTA (reward), nucleus of the solitary tract (NTS, autonomic regulation), LC (anxiety and aversive behaviors) and lateral substantia nigra (SNL, appetitive and aversive learning) [47, 48, 49, 50] (**Fig. 6**).

So far, I have exclusively mentioned the major glutamatergic inputs and outputs that the BLA receives and sends, but it is crucial to understand the functions of the GABAergic inputs and outputs. In a study from Liu et al. 2021, anterograde tracing was employed in order to follow efferent projections of the BLA to other brain regions. Intra-amygdala GABAergic projections were quantified, but long-distance GABAergic projections to distant brain regions were also shown, including the olfactory bulbs, cerebral cortex, septum, striatum, and hippocampus [51].

Long range projections neurons have been shown arise from SOM^+ cells expressing high levels of nNOS [10], a portion of which has been found to project to both medial thalamic nucleus (MDm) as well as mPFC [52].

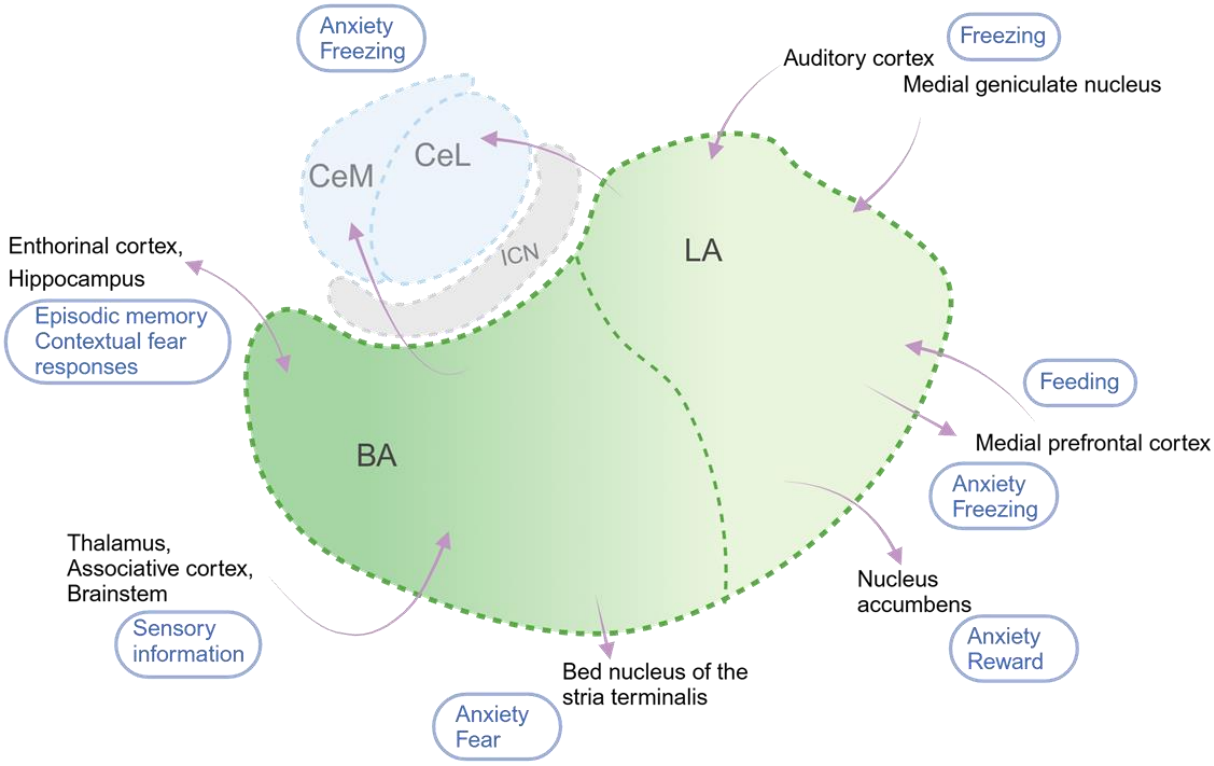

Fig. 6 - Main inputs and outputs of the BLA.

Regulatory inputs coming from areas such as auditory cortex, medial geniculate nucleus, medial prefrontal cortex, thalamus, brainstem, associative and enthorinal cortex, hippocampus is processed within either the LA or BA, which send outputs to either enthorinal cortex, hippocampus, Nucleus accumbens, bed nucleus of stria terminalis, prefrontal cortex, CeM, CeL in order to regulate a variety of behavioral responses (eg. Freezing, anxiety, sensory associations, social interactions, arousal, feeding, reward). Modified from Eduardo E. Benarroch, 2015 [49]. Figure created with BioRender.

1.2 Functional roles of the BLA

1.2.1 BLA role in emotional valance

The BLA, by receiving and integrating inputs form a diverse array of other brain regions, is able to compute and mediate "*valence processing*" or "*valence driven*" behaviors. Neurons in the BLA are specialised in encoding both positive and negative stimuli (or valence coding) [53]. Neuromodulatory inputs to the BLA play a key role in valence coding in the BLA. Such inputs include the basal forebrain, which provides cholinergic inputs that control both appetitive and aversive stimuli, the dorsal raphe nucleus (DRN), which provides serotonergic inputs that primarily act via 5-HT2 receptors found on BLA glutamatergic and PV-positive INs. Serotonin release is usually caused by increased stress, fear and anxiety and it has been shown that knockdown of the 5-HT2 receptor reduces fear expression and has anxiolytic effects. The ventral tegmental area (VTA) provides dopaminergic inputs to the BLA. These inputs have been shown to facilitate auditory-cue induced fear memory, as specific VTA to BLA projections become activated during aversive stimuli (i.e. footshocks) [54] . Optogenetic studies have been used to demonstrate how BLA axon terminals are able to control and potentially drive motivated behaviors – for example, photoactivation of BLA axon terminals in the vHPC and CeA can not only regulate anxiety-driven behaviors (as mentioned also in chapter 1.1.3) but are also able to increase freezing in response to aversive stimuli and promote defensive behaviors [55, 3]. The mPFC is also a crucial target of BLA axons, which project to both PL and infralimbic cortex (IL). These regions are involved in the regulation of fear expression and fear extinction respectively[19]. Previous findings identified that BLA neurons projecting to the IL or PL are characterized

by Ppp1r1b^{+} and Rspo2^{+} expression, respectively[53]. A recent study from our lab further dissected the role of Rspo2^{+} PNs in promoting fear conditioning and freezing responses [13]. These findings illustrate how heterogeneous populations in the BLA can regulate fear-related behaviors in opposite ways by connecting with distinct downstream brain areas. Besides regulating fear behaviors, the PFC coordinates reward-seeking behaviors. As the PL and IL are functionally heterogeneous, when activated by glutamatergic inputs from the BLA they mediate opposing behavioral responses. For example, activity of the BLA can either drive the seeking of substances of abuse when activating the IL cortex or inhibit such seeking when activating the PL cortex [56].

In addition to extrinsic inputs to and outputs from the BLA, other studies suggest that transmission between different areas of the BLA, as well as between different cell populations, has an important role in regulating behavior. Research has demonstrated that in the BLA, neurons regulating positive and negative valence are distinct, with negative-valence neurons located in the anterior region and positive-valence neurons in the posterior region. These populations are generally non-overlapping and may only intermingle at the transition between the two regions [57]. In a study from Kim et al., 2016, BLA neurons were categorized depending on which stimulus they coordinate - negative stimuli such as foot-shocks, trimethylthiazoline (TMT, a compound present in fox urine), or aversive gustatory stimuli (quinine, bitter taste) were shown to activate neurons present in the anterior part of the BLA and characterized by the marker gene Rspo2. Positive stimuli such as social interactions, rewarding or appetitive food, activated neurons in the posterior part of the BLA and characterized by the marker Ppp1r1b [53]. Besides these two

neuronal populations, other neurons have been recently included in the group of glutamatergic neuronal ensembles that contribute to overall BLA valence. For example, Lypd1^{+} neurons have been classified as positive valence neurons, controlling normal food intake, and Etv1-positive neurons which are classified as mixed-valence neurons as they are not only activated during aversive stimuli but also during social interactions[13].

1.2.2 Circuitry for fear and anxiety

The neural circuits underlying the learning of threat-associated cues and the generation of defensive responses have been extensively investigated, for example through the use of Pavlovian fear conditioning. The amygdala, in particular the BLA, plays a crucial role in the processing of fear-related behaviours [58], which are typically acute, stimulus-driven responses that help organisms react to imminent danger. Pavlovian fear conditioning paradigms are characterized by a neutral conditioned stimulus (CS), a light or a tone stimulus, that can be presented together with an aversive unconditioned stimulus (US), such as a foot-shock[59]. This results in an association between what is normally a neutral stimulus and fear-inducing stimulus, resulting in fear-related behaviours in response to said neutral stimulus. The combination of CS and US promotes long-term potentiation (LTP) of the synapses that relay CS-related information. This results in the formation of aversive memories, resulting in the CS being capable of inducing fear and/or defensive responses even if presented days, weeks, or months after initial conditioning [58]. Both BA and LA are involved in the integration of sensory information, thus contributing to the formation of associative fear memories [59]- the projections from the BLA to the CeA are also of importance, as the activity of these projections is crucial for

orchestrating defensive behaviours. BLA inhibitory microcircuits play a crucial role in the regulation and expression of fear conditioning. Research has demonstrated that BLA-INs are powerful regulators of the activity of BLA-PNs, and are thus essential for driving fear learning [58].

Thus far different classes of INs have been studied in association with aversive behaviours (**Fig. 7A**). Recent studies using *in vivo* recordings of INs in BLA have focused on the activity of VIP, PV, SOM and CCK neurons. In general, VIP neurons are activated after US onset and by providing inhibition to all other BLA INs, promote disinhibition of PNs, the principle cells responsible for fear-encoding[60]. In turn, PV and VIP interneurons strengthen their inhibitory output when excited by PNs, thus resulting in feedback inhibition[60] (**Fig. 7B**). When an auditory CS is presented together with an US, there is an increase in the activity of PV neurons, driven by the activation of PNs, whereas firing of SOM interneurons is silenced [61] (**Fig. 7C**). Direct synaptic connections between PV-INs and SOM-INs has been revealed to be the main circuit through which SOM interneurons become silenced during such conditioning. The feedforward inhibition of SOM-INs results in dendritic disinhibition in local PNs, thereby enhancing the integration of auditory CS-driven inputs [61].

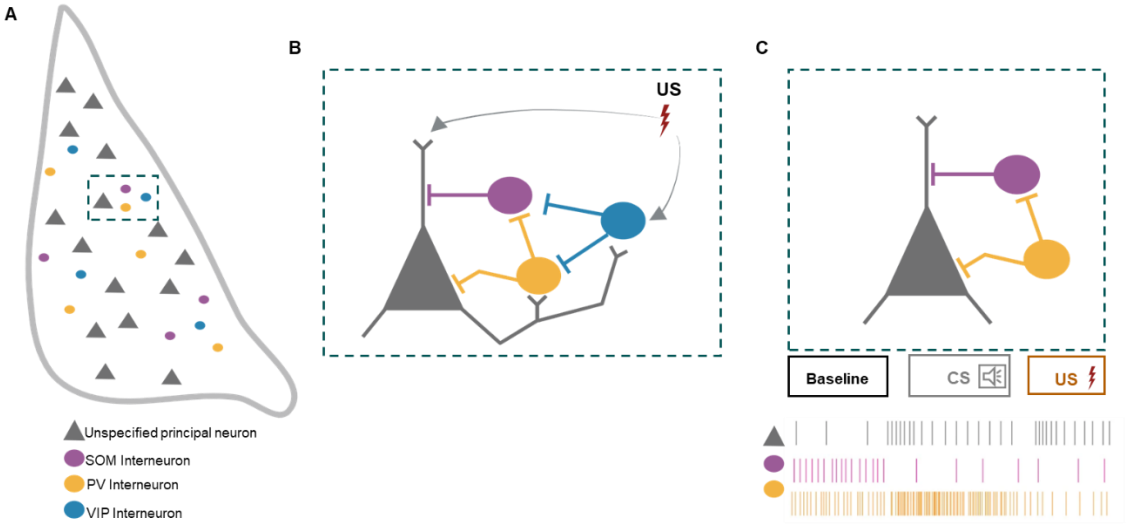

Fig. 7 – Fear microcircuits in the BLA.

(A) Representative image of the BLA with integrated PNs (grey), SOM-INs (purple), PV-INs (yellow) and VIP-INs (blue). **(B)** Fear microcircuits at US onset, VIP-INs activity increases providing inhibition to both SOM- and PV-INs and disinhibition onto PNs which in turn excite both PV- an VIP-INs, resulting in feedback inhibition. **(C)** CS and US, together increase activity of PV neurons, driven by the activation of PNs, whereas firing of SOM interneurons is silenced. Modified from Janak, P. & Tye, K. (2015)[47], Cattani et al., (2024)[60]. Figure created with BioRender.

CCK neurons mediate both fear expression and fear extinction, i.e. the reduction in fear responses. CCK neurons provide strong inhibition towards a subclass of PNs that project to the PL and modulate fear responses through this amygdalo-cortical circuit during fear expression. In contrast, due to high levels of diacylglycerol lipase alpha (DGLα) during fear extinction phase, PNs-that project to the IL increase their activity. This depolarization induces a release in endocannabinoids, causing a decrease in CCK-mediated inhibition [45]. Another crucial paradigm used to understand the roles of the BLA in fear and anxiety is contextual fear conditioning (CFC). Unlike paradigms involving auditory or visual conditioned stimuli (CS), this approach associates the aversive stimulus with the context itself. Typically, on the first experimental day, the animal is introduced to a novel environment, which may be inherently anxiogenic, where it receives an aversive stimulus such as a foot shock. On the following day, the animal is placed back into the same environment without the aversive stimulus being presented. This context-based association is sufficient to elicit a freezing response from the animal [62]. Interestingly, studies performed in chronically epileptic mice, have shown that the ablation of PV-INs from the BLA (a typical mechanism for models of amygdala-related chronic epilepsy) is sufficient to disrupt fear learning and recall [63], highlighting the role that PV-INs have not only during cued-fear conditioning, but also in contextual fear behaviours. Moreover, PV neurons show dual activity based on stimuli expectation, for example they show lower activity during fear learning when the US event is expected compared to when the stimulus is presented unexpectedly – suggesting that fear-learning circuits in the BLA maintain

selectivity for specific US sensory features, allowing for a quick adjustment of fear associations even when new sensory features of US are presented [64].

In addition to learned threats, it is important to study other types of threats that are innate, or unlearned. Different brain regions use distinct coding mechanisms to process this information and drive innate fear behaviours.

For instance, innate threats can be elicited during experiments by using different aversive odours or looming stimuli – these strategies have the ability to evoke defensive behaviours which include freezing or escape reactions that are essential for survival. Amongst aversive odours, trimethylthiazoline (TMT) and 4-methylthiazoline (4MT) elicit the most potent fear responses. TMT is an odorant that it is extracted from fox urine, and is the main substance used to induce freezing behaviors in mice, whereas the 4MT is a related odorant, that induces aversion but not immobility in mice[65]. Distinct odour valence refers to whether an odour elicits an approach or avoidance response. The latter can be achieved by using either TMT of 4MT, as described above, whereas approach responses can be elicited by using appetitive odours such as 2-phenylethanol (2PE) and peanut oil (PEA). This mechanism of valence coding for odorants, has been recently studied in relation to the cortical amygdala (plCoA), being one of the main regions able to mediate innate attraction or aversion to odours[66]. Molecularly defined glutamatergic neurons within the plCoA are able to encode for different odour identities, and the characterization of their downstream outputs has shown to mainly target regions involved in the regulation of valence and emotions, among which we find the BLA, NAc, BNST and MeA [66]. Looming stimuli can also successfully elicit an innate fear response

- this is a visual cue that simulates an object rapidly approaching the observer from above, creating the perception of an imminent predator attack [67].

In addition to behavioural paradigms used to study fear, several other key paradigms have been employed to investigate the role of the BLA in regulating anxiety-related behaviors, which represent a more sustained, context-dependent state triggered by perceived or potential threats. The most commonly used paradigms include the elevated plus maze (EPM), open field test (OFT), elevated zero maze, and light-dark box [68]. In general, these tasks leverage rodents' natural tendencies to explore unfamiliar environments while avoiding open, exposed, and bright zones where they may feel more vulnerable to threats. These tasks are valuable for distinguishing and more effectively studying mice with an anxious phenotype, as these animals tend to spend more time in the enclosed or “safe” areas of the apparatus compared to less anxious animals. In the EPM, the more anxiogenic areas are represented by the open arms, where mice can explore over and down the maze, in contrast to the walled arms. The OFT operates on a similar principle; however, in this case, the more anxiogenic area is the center of the field, which is usually avoided by anxious mice that tend to spend more time in the corners or close to the edges[68]. Moreover, neurotransmitter and neuromodulatory systems, particularly the role of glutamate, GABA, serotonin and dopamine, are crucial in modulating these threat responses[69]. Studies have shown that compounds that positively modulate $GABA_A$ receptors can potentially help in modulating stress-related memory deficits, depressive symptoms, and may also address dopaminergic dysfunction linked to schizophrenia and amygdala activity associated with fear and anxiety[70]. Serotonin has also been shown to play a

very important role in the modulation of fear responses. Serotonergic transmission becomes significantly activated during conditioned fear and remains unchanged during unconditioned stimuli, thus highlighting its dual role in anxiety disorders[71]. Additionally, 5-HT deficiency gives rise to an increase in fear recall during Pavlovian fear conditioning, and positively effects the extinction phase at later stages of conditioning [72]. These findings are particularly relevant to understanding the pathophysiology of affective and anxiety disorders, and highlight clinically relevant avenues for therapeutic intervention.

In addition to the role of NDNF INs in the BLA I have also studied their functions in Huntington's disease (HD), for this reason the next chapters will focus on the circuits that NDNF INs form in the cortex and their role in HD mouse models used in my research.

1.3 Interneurons in the mouse neocortex

1.3.1 NDNF neurons: what do we know so far?

NDNF INs have been identified as specific subpopulation of layer 1 (L1) cells in the neocortex. In a study conducted by Abs et al., 2018[35], the authors employed *In Situ Hybridization* to probe for a various range of INs markers, demonstrating a strong co-expression of Ndnf, Reln, Npy and nNos, whose expression was similarly and consistently found in NGF^+ cells, confirming their classification within the NGF cells family. The properties of NDNF INs in L1 differ compared to other already well-known cortical interneuron populations, such as those expressing PV, SOM, or VIP. Electrophysiological studies have identified distinctive characteristics of NDNF INs, including the slow inhibition

mediated by $GABA_B$ receptors they elicit in other neurons. These neurons exhibit persistent firing (PF), a late-spiking phenotype, and slow inhibitory kinetics in the postsynaptic responses they induce [73]. Moreover, they provide long range top-down inhibition onto all other classes of INs in lower layers 2/3 of the neocortex, whilst together with SOM, simultaneously modulating distal apical cortico-pyramidal neurons (CPNs) dendrites (**Fig. 8**) [73].

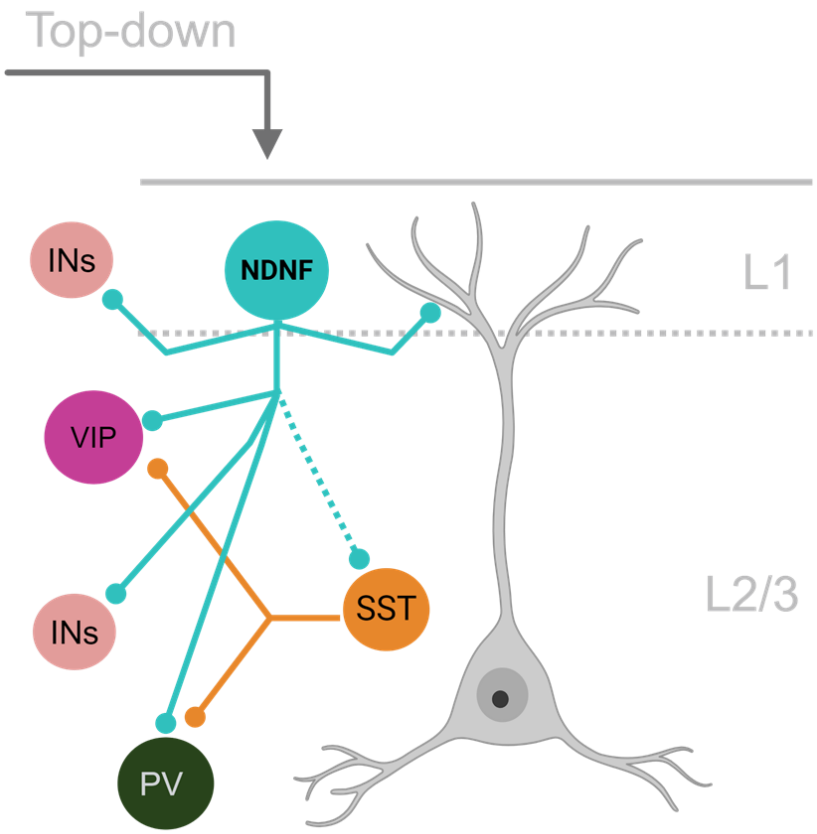

Fig. 8 – NDNF microcircuits in the L1 and L2/3 of the cortex.
L1 NDNF-INs provide top-down inhibition to L2/3 INs as well as regulating distal apical cortico-pyramidal neurons. Adapted and modified from Jan Hartung et al., (2024)[73]. Figure created with BioRender.

In the neocortex, IN activity varies depending on the subtype. For example, PV INs are responsible for feedforward inhibition of CPNs, regulating their excitability and influencing gamma oscillations. SOM-INs provide feedback inhibition to CPN dendrites, influencing signal integration and beta oscillations, thereby controlling spine dynamics. VIP INs disinhibit CPNs by inhibiting both SOM and PV INs [73]. For the purpose of this thesis, in the next chapter, I will talk in depth about IN roles in neurodegenerative diseases, with a focus on Huntington's Disease (HD).

1.3.2 Interneuron vulnerability in Huntington's disease

HD is a debilitating disorder that presents a diverse spectrum of clinical symptoms. This disorder affects about 5-10 people per 10,000 [74] and onset of symptoms is between the age of 35 and 45, although in more rare cases it can manifest before the age of 21 (juvenile HD) [75]. The progression of HD can generally be described in distinct phases. Phase I typically begins with psychiatric and cognitive symptoms. This is followed by a second phase when involuntary movements become the predominant feature. In the third phase, patients often experience bradykinesia, weight loss, and dementia, with the disease ultimately leading to death, usually occurring 15 to 20 years after disease onset [76].

HD is caused by a CAG triplet expansion of more than 35 repeats in exon 1 of the huntingtin (*HTT*) gene, giving rise to the mutant *HTT* gene (mHTT). The CAG repeats of mHTT result into an expanded polyglutamine (polyQ) tract at

the amino terminus of the HTT protein [76] causing protein aggregations (also referred to as inclusions bodies, **Fig. 9**) in a gain-of-function like toxicity hypothesis [77,78].

Given the crucial role of interneurons in maintaining cortical excitation-inhibition balance and modulating CPN activity, any disruption to their function can have a profound impact on cortical activity. In neurodegenerative diseases such as Huntington's Disease (HD), this delicate balance is disrupted, potentially contributing to neuronal degeneration. Understanding how the dysfunction of specific interneuron populations contributes to the pathophysiology of HD can provide valuable insights into the mechanisms underlying cortical degeneration and dysfunction in this condition (see manuscript 2, 2.2.3). Neuropathological studies of human post-mortem brains have highlighted this by revealing a reduction in both cortical areas and white matter, along with a significant cell loss [79].

Neurodegeneration in HD patients can be seen mainly in the striatum and motor cortex[76]. In the striatum, GABAergic spiny projection neurons (SPNs) - also referred as medium spiny neurons (MSNs) - undergo progressive degeneration. Loss of GABAergic SPNs leads to striatal brain atrophy (**Fig. 9**), as shown in human post-mortem brain sections. While it is well documented that CPNs are especially susceptible to degeneration in HD, there is also evidence of region-specific interneuron degeneration[79]. In the cortical motor and premotor areas, locally projecting GABAergic INs also undergo molecular and electrophysiological changes during HD progression. Studies in animal models of HD have shown that loss of SOM and VIP expression is directly proportional to disease progression, corresponding with a faster rate of mHTT

inclusion formation - however the total IN number remains unchanged [80]. Moreover, the role of dysfunctional interneurons in overall cortical degeneration in HD has been shown to be linked to an increase in excitability of CPNs, with this hyperexcitability shown to contribute to the cortical pathogenesis in HD [81]. In the motor cortex (M1) of HD patients, significant cell loss of CB^+ interneurons can be seen prominently at a later stage from HD onset, when motor symptoms are already present [79]. In summary, these studies emphasise the significance of both striatal and cortical neural degeneration in disease manifestation.

In this thesis we will further discuss the functionality of NDNF INs in the M1 of a mouse model of HD disease, as so far, no research has been done on the matter (see manuscript 2). NDNF proteins have shown promising potential for treating neurodegenerative diseases and nerve injuries, by supporting neuronal survival, migration, and neurite growth, and they could provide the basis for developing therapies for conditions involving neuronal degeneration and damage [33].

1.3.3 The R6/2 mouse model of HD

The R6/2 transgenic mice, the first line developed for studying HD, remain one of the most widely used and well-characterized models [82]. Their ability to replicate multiple aspects of HD phenotype and pathology makes them an invaluable tool for HD research and particularly well-suited for screening new therapeutic compounds [83]. The R6/2 line expresses exon 1 of the human *HTT* gene and contains about 150 CAG repeats [84]. This line exhibits a very aggressive disease phenotype that results in a very short life span of only 3 to 5 months and displays prominent changes in both physiology and behaviour [76]

(**Fig. 9**). R6/2 mice show HD-like symptoms that include hypoactivity, motor imbalance, and coordination deficits, accompanied by learning impairments and an anxiogenic phenotype. Although animal models of HD disease are widely used and remain important tools to study HD, they do exhibit certain differences in key aspects of human HD pathophysiology. For example, longer CAG tracts in R6/2 mice correlate with delayed disease onset [85] which might be caused by a reduced expression of mHTT [85]. In contrast, in humans longer CAG repeats are associated with an earlier onset of the disease [86].

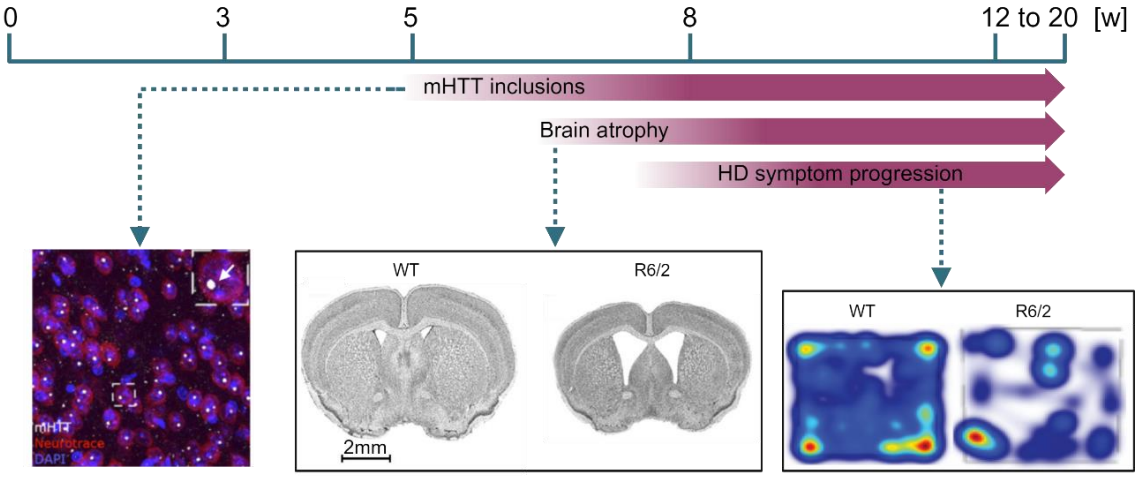

Fig. 9 – Disease progression in the R6/2 mouse model for HD.

The R6/2 mouse model widely used for studying HD disease, shows fast and severe pathology progression. At 5 weeks, it is possible to study mHTT inclusion bodies in neurons, followed by brain atrophy and prominent changes in behavioral phenotypes. The R6/2 mice usually die in a time window between 12 and 20 weeks of age. Confocal image showing mHTT aggregates in the motor cortex was taken by Kerstin Voelkl. Images of brain sections from WT and R6/2 mice were taken from Stack et al. (2005) [87] . Heat maps of open field experiments comparing WT and R6/2 mice were done by Sara Gutiérrez-Ángel. Figure created with BioRender and adapted from Dennis Feigenbutz "Temporally resolved single-nucleus RNA-sequencing profiling of the cortex reveals mechanisms of neuronal vulnerability in Huntington's disease", Doctoral Thesis, Ludwig Maximilian University of Munich, 2024[143].

1.4 Advanced techniques for studying neuronal cell types and circuit dynamics

1.4.1 Spatial mapping of neuronal cell types with HCR™ RNA-FISH

To visualize RNA molecules within brain tissue, in situ hybridization (ISH) is commonly used and in this thesis, we applied the HCR™ RNA-FISH protocol for fixed frozen brain tissue sections[104]. This technique begins with the identification of target genes and the design of complementary probes that can selectively bind to the corresponding RNA transcripts. Thin brain sections, typically 20µm or less in thickness, are prepared using a cryostat and mounted onto slides, where they are stored frozen at -80°C until processed. Upon application, the probes hybridize to their targets, and gene expression is subsequently visualized through either fluorescent or chromogenic signal amplification. More recent advances, such as sequential multiplexed fluorescent in situ hybridization (smFISH), allow for the detection of a large number of transcripts in a single tissue section by employing repeated cycles of hybridization and signal detection[13].

1.4.2 Single nucleus RNA sequencing profiling

Single-nucleus RNA sequencing (snRNA-seq) has increasingly become a valuable approach for transcriptomic profiling. In fact, unlike single-cell RNA-sequencing, which captures RNA from whole cells, snRNA-seq isolates nuclei offering a more reliable alternative for detection of fragile or tightly interconnected tissues[141]. In our study (refer to Manuscript 2), we adapted established protocols for nuclear isolation[141,142], beginning with gentle mechanical homogenization in a protective sucrose-based buffer. Following

tissue disruption, nuclei were enriched through filtration and density gradient centrifugation. The resulting nuclear suspension was stained, counted, and adjusted to the appropriate concentration for downstream processing. For sequencing, nuclei were encapsulated into droplets using the 10X Genomics Chromium system, where barcoded gel beads captured mRNA from individual nuclei. Libraries were prepared using the Chromium Single Cell 3' reagent kit (v3.1) and sequenced on a NovaSeq6000 platform. Raw sequencing data were processed with Cell Ranger (v4.0), aligning reads to the mouse reference genome (GRCm38) with inclusion of intronic sequences to capture the nuclear transcriptome enabling high-throughput profiling of gene expression at single-nucleus resolution[143].

1.4.3 Viral strategies and optogenetic manipulations

The ability to specifically activate or inhibit neurons with temporal precision has become a powerful tool, allowing researchers to explore the causal roles of specific neuronal manipulations in animal behavior[88]. Optogenetic manipulation combines genetic targeting with optical stimulation. Specifically, the DNA encoding a sensory photoreceptor, sourced from a microorganism, plant, or animal, can be cloned under the regulation of control elements that enable targeting specific host cells. This DNA is then packaged into a viral or bacterial vector and injected into the organism of interest. The targeted cell will then express a light-sensitive protein, allowing its activity to be controlled with light[89]. For instance, adeno-associated virus (AAV) vectors can be engineered to carry optogenetic actuators to be expressed under specific promoters, which can then be delivered directly to a rodent brain parenchyma or via systemic injection, enabling the targeting of specific brain regions or widespread brain

populations [89]. Transgenic expression of the AAVs can be achieved by using Cre or Flpo driver mouse lines, that express into a specific cellular population of interest [89] . Light-sensitive transmembrane proteins are defined as opsins [88], and respond to light by either moving ions in or out of the cell or by opening ion channels [89]. For optical silencing, proteins such as halorhodopsin and archaerhodopsins are used, while channelrhodopsins (i.e, chronos and chrimson) enable optical activation. Amongst microbial opsins there is the *Natronomonas pharaonis* halorhodopsin (Halo/NpHR), which is a light-driven inward chloride pump [88] , that together with Jaws derived from *Haloarcula salinarum* [90] allow for a reliable neuronal inhibition. Another very powerful inhibitory tool is the gene archaerhodopsin-3 (Arch) derived from *Halorubrum sodomense* that has been shown to be able to inhibit neurons in the mouse brain with almost 100% of success when illuminated with yellow light [88]. This very efficient form of inhibition has a very peculiar mechanism that differs from light-driven chloride channels, as it is able to spontaneously recover from inactive states in response to light [88]. Other microbial opsins are membrane-bound ion transport proteins, with channelrhodopsin-1 (ChR1) and ChR2 functioning as light-gated proton channels derived from the green alga *Chlamydomonas reinhardtii*. Upon absorbing a photon, these channels rapidly open, allowing for increased permeability to both monovalent and divalent cations, leading to cell depolarization through illumination [91]. Visualization of these opsins is achieved via fluorescent proteins that are packed within the AAV to be delivered. Different brain areas can be manipulated via implanted optical fibers from which light can be delivered, with experiments typically conducted at least four weeks after the viral delivery to allow sufficient expression.

1.4.4 *In vivo* calcium imaging

To investigate how neuronal activity changes *in vivo* as mice explore or experience specific contexts, researchers employ tools that enable temporally precise recordings of neuronal activity. One way to study the activity of specific circuits is through *in vivo* calcium imaging. During periods of high neuronal activity, calcium levels fluctuate dynamically, and these changes can be observed using genetically encoded calcium indicators (GECIs), such as GCaMP [92], which can be targeted to specific cell types to record their activity. GCaMP, is the most widely used calcium sensor which acts by signaling calcium concentration changes in the intracellular compartment – when calcium concentration rises within neurons during activity, the resulting increase in fluorescence indicates changes in neuronal firing [92]. Two-photon microscopy is a powerful tool for *in vivo* imaging, offering exceptional cellular and subcellular spatial resolution. However, a notable limitation is the need to head-fix the mice, restricting natural movement during behavioral experiments [93]. Alternative techniques, while offering lower resolution, enable calcium imaging in freely moving animals, providing valuable insights into neuronal activity. Two key methods include mini-epifluorescent microscopes paired with gradient index (GRIN) lens [94] microendoscopes and fiber photometry [95]. These compact, lightweight devices are designed to be mounted on the animal's head, facilitating recordings of neuronal activity even in deep brain regions. Notably, mini-epifluorescent microscopes allow researchers to repeatedly measure somatic calcium activity across hundreds of genetically and spatially defined neurons within the same animal [94].

1.5 Thesis aims

Although NDNF INs have been studied in areas such as cortical layer 1 and the hippocampus, their contributions to local circuit modulation and behavioral regulation in the BLA and M1 remain largely unexplored. This study aims to characterize and validate, for the first time, the functional roles of NDNF INs in these two brain regions. In the BLA, the present study explores how NDNF INs influence fear-related behaviors by examining their activity patterns during exposure to aversive stimuli using *in vivo* calcium imaging, as well as assessing their behavioral relevance through optogenetic manipulations. In parallel, this thesis examines how NDNF INs in M1 contribute to circuit dysfunction in Huntington's disease (HD). Using a combination of single-nucleus RNA sequencing, *ex vivo* electrophysiology, and *in vivo* two-photon imaging in the R6/2 mouse model, this study characterises transcriptomic changes, intrinsic excitability, and behavioral activity of these neurons during motor tasks at different disease stages. Overall, this work aims to uncover how NDNF INs contribute to both healthy and pathological brain function, highlighting their importance in maintaining excitatory-inhibitory balance and regulating animal behaviors.

2. MANUSCRIPTS

The two manuscripts included in this thesis are currently *in preparation* and have not yet been submitted to a peer-reviewed scientific journal.

2.1 Conditioned and innate fear responses are mediated by basolateral amygdala Ndnf-expressing neurons

Manuscript 1: "**Conditioned and innate fear responses are mediated by basolateral amygdala Ndnf-expressing neurons**"

Ylenia Mastrodicasa*, Federica Fermani, Maria Fernanda Frutos Marquez, Rüdiger Klein

YM and RK conceptualized the study and designed the experiments. YM performed most of the experiments. FF supported with *in vivo* calcium recording experiments and analysis, MFFM performed and analysed *in situ* hybridization experiments and assisted with immunohistochemistry, histology, microscopy, and image processing. YM and RK wrote the manuscript with inputs form all authors. RK supervised and provided funding.

My contribution to this manuscript in detail:

- For this study I participated in designing the experiments, performing experiments, data analysis, image processing, creating graphs and visuals for experimental paradigms, wrote and edited the manuscript.
- I performed stereotaxic injections and procedures, including optic fibers implants and participated in GRIN lens and baseplate implants.
- I performed and analysed behavioral experiments, including cFos experiments.
- I collected and analysed monosynaptic rabies tracings data.
- I designed and supervised *in situ* hybridization experiments and analysis.

Conditioned and Innate Fear responses are mediated by Basolateral Amygdala Ndnf-expressing neurons

Ylenia Mastrodicasa[1,2*], Federica Fermani[1,3], Maria Fernanda Frutos Marquez[1], Rüdiger Klein[1,4]

[1]Department of Molecules – Signaling – Development, Max Planck Institute for Biological Intelligence, 82152 Martinsried, Germany

[2]Graduate School of Systemic Neurosciences, Ludwig-Maximilians-Universität München, 82152 Martinsried, Germany

[3]Cellular Neurobiology, Department of Behavioral and Molecular Neurobiology, University of Regensburg, Regensburg, Germany

[4]Lead contact

Correspondence: ruediger.klein@bi.mpg.de (R.K.)

2.1.1 Abstract

The basolateral amygdala (BLA) is an integration center that regulates responses to both positive and negative behavioral stimuli. Although it is primarily composed of excitatory pyramidal neurons (PNs), the role of local inhibitory microcircuits in modulating BLA activity and mediating amygdala-related cognitive processes remains poorly understood. In this study we characterize neuron-derived neurotrophic factor (NDNF)-positive neurons in the BLA and their role during fear-related behaviors. Firstly, we employed high-resolution RNA fluorescence *in situ* hybridization (RNA-FISH) to reveal that BLA^{Ndnf} neurons are predominantly GABAergic, with 93.5% co-expressing Gad1. These neurons also express canonical neurogliaform cell (NGFC) markers such as Reln, Lamp5, and Npy, while showing little overlap with major interneuron subtypes (Sst and Pvalb), confirming that BLA^{Ndnf} neurons represent a distinct interneuron population in the BLA. To explore their role during fear processing, we examined cFos expression following a contextual fear conditioning (CFC) paradigm. BLA^{Ndnf} neurons exhibited significantly elevated cFos levels during fear acquisition, but not during fear recall, indicating selective activation by acute aversive stimuli. By performing *in vivo* Ca^{2+} imaging we identified two distinct neural ensembles of BLA^{Ndnf} neurons that encode negative stimuli during contextual fear conditioning and odour-induced innate fear. One ensemble exhibited reduced activity during fear conditioning and trimethylthiazoline (TMT, fox odour) exposure, while the second ensemble displayed increased activity. In line with these activity patterns, optogenetic loss-of-function experiments indicated that the activity of BLA^{Ndnf} neurons was necessary to promote freezing in response to aversive stimuli. Monosynaptic Rabies tracing revealed significant inputs from the cortical amygdala to BLA^{Ndnf} neurons, consistent with these neurons playing a role in the regulation of odour-induced fear responses. These findings suggest that two ensembles of BLA^{Ndnf} neurons differentially regulate aversive stimuli, both conditioned and innate, thereby contributing to the modulation of BLA microcircuits and shaping the overall response to negative states, ultimately influencing animal behavior.

2.1.2 Introduction

Emotions are associated with a wide range of behavioral and physiological responses, requiring various processes including the decoding and evaluation of different valence stimuli. These processes work together to shape a broad spectrum of behaviors and cognitive functions[96]. Emotions can be triggered by both innate and learned stimuli, the response to which can change in different contexts[97]. Classically, the neural circuits

involved in the regulation of fear and anxiety are mainly located in the amygdala, medial prefrontal cortex (mPFC), entorhinal cortex (EC), bed nucleus of the stria terminalis (BNST) and hippocampus[96, 49]. The recruitment of each of these regions, can differ depending on the strength and type of stimulus (conditioned, unconditioned or innate), hormonal responses to potential threats, neurotransmitter release and internal states of the animal[98, 99].

Here we focus on the basolateral amygdala (BLA), a region important for emotional processing, which integrates and processes behaviors driven by valence. BLA-associated behaviors include aversive responses, learning and memory, anxiety, reward, and social interactions[59, 58, 100, 13] .

Neurons in the BLA are specialized in encoding both positive and negative emotional experiences, contributing to the animal's ability to distinguish and respond appropriately to rewarding or aversive stimuli[53]. Studies on the mechanisms by which the BLA regulates aversive responses, both conditioned and innate, have focused on how fear memories are processed in reaction to recurring threats. Gaining insights into physiological circuit mechanisms of fear and anxiety can help us understand how they may become dysfunctional in fear- and anxiety-related conditions.

The BLA is characterized by different neural ensembles, known to differentially modulate the emotional valence of external stimuli. These ensembles are mainly composed of glutamatergic pyramidal principal neurons (PNs), which comprise approximately 80% of the total BLA neuron population. However, these PNs are tightly regulated by GABAergic interneurons (INs), which, despite their lower abundance (~20% of total BLA neurons), play critical roles in processing fear-related stimuli. Thus far, the activity of different classes of BLA-INs have been studied during aversive behaviors. Recent studies using *in vivo* recordings of INs in BLA have elucidated the role that vasoactive intestinal peptide (VIP), parvalbumin (PV), and somatostatin (SOM)- expressing INs play in associative fear memory formation. Specifically, optogenetic inhibition of VIP-INs during presentation of an unconditioned stimulus (US) in Pavlovian fear conditioning paradigms is known to impair associative learning[45]. In contrast, inhibition or excitation of PV-INs increases and impairs fear learning respectively during US[64]. Moreover, chemogenetic inhibition of SOM-INs during contextual fear conditioning experiments, elucidated their role in facilitating fear memory recall[101].

Studies in layer 1 (L1) of the neocortex, identified a novel IN subclass, neuron-derived neurotrophic factor (NDNF) neurons, and revealed that they co-express Reelin (Reln)

and Neuropeptide Y (Npy) suggesting that L1 NDNF INs may correspond to neurogliaform cells (NGFCs)[35]. In the auditory and prefrontal cortex, NDNF-INs act as "master regulators"[35], where they provide top-down inhibition of all other classes of INs in layers 2/3[73] and control L1 distal apical dendrites of pyramidal cells. Moreover, *in vivo* experiments showed that L1 NDNF INs exhibit increased activity in response to conditioned stimuli following fear learning, while their responses are reduced in the absence of associative fear learning, indicating the significance of experience in shaping their activity[35]. A recent study[36] employed different viral approaches to specifically target NDNF cells in the BLA. This study describes NDNF neurons both electrophysiologically and morphologically for the first time in the BLA, and further confirmed their nature as NGFCs by demonstrating co-expression of Npy and Reln in the BLA. However, the behavioral and functional relevance that NDNF INs have in the BLA remains entirely unknown.

Our study sheds light on the critical functions that BLA^{Ndnf} neurons play in modulating fear-related behaviors. Through a combination of optogenetic and *in vivo* Ca^{2+} imaging experiments, we demonstrate that BLA^{Ndnf} neurons play a crucial role in encoding responses to aversive stimuli. Optogenetics was employed to causally manipulate BLA^{Ndnf} neuron activity with temporal precision, allowing us to directly test their functional contribution to behavior during fear acquisition and innate fear paradigms. *In vivo* Ca^{2+} imaging enabled us to monitor the real-time activity of individual BLA^{Ndnf} neurons in awake freely-moving animals, revealing changes of neural ensembles dynamics in response to aversive stimuli. Specifically, optogenetic loss-of-function in contextual fear conditioning experiments, results in a significant reduction in freezing behavior during the fear acquisition phase, but not during memory recall, suggesting that the activity of BLA^{Ndnf} neurons impacts on fear responses during learning, but not during memory formation. Similar findings were obtained during odour-induced innate fear, where photoinhibition of BLA^{Ndnf} neurons in the presence of TMT significantly decreases freezing behavior. *In vivo* single cell Ca^{2+} imaging reveals the presence of two functionally distinct BLA^{Ndnf} neuron ensembles which have opposite activity patterns in response to aversive stimuli. These results suggest a model in which a freezing-on BLA^{Ndnf} ensemble, positively modulates freezing when fearful stimuli are presented. It also suggests the presence ensemble, a separate freezing-off BLA^{Ndnf} ensemble, that negatively modulates freezing.

2.1.3 Results

2.1.3.1 NDNF neurons are predominantly GABAergic and express typical NGFCs markers in the BLA

Previous studies have identified Ndnf as a genetic marker specific to NGFCs in L1 of the neocortex, the hippocampus, and the BLA[35,36,39,102]. This was demonstrated using in situ hybridization and immunohistochemistry (IHC), confirming co-expression with typical NGFC markers such as Npy, Reln, and nNOS[103]. Additionally, in neocortical L1 the majority of Ndnf$^+$ cells co-express Gad1, while only a small proportion co-localize with the glutamatergic marker Slc17a7, supporting the classification of Ndnf$^+$ cells as GABAergic. Most research on Ndnf$^+$ cells in the BLA has utilized a combination of viral strategies and IHC techniques; however, RNA fluorescence in situ hybridization (RNA-FISH) data for the BLA is not yet available. A previous study using single-nucleus RNA sequencing (snRNA-Seq) analysis revealed a subpopulation of Ndnf/Lamp5/Reln-expressing neurons in the BLA[13]. To confirm these findings, we employed hairpin chain reaction (HCR) high-resolution RNA-FISH[104]. Using C57BL/6NRj mice of both sexes, we probed for various mRNA combinations in the BLA, including Ndnf/Gad1/Slc17a7, Ndnf/Reln/Cck, Ndnf/Pvalb/Sst, Ndnf/Lamp5, and Ndnf/Npy. Our study shows that there is an even distribution of Ndnf$^+$ cells in a coronal BLA section, albeit with a slight basal preference, without any differences in density across the anterior-posterior brain axis. Ndnf$^+$ cells were sparsely distributed, with an average of 13 Ndnf$^+$ cells/20µm slice in the BLA (**Fig. 1a and e**). Quantitative analysis of cryoprotected brain slices was performed using a hybrid approach. Analysis was performed with HALO software automated cell count followed by a manual color-coding system when necessary (all data are reported as mean ± SEM, **Fig. 1f**; **Fig 2d-e**). These data show that 93.5 ± 3.3% of Ndnf$^+$ cells co-localize with Gad1 and only 12.3 ± 1.4% with Slc17a7 (**Fig. 1b**). These results strongly support evidence provided by Abs et al. (2018) and Guo et al. (2021) that Ndnf$^+$ cells are overwhelmingly GABAergic. Importantly our analysis shows that 11% of Ndnf$^+$ cells expressing Slc17a7 simultaneously expressed Gad1. It can therefore be concluded that the majority of Ndnf/Slc17a7 expressing cells belong to the cluster of cells that also expresses Gad1, whilst approximately 1.2% express Slc17a7 exclusively. Further, our data show that 81.4 ± 6.7% and 90 ± 3.3% express Reln and Lamp5 respectively (**Fig. 1c**) and 80.8 ± 3.5% of Ndnf$^+$ cells express Npy (**Fig. 1d**). These results are consistent with currently available literature[13,35,36,39]. Furthermore, 37 ± 7.3% of Ndnf$^+$ cells express Cck (**Fig. 2a and d**) and 35.4 ± 6.1% express Nos1 (**Fig. 2b and d**). To exclude the possibility that Ndnf$^+$ cells belong to one of the other main interneurons

(INs) classes, we analysed for co-localization levels of Ndnf with Sst and Pvalb. Analyses revealed that Ndnf INs have low colocalization levels with both Sst (3.7 ± 2%) and Pvalb (4 ± 2%) (**Fig. 2c and d**) ruling out the possibility that Ndnf$^+$ cells belong to the Sst$^+$ or Pvalb$^+$ interneuron populations. Finally, we analysed the co-expression of specific subtype markers with Ndnf. We found that the main marker that co-localize with Ndnf is Reln (27.6 ± 4.2%), followed by Npy (15.7 ± 2.2%), Gad1 (15.5 ± 4%), Nos1 (7.4 ± 4.6%) and Lamp5 (5 ± 2.3%), (**Fig. 2e**). These findings are consistent with recent studies that used single-nucleus RNA sequencing to analyse the molecular composition of the BLA and show that Ndnf INs belong to a subpopulation of Reln/Lamp5 cell cluster[13].

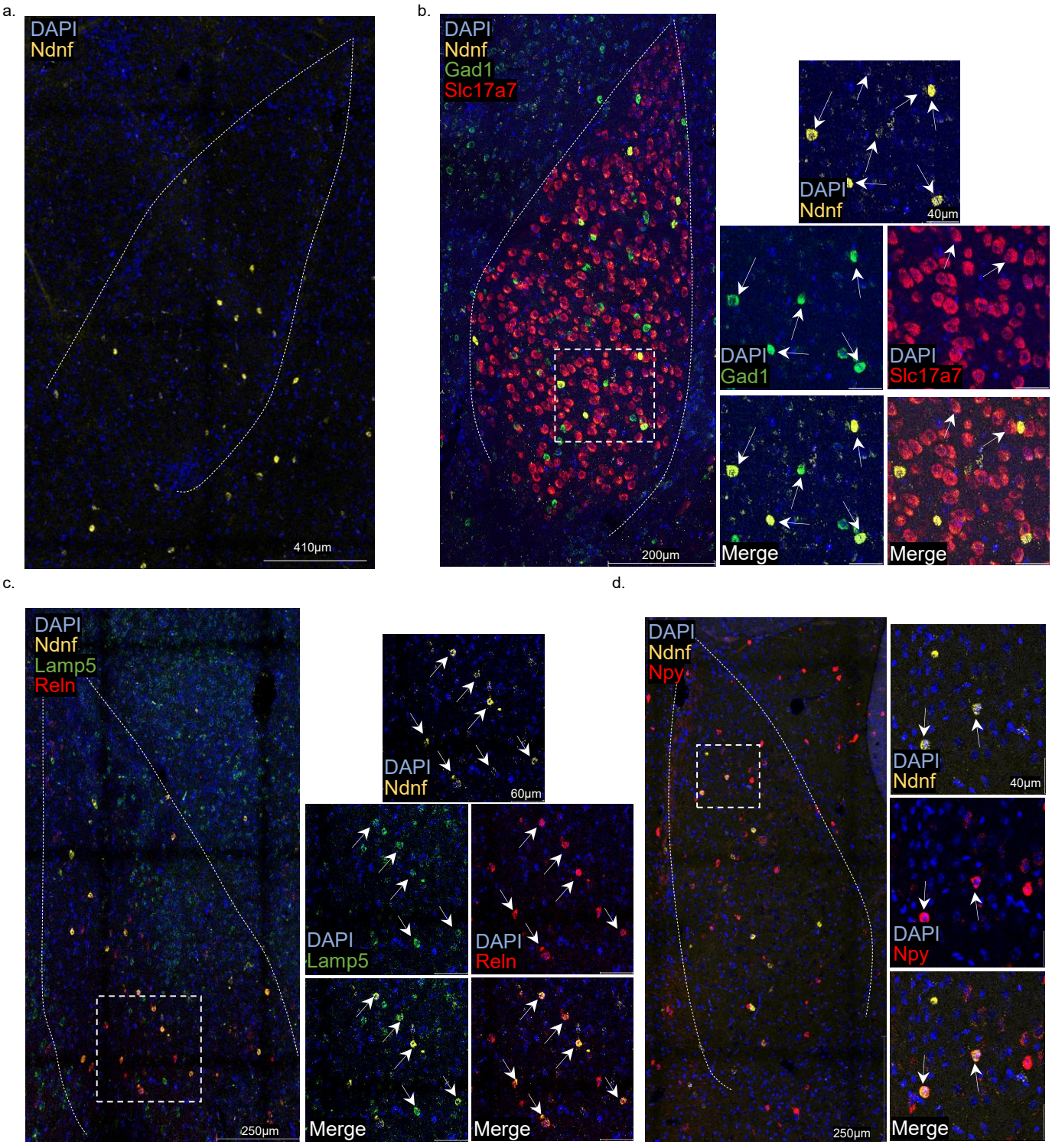
a.
DAPI
Ndnf
410µm
b.
DAPI
Ndnf
Gad1
Slc17a7
200µm
DAPI
Ndnf
40µm
DAPI
Gad1
DAPI
Slc17a7
Merge
Merge
c.
DAPI
Ndnf
Lamp5
Reln
250µm
DAPI
Ndnf
60µm
DAPI
Lamp5
DAPI
Reln
Merge
Merge
d.
DAPI
Ndnf
Npy
250µm
DAPI
Ndnf
40µm
DAPI
Npy
Merge
e.
# of Ndnf+ cells / 20µm slice
% Ndnf+ cells
Experimental Animal
WT1
WT2
WT3
WT4
WT5
WT6
WT7
WT8
WT9
Total
f.
Mean ± SEM
% Ndnf expressing respective marker
Gad1
Npy
Reln
Lamp5
Reln/Lamp5
Slc17a7
Slc17a6

Figure 1. NDNF-INs are predominantly GABAergic and express typical NGFC markers

a. Representative image of HCR RNA-FISH for Ndnf (yellow) localization in the BLA.

b. Representative image of whole slice HCR and close-ups of Ndnf (yellow), Gad1 (green), Slc17a7 (red), and DAPI in BLA, indicated by arrowheads. Scale bar BLA: 200 µm, scale bar zoomed in images: 40 µm.

c. Representative images of HCR RNA-FISH for Ndnf (yellow), Lamp5 (green), Reln (red) and DAPI in the BLA, indicated by arrowheads. Scale bar BLA: 250 µm, scale bar zoomed in images: 60 µm.

d. Representative images of HCR RNA-FISH for Ndnf (yellow) Npy (red) and DAPI in the BLA, indicated by arrowheads. Scale bar BLA: 250 µm, scale bar zoomed in images: 40 µm.

e. Percentage of $Ndnf^+$ cells expressed in 20 µm-thick coronal brain sections for each experimental animal used in this study (n= 9).

f. Percentage of $Ndnf^+$ cells expressing Gad1, Npy, Reln, Lamp5, Reln/Lamp5, Slc17a7, Slc17a6 in the BLA of 20 µm-thick coronal brain sections (For Gad1, Npy, Reln/Lamp5, Slc17a7, Slc17a6, n= 3. For Reln and Lamp5, n= 6). Dots represent each experimental animal. Data are presented as mean ± SEM.

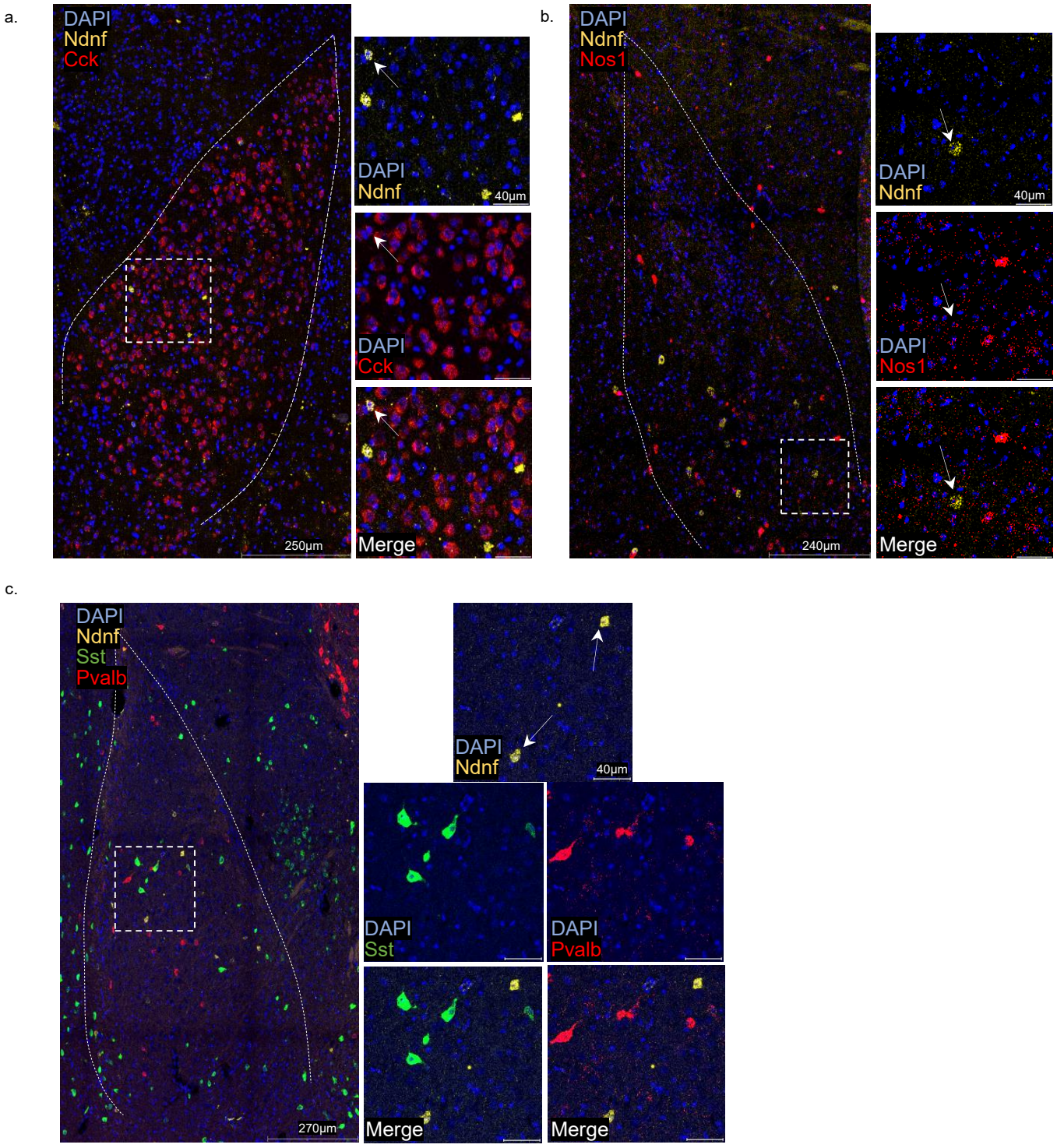
a.
DAPI
Ndnf
Cck
250µm
DAPI
Ndnf
40µm
DAPI
Cck
Merge
b.
DAPI
Ndnf
Nos1
240µm
DAPI
Ndnf
40µm
DAPI
Nos1
Merge
c.
DAPI
Ndnf
Sst
Pvalb
270µm
DAPI
Ndnf
40µm
DAPI
Sst
DAPI
Pvalb
Merge
Merge
d.
% Ndnf expressing respective marker
50
40
30
20
10
0
Cck
Nos1
Sst
Pvalb
e.
% of markers expressing Ndnf
Mean ± SEM
60
40
20
0
Gad1
Npy
Reln
Lamp5
Slc17a7
Slc17a6
Cck
Sst
Pvalb
Nos1

Figure 2. NDNF-positive cells do not overlap with other interneurons population of the BLA

a. Representative images of HCR RNA-FISH for Ndnf (yellow), Cck (red), and DAPI in the BLA, indicated by arrowheads. Scale bar BLA: 250 µm, scale bar zoomed in images: 40 µm.

b. Representative images of HCR RNA-FISH for Ndnf (yellow), Nos1 (red), and DAPI in the BLA, indicated by arrowheads. Scale bar BLA: 240 µm, scale bar zoomed in images: 40 µm.

c. Representative images of HCR RNA-FISH for Ndnf (yellow), Sst (green), Pvalb (red), and DAPI in the BLA, indicated by arrowheads. Scale bar BLA: 270 µm, scale bar zoomed in images: 40 µm.

d. Percentage of Ndnf cells expressing Cck, Nos1, Sst, Pvalb in the BLA of 20 µm-thick coronal brain sections (For Cck, n= 2. For Nos1, Sst, Pvalb, n= 3). Dots represent each experimental animal. Data are presented as mean ± SEM.

e. Percentage plotted for each marker (Cck, Nos1, Sst, Pvalb) expressing Ndnf in the BLA of 20 µm-thick coronal brain sections (For Cck, n= 2. For Nos1, Sst, Pvalb, n= 3). Dots represent each experimental animal. Data are presented as mean ± SEM.

2.1.3.2 NDNF neurons are activated by aversive stimuli

The amygdala, in particular the BLA, has been long studied for its important role in the processing of fear-related behaviours[58]. Recent studies using *in vivo* recordings of INs in BLA have focused on the role that VIP, PV, SOM and CCK neurons play in the regulation of aversive stimuli[45,60,61]. A key paradigm for investigating the role of the BLA in fear and anxiety is contextual fear conditioning (CFC). Unlike Pavlovian Fear Conditioning that uses auditory or visual cues as conditioned stimuli (CS), CFC associates an aversive experience with the context itself. On the first day of the experiment, the animal is introduced to a novel environment, often inherently anxiety-inducing, where it receives an aversive stimulus, such as a foot shock. When the animal is re-exposed to the same environment the following day, without the aversive stimulus, the context alone triggers the animal freezing response[62]. Therefore, to begin investigating the function of NDNF INs, we asked if aversive stimuli would increase the expression of the activation marker cFos during CFC. For this purpose, Ndnf-ires-cre-ERT2 crossed with Ai9-Tdtomato mice were used. A first group of mice that was placed in a contextual fear chamber and did not receive any foot shock, served as a control group. Mice that received the shocks (fear acquisition) were further divided into two groups, one of which was placed in the chamber again after a 24h memory consolidation phase (fear recall) (**Fig. 3a**). All three groups were subsequentially perfused after 60 minutes waiting time in order to allow maximal expression of the immediate-early gene c-Fos, which serves as a marker for neuronal activity. After immunohistochemical staining to visualize c-Fos expression (**Fig. 3b**), we found that BLA cells were heterogeneously activated by the negative stimuli, and that the majority of NDNF INs were significantly activated during fear acquisition but not during fear recall when compared to controls (**Fig. 3c**). Similarly, previous studies have shown that PV, SOM, and CCK GABAergic neurons in the BLA are strongly activated by foot shocks[105]. Our data extend this understanding by providing evidence that NDNF INs significantly contribute to BLA fear microcircuits. Like other GABAergic neurons, NDNF INs are modulated by aversive stimuli, suggesting their involvement in the processing of fear-related information in the BLA.

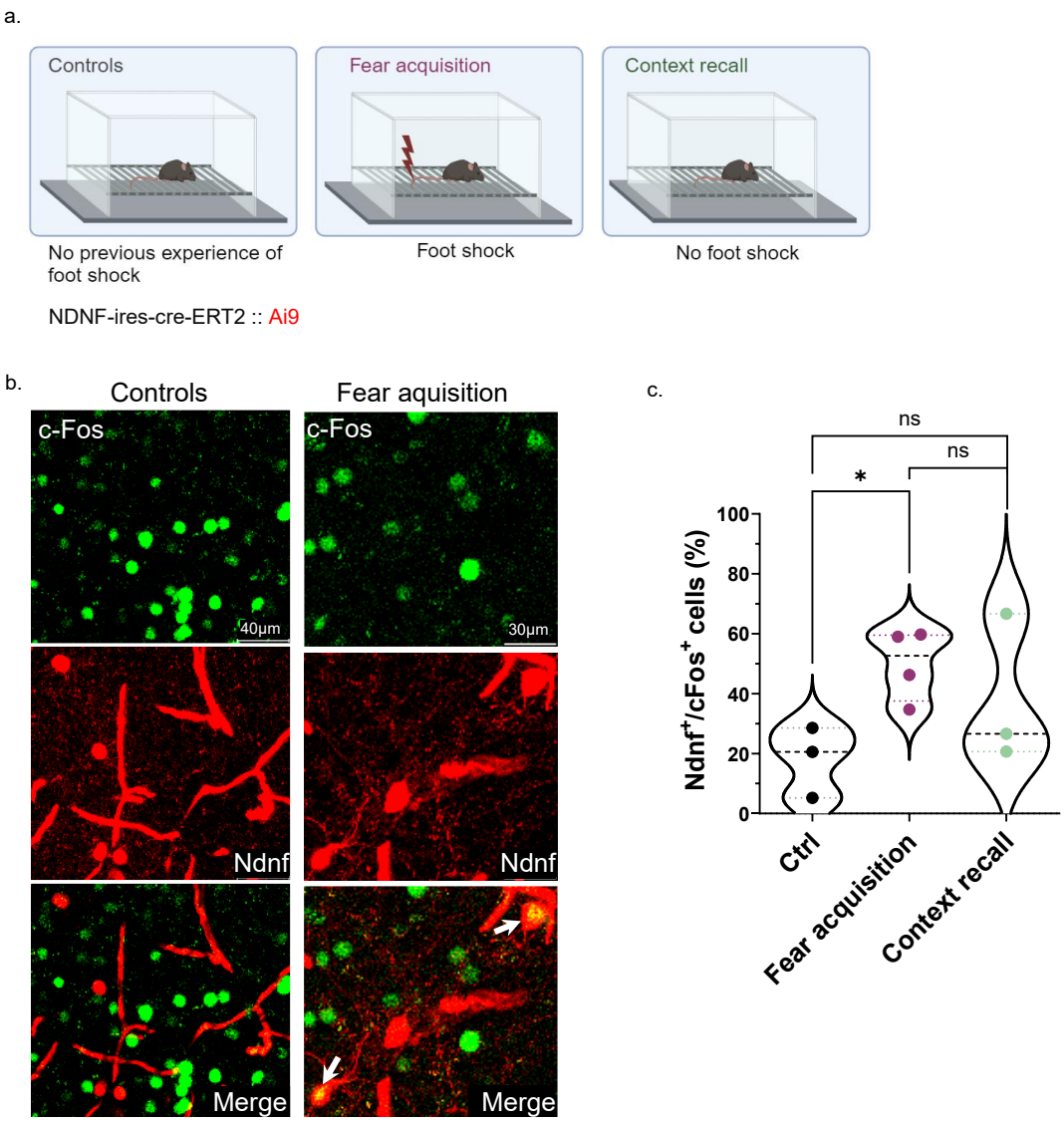

Figure 3. Aversive stimuli activate NDNF neurons during Contextual Fear Conditioning

a. Scheme depicting the Contextual Fear Conditioning (CFC) paradigm.

b. Representative images of c-Fos staining (green) in the BLA of Ndnf-Ai9 (red) mice 60-min after CFC experiments. Arrows indicate double-positive cells in the fear acquisition condition. Scale bar, 30µm.

c. Percentage of NDNF$^+$ INs colocalizing with c-Fos$^+$ cells, for control (ctrl), fear acquisition and context recall conditions. unpaired t test between ctrl and fear acquisition groups, p=0.0172, t=3.503. unpaired t test between fear acquisition and context recall groups, p= 0.4319, t=0.8545. unpaired t test between ctrl and context recall groups, p= 0.2823, t=1.241.

2.1.3.3 Photoinhibition of Ndnf-positive neurons reduces anxiety-like behavior and promotes exploratory activity

To study the role that NDNF INs play in anxiogenic situations, we first asked if optogenetic inhibition or activation of NDNF INs would alter the behavior during open field exploration. The classical view of this behavior is that mice prefer to spend more time in the periphery (corners) of the open field arena rather than the center, which represents the most anxiogenic zone. Stereotactic bilateral injections into the BLA were performed using either AAV-EF1a-DIO-eNpHR3.0-mcherry or AAV-EF1a-double floxed-hChR2(H134R)-EYFP in tamoxifen inducible Ndnf-ires-cre-ERT2 mice, expressing halorhodopsin (eNpHR3.0) or channelrhodopsin (ChR2) respectively, to target BLA^{Ndnf} (**Fig. 4a**). Viruses expressing only mCherry or eGFP fluorescent proteins were used in control experiments. Expression of both viruses was validated for all animals tested for this behavior (**Fig. 4b and c**). Following adenovirus injection, we placed one optic fibre in each hemisphere in order to achieve specific photoinhibition or photoactivation of BLA^{Ndnf}. Animals were placed in the open field chamber for 10 minutes while being bilaterally photoinhibited or photoactivated for the entirety of the session (**Fig. 4d and j**). Correlation analysis between the distance travelled and time spent in the central area of the field was significantly different in photoinhibited BLA^{Ndnf} neurons, indicative of increased levels of exploratory behavior. In contrast, no changes can be seen in control mice (**Fig. 4e**). Photoinhibition of BLA^{Ndnf} neurons produced no significant changes between eNpHR3.0-mcherry and mCherry control mice in the time spent in the center or corners of the OF, number of visits (frequency) in each zone, velocity and time spent moving (**Fig. 4f-g**). Photoactivation was insufficient to induce any change in either animal locomotion nor exploration behaviors (**Fig. 4k-n**). These data suggest that BLA^{Ndnf} neurons, are sufficient to promote exploration of the anxiogenic central area. In contrast, no such changes were observed in control mice, stressing the specificity that BLA^{Ndnf} neurons have in modulating exploratory behavior. We next asked whether BLA^{Ndnf} neurons are required for promoting anxiety-like states. In order to achieve this, we stereotactically injected AAVs expressing eNpHR3.0 in a Cre-dependent manner, bilaterally into the BLA, followed by optic fibre implantation. Four weeks later, animals were tested in the elevated plus maze (EPM) paradigm for 10 minutes while being bilaterally photoinhibited for the entirety of the session (**Fig. 4o**). Typically, the closed arms of the EPM represent a safe area, where mice normally spend the majority of their time, avoiding going to the center or the open arms of the arena which are more anxiogenic. We found that in both experimental groups, mice spent more time in the closed arms compared to the open arms, however inhibition of eNpHR3.0 expressing mice significantly decreased the time spent in the closed arms

compared to control mice and subsequently spent significantly more time in the center (**Fig. 4p**), choosing to explore the open arms more frequently compared to the closed ones (**Fig. 4q**). Therefore, photoinhibited eNpHR3.0 mice showed increased exploratory behavior on the EPM, by transitioning from the closed arms to the center and open arms more frequently. These data reveal that BLA^{Ndnf} neurons are necessary to efficiently balance animal's exploratory drive and anxiety-like behaviors.

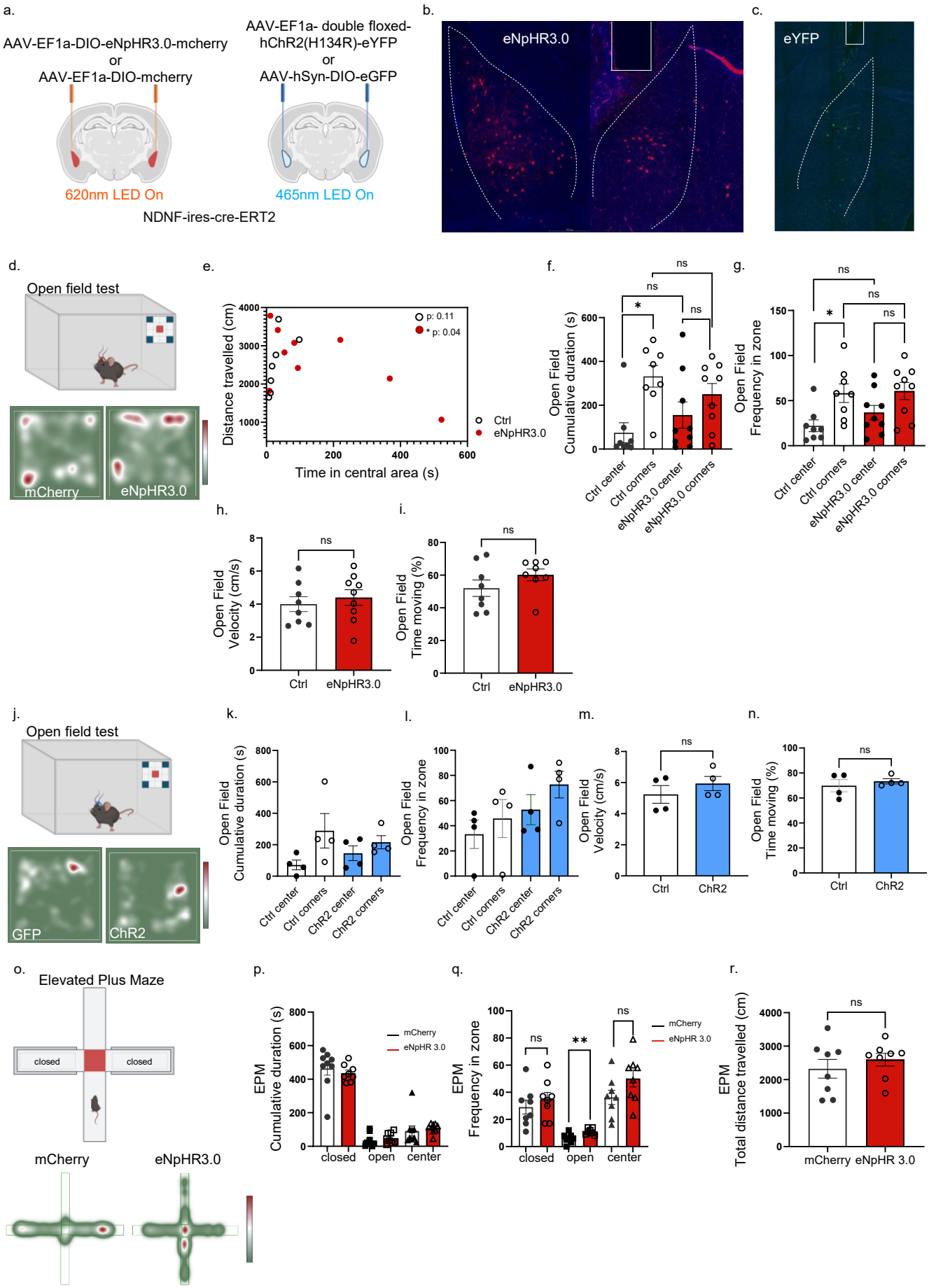
a.
AAV-EF1a-DIO-eNpHR3.0-mcherry
or
AAV-EF1a-DIO-mcherry
620nm LED On
AAV-EF1a- double floxed-
hChR2(H134R)-eYFP
or
AAV-hSyn-DIO-eGFP
465nm LED On
NDNF-ires-cre-ERT2
b.
eNpHR3.0
c.
eYFP
d.
Open field test
mCherry
eNpHR3.0
e.
Distance travelled (cm)
Time in central area (s)
p: 0.11
* p: 0.04
Ctrl
eNpHR3.0
f.
Open Field
Cumulative duration (s)
Ctrl center
Ctrl corners
eNpHR3.0 center
eNpHR3.0 corners
g.
Open Field
Frequency in zone
h.
Open Field
Velocity (cm/s)
i.
Open Field
Time moving (%)
j.
Open field test
GFP
ChR2
k.
Open Field
Cumulative duration (s)
Ctrl center
Ctrl corners
ChR2 center
ChR2 corners
l.
Open Field
Frequency in zone
m.
Open Field
Velocity (cm/s)
n.
Open Field
Time moving (%)
o.
Elevated Plus Maze
closed
closed
mCherry
eNpHR3.0
p.
EPM
Cumulative duration (s)
mCherry
eNpHR 3.0
closed
open
center
q.
EPM
Frequency in zone
r.
EPM
Total distance travelled (cm)
mCherry
eNpHR 3.0
ns

Figure 4. Photoinhibition of BLA^{Ndnf} neurons reduces anxiety-like behavior and promotes exploratory activity

a. Scheme representing the viruses injected bilaterally into the BLA of Ndnf-Cre mice with optic fiber placement.

b-c. Representative images of eNpHR3.0-mCherry and ChR2-eYFP expression in the BLA of Ndnf-Cre mice.

d. Scheme depicting the open field behavioral paradigm with representative heatmaps for both controls-mCherry and eNpHR3.0-mCherry groups.

e. Correlation analysis between the distance travelled (cm) and time spent in the central area (s) of the open field is significantly different in photoinhibited BLA^{Ndnf} neurons (n= 9). No changes can be seen in control mice (n=8). eNpHR3.0-mCherry: correlation analysis, p= 0.0488; controls-mCherry: correlation analysis, p= 0.1163.

f. Effect of BLA^{Ndnf} photoinhibition on cumulative duration (s) spent in either center zone or corners of open field arena in Ndnf-cre mice, analysed for controls-mCherry (white, n= 8) and eNpHR3.0-mCherry (red, n= 9). Main effect controls-eNpHR3.0 zones: Two-way ANOVA, F (8, 22) =0.10, P= 0.99; Main effect groups: Two-way ANOVA, F (3, 22) = 3.392, p=0.03. Tukey post-hoc test *P= 0.030. Values = Mean± SEM.

g. Effect of BLA^{Ndnf} photoinhibition on entries frequency in either center zone or corners of open field arena in Ndnf-cre mice, analysed for controls-mCherry (white, n= 8) and eNpHR3.0-mCherry (red, n= 9). Main effect controls-mCherry zones: Two-way ANOVA, F (1, 30) = 11.79, p=0.0018; Tukey post-hoc test p= 0.0384. Main effect groups: Two-way ANOVA, F (1, 30) = 0.9382, p=0.3405. Values = Mean± SEM.

h. No effect of BLA^{Ndnf} photoinhibition on velocity (cm/s), analysed for controls-mCherry (white, n= 8) and eNpHR3.0-mCherry (red, n= 9). Unpaired t-test, p= 0.5600.

i. Effect of BLA^{Ndnf} photoinhibition on time spent moving (%) in the whole open field arena in Ndnf-cre mice, analysed for controls-mCherry (white) and eNpHR3.0-mCherry (red). Unpaired t-test, p= 0.2083.

j. Scheme depicting the open field behavioral paradigm with representative heatmaps for both controls-eGFP and ChR2-eYFP groups.

k. Effect of BLA^{Ndnf} photoactivation on cumulative duration (s) spent in either center zone or corners of open field arena in Ndnf-cre mice, analysed for controls-eGFP (white, n= 4) and ChR2-eYFP (blue, n= 4). Main effect zones: Two-way ANOVA, F (1, 12) = 4.882, p=0.0473. Values = Mean± SEM.

l. No effect of BLA^{Ndnf} photoactivation on entries frequency in either center zone or corners of open field arena in NDNF-cre mice, analysed for controls-eGFP (white, n= 4) and ChR2-eYFP (blue, n= 4).

m. No effect of BLA^{Ndnf} photoactivation on velocity (cm/s) in the whole open field arena in Ndnf-cre mice, analysed for controls-eGFP (white, n= 4) and ChR2-eYFP (blue, n= 4). Unpaired t-test, p= 0.3741.

n. No effect of BLA^{Ndnf} photoactivation on time spent moving (%) in the whole open field arena in Ndnf-cre mice, analysed for controls-eGFP (white) and ChR2-eYFP (blue). Unpaired t-test, p= 0.5307.

o. Scheme depicting the elevated plus maze behavioral paradigm with representative heatmaps for both controls-mCherry and eNpHR3.0-mCherry groups.

p. Effect of BLA^{Ndnf} photoinhibition on cumulative duration (s) spent in either center zone, open or closed arms of elevated plus maze arena in Ndnf-cre mice, analysed for controls-mCherry (white, n= 8) and eNpHR3.0-mCherry (red, n=8). NDNFclosed: Mann-Whitney test p= 0.0379. NDNFopen: Mann-Whitney test p= 0.1304, NDNFcenter: Mann-Whitney test p= 0.020.

q. Effect of BLA^{Ndnf} photoinhibition on entry frequency in either center zone, open or closed arms of elevated plus maze arena in Ndnf-cre mice, analysed for controls-mCherry (white, n= 8) and eNpHR3.0-mCherry (red, n= 8). NDNFclosed: Mann-Whitney test p= 0.3921. NDNFopen: Mann-Whitney test p= 0.005. NDNFcenter: Mann-Whitney test p= 0.1378.

r. Effect of BLA^{Ndnf} photoinhibition on the total distance travelled in the whole elevated plus maze arena in Ndnf-cre mice, analysed for controls-mCherry (white, n= 8) and eNpHR3.0-mCherry (red, n= 8). Mann-Whitney test p= 0.7209.

2.1.3.4 BLA^{Ndnf} neurons are necessary for expression of fear behavior

Next, we tested the function of NDNF INs during fear conditioning and examined whether photoinhibition of these cells would affect freezing behavior and if they have a role in fear memory formation in two conditions: animals naïve to the aversive cue and those previously exposed to the stimuli (foot shocks).

To address the first condition, on day 1 (fear acquisition) we placed eNpHR3.0-expressing mice and mCherry controls, in the CFC chamber for 360 seconds, during which mice received three shocks (2s each, 1.1A) after a pre-stimuli period of 2-minutes. The animals were left in the chamber for an additional 2 minutes in order to asses freezing (considered as the complete lack of movement from tail to animal's nose tip, at exception of breathing movements) during a post-conditioning phase. Photoinhibition was applied throughout the behavioral test. During day 2 (fear recall), mice were again placed in the CFC chamber. During this time no photoinhibition and foot shocks were applied (**Fig. 5a**). The fraction of time that mice spent freezing and being immobile, were analysed and monitored for the entirety of the behavior. On day 1, control animals exhibited low freezing behavior when first placed in the chamber and freezing time increased significantly after the conditioning phase (**Fig. 5c**). In contrast, freezing time in the NDNF INs photoinhibited mice did not increase post conditioning (**Fig. 5d**) and it is significantly reduced compared to control mice (**Fig. 5e** and **Fig. 5b**, heatmap for day 1). These results suggest that the activity of BLA^{Ndnf} neurons is required to express freezing behavior during fear acquisition in day 1 and indicate that the freezing behavior observed after conditioning is not influenced by their initial internal state, but rather is a direct result of the conditioning process itself. On day 2, control animals when introduced to the same context, continue expressing freezing behavior indicating that fear memory was formed (**Fig. 5e**). NDNF neuron photoinhibited mice also displayed increased freezing behavior on day 2, suggesting that NDNF neuron activity is not required for expression of fear memory during fear recall (**Fig. 5e** and **Fig. 5b**, heatmap for day 2). These results are supported by the fact that NDNF INs photoinhibited mice show increased immobile time (characterized by the animal's stillness with occasional head movements) and much reduced locomotor activity during day 2, as compared to day 1, similar to control mice (**Fig. 5f-h**). We next asked whether the expression of fear memory on day 2 is influenced by NDNF INs activity. We followed the same CFC paradigm as described above, but this time we photoinhibited NDNF INs only on day 2 and not on day 1 (**Fig. 5i**). As before, control mice behaved largely as expected with significantly increased freezing on day 1 (**Fig. 5j**), although freezing on day 2 was significantly lower than on day 1 (**Fig. 5l**).

The eNpHR3.0-expressing mice in the absence of photoinhibition also learned the fear conditioning test and showed significantly increased freezing behavior on day 1 (**Fig. 5k**). We found no significant differences in either the time spent freezing nor immobile between day 1 (no photoinhibition) and day 2 (with photoinhibition) in the NDNF INs manipulated mice (**Fig. 5l and m**). Photoinhibition also led to a decrease in exploratory time on day 2 (**Fig. 5n**), indicating that all animals retained a memory of the aversive context experienced on day 1. Together these results show that BLA^{Ndnf} neurons are necessary for fear expression during conditioning, but not for fear memory recall.

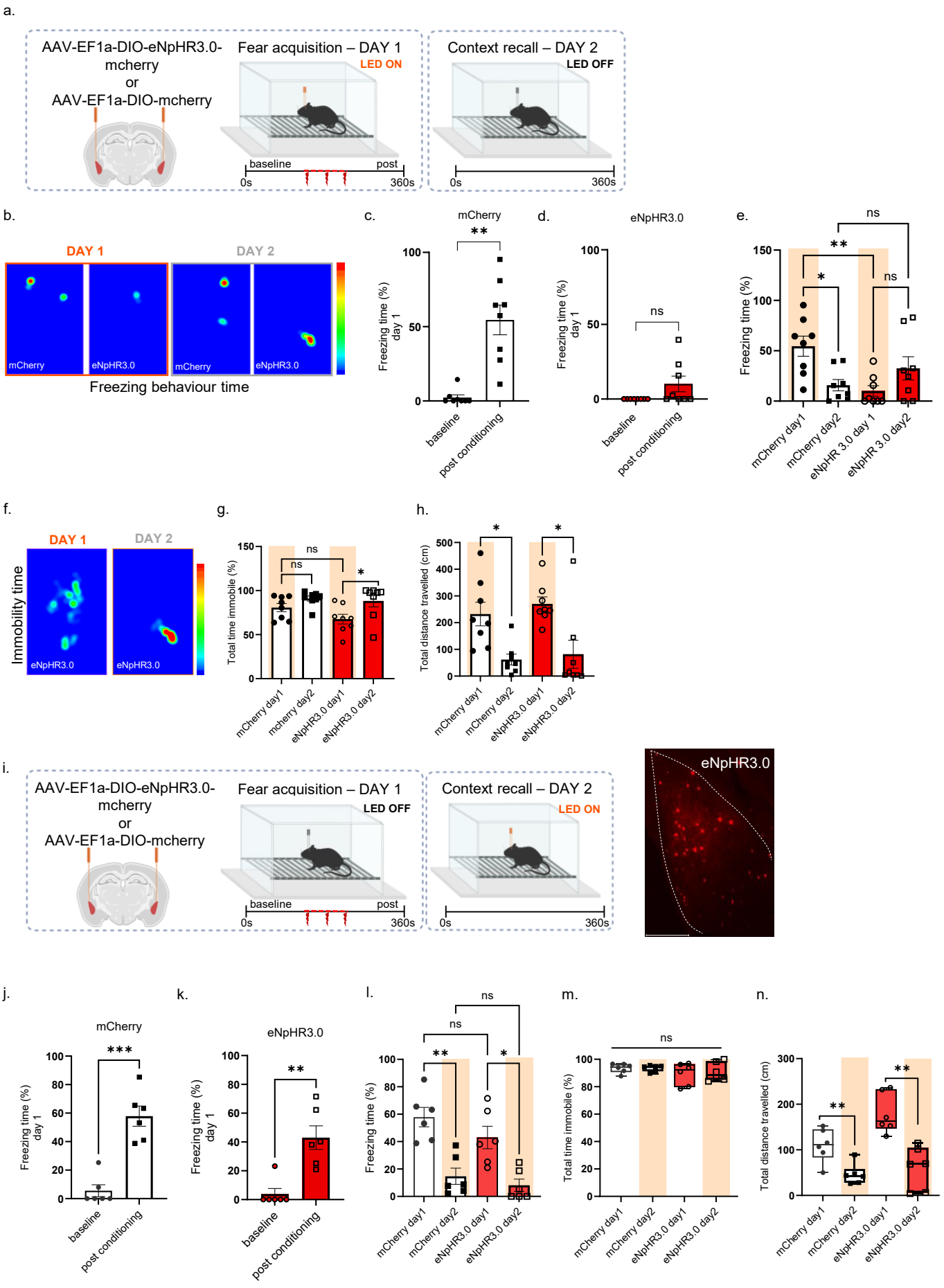
a.
AAV-EF1a-DIO-eNpHR3.0-mcherry
or
AAV-EF1a-DIO-mcherry
Fear acquisition – DAY 1
LED ON
baseline
post
0s
360s
Context recall – DAY 2
LED OFF
0s
360s
b.
DAY 1
DAY 2
mCherry
eNpHR3.0
mCherry
eNpHR3.0
Freezing behaviour time
c.
mCherry
**
Freezing time (%) day 1
baseline
post conditioning
d.
eNpHR3.0
ns
Freezing time (%) day 1
baseline
post conditioning
e.
ns
**
*
ns
Freezing time (%)
mCherry day1
mCherry day2
eNpHR 3.0 day 1
eNpHR 3.0 day2
f.
DAY 1
DAY 2
Immobility time
eNpHR3.0
eNpHR3.0
g.
ns
ns
*
Total time immobile (%)
mCherry day1
mcherry day2
eNpHR3.0 day1
eNpHR3.0 day2
h.
*
*
Total distance travelled (cm)
mCherry day1
mCherry day2
eNpHR3.0 day1
eNpHR3.0 day2
i.
AAV-EF1a-DIO-eNpHR3.0-mcherry
or
AAV-EF1a-DIO-mcherry
Fear acquisition – DAY 1
LED OFF
baseline
post
0s
360s
Context recall – DAY 2
LED ON
0s
360s
eNpHR3.0
j.
mCherry
***
Freezing time (%) day 1
baseline
post conditioning
k.
eNpHR3.0
**
Freezing time (%) day 1
baseline
post conditioning
l.
ns
ns
**
*
Freezing time (%)
mCherry day1
mCherry day2
eNpHR3.0 day1
eNpHR3.0 day2
m.
ns
Total time immobile (%)
mCherry day1
mCherry day2
eNpHR3.0 day1
eNpHR3.0 day2
n.
**
**
Total distance travelled (cm)
mCherry day1
mCherry day2
eNpHR3.0 day1
eNpHR3.0 day2

Figure 5. BLA^{Ndnf} neurons are necessary for expression of fear behavior

a. Scheme representing the virus injected bilaterally into the BLA of Ndnf-Cre mice with optic fiber placement together with CFC behavioral paradigm.

b. Representative heatmaps of average freezing time during CFC for both controls-mCherry and eNpHR3.0-mCherry groups during day 1 and day 2.

c. Percentage of freezing time during day 1 at baseline and after conditioning for controls-mCherry (n=8) expressing mice. Paired t test, p=0.0020, t=4.777.

d. Percentage of freezing time during day 1 at baseline and after conditioning for eNpHR3.0-mCherry (n=8) expressing mice. Paired t test, p= 0.0954, t=1.927.

e. Percentage of the time spent freezing on day 1 paired with photoinhibition and day 2 with no photoinhibition of BLA^{Ndnf} neurons, (mCherry, n=8 - eNpHR3.0, n=8). Two-way ANOVA, Bonferroni's multiple comparison test *P= 0.0287, **P=0.0097.

f. Representative heatmaps of average immobility time or both controls-mCherry and eNpHR3.0-mCherry groups during day 1 and day 2 of CFC.

g. Percentage of total immobility time on day 1 paired with photoinhibition and day 2 with no photoinhibition of BLA^{Ndnf} neurons. Unpaired t test of eNpHR3.0- expressing mice (n=8) compared to controls (n=8), (day 1), p= 0.0886, t=1.830. Paired t test of eNpHR3.0- expressing mice between day 1 and day 2, p= 0.0209, t=2.966. Paired t test of controls-mCherry expressing mice between day 1 and day 2, p= 0.1521, t=1.607.

h. Effect of photoinhibition of BLA^{Ndnf} neurons on the total distance travelled during CFC. Paired t test of controls-mCherry expressing mice between day 1 and day 2, p= 0.0150, t=3.202. Paired t test of eNpHR3.0- expressing mice between day 1 and day 2, p= 0.0126, t=3.329.

i. Scheme representing the virus injected bilaterally into the BLA of Ndnf-Cre mice with optic fiber placement together with CFC behavioral paradigm. Representative image of AAV injection site in BLA.

j. Percentage of freezing time during day 1 at baseline and after conditioning for controls-mCherry (n=6) expressing mice. Paired t test, p=0.0005, t=7.885.

k. Percentage of freezing time during day 1 at baseline and after conditioning for eNpHR3.0-mCherry (n=6) expressing mice. Paired t test, p= 0.0084, t=4.206.

l. Freezing time (%) on day 1 with no photoinhibition and day 2 paired with photoinhibition of BLA^{Ndnf} neurons. Two-way ANOVA, **p=0.0018, *P=0.0103.

m. No difference in the time spent immobile can be seen between eNpHR3.0- and control-expressing mice or between days. (Unpaired t test day 1 p= 0.2740, t=1.157; unpaired t test day 2 p= 0.3753, t=0.9280).

n. A decrease in the total distance travelled (cm) during photoinhibition in day 2, can be seen for both eNpHR3.0- and control-expressing mice (paired t test eNpHR3.0 p= 0.0087, t=4.176; paired t test controls p= 0.0016, t=6.184).

2.1.3.5 Photoinhibition of BLA^{Ndnf} neurons decreases the freezing response to innate threat

Next, we aimed to determine whether BLA^{Ndnf} neurons regulate the innate fear response to the predator odour TMT (a fox urine derivative). During the behavioral test, mice were placed in an enclosed cage for 10 minutes, divided into two phases: a 5-minute baseline period, during which a filter paper was attached to the side of a circular sliding door without photoinhibition, and a 5-minute TMT exposure period. In the TMT phase, 5 µL of TMT was applied to the same filter paper used during baseline, and photoinhibition was activated throughout this entire phase (**Fig. 6a**). Freezing and rearing behaviors were monitored under both light-off (baseline) and light-on (TMT) conditions (**Fig. 6b**). We found that both eNpHR3.0- and mCherry-expressing mice showed significantly higher levels of freezing during the TMT phase compared to the baseline condition. (**Fig. 6c and d**). Interestingly, eNpHR3.0-expressing mice showed a significantly reduced freezing behavior compared to mCherry control mice during the TMT phase (**Fig. 6e**) with no significant effects seen for either the time spent immobile nor exploring the arena (**Fig. 6f and g**). Taken together these findings suggest that BLA^{Ndnf} neurons contribute to fear responses positively by enhancing the freezing response to innate threats, such as TMT. When evaluating whether rearing behavior was affected by the inhibition of BLA^{Ndnf} neurons, we did not find significant differences between baseline and TMT exposure times, nor between eNpHR3.0-expressing mice and mCherry controls (**Fig. 6h-j**). Previous studies have shown that rearing occurs less during high fear or very low anxiety states, and peaks when the animal experiences low fear but relatively high anxiety[106]. Therefore, rearing behavior is contextually sensitive and depends on the interplay between fear and anxiety states. The stability of rearing across conditions suggests that NDNF INs do not significantly modulate this behavior in high-fear contexts. This aligns with our earlier finding that BLA^{Ndnf} neurons help balance exploratory drive and anxiety-like behaviors and this strictly depends on the contextual cues. Therefore, when mice face a strong aversive stimulus (i.e. TMT), the motivation to explore is independent of whether NDNF INs are active or inhibited.

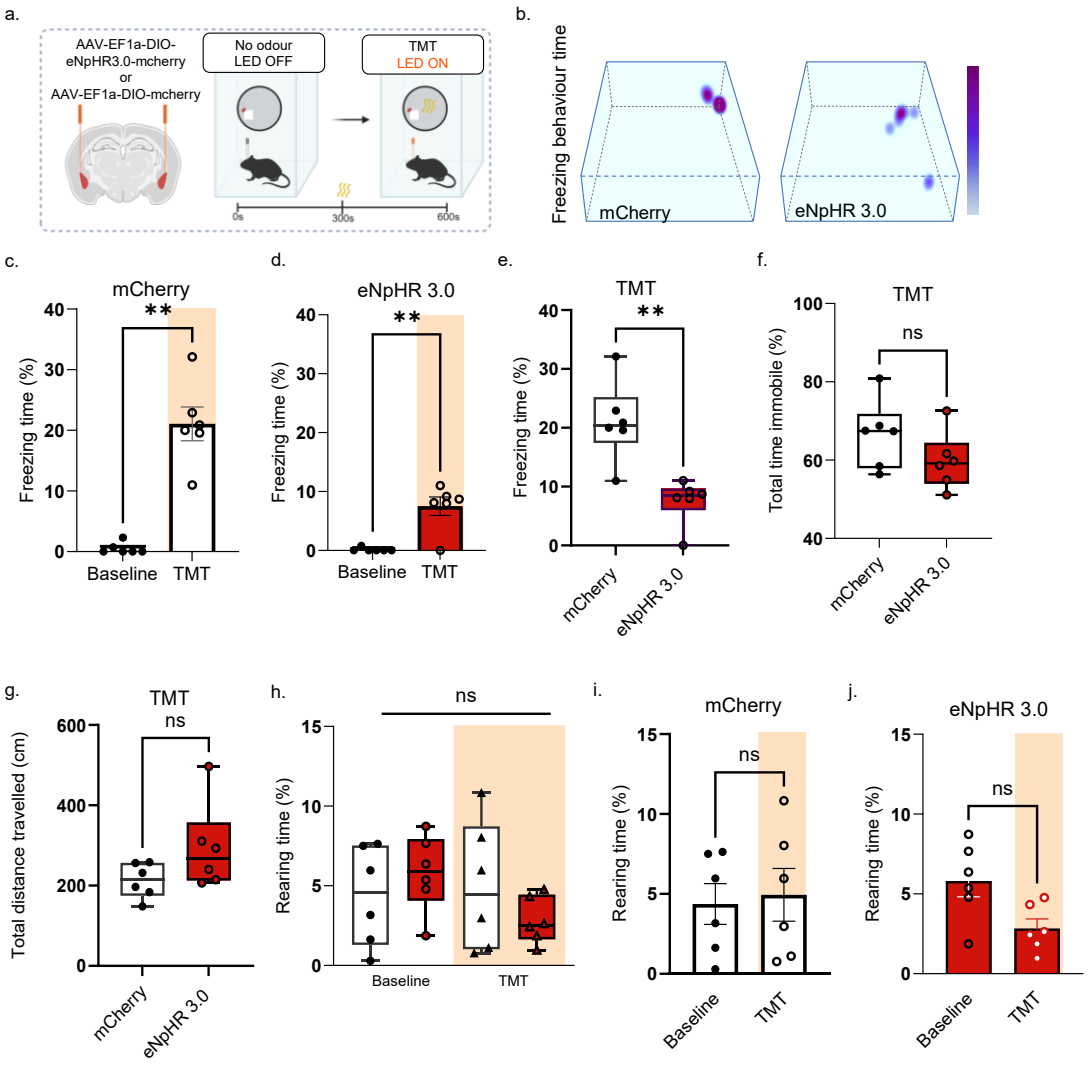

Figure 6. Photoinhibition of BLA^{Ndnf} neurons decreases the freezing response to innate threat

a. Scheme representing the virus injected bilaterally into the BLA of Ndnf-Cre mice with optic fiber placement together with innate threat behavioral paradigm.

b. Representative heatmaps with average freezing behavior time of both mCherry-controls and eNpHR 3.0 mice.

c. Freezing time increases during TMT exposure time in mCherry controls (n=6). (Paired t test p= 0.0011, t=6.693).

d. Freezing time increases during TMT exposure time in eNpHR3.0-expressing mice (n=6). (Paired t test p= 0.0046, t=4.880).

e. Percentage of freezing time decreases in photoinhibited eNpHR3.0-expressing mice during TMT exposure compared to baseline controls. (Unpaired t test p= 0.0017, t=4.255).

f. No difference in the time spent immobile can be seen between eNpHR3.0- and control-expressing mice during TMT exposure time. (Unpaired t test p= 0.1753, t=1.459).

g. Total distance travelled (cm) is not significantly different between eNpHR3.0- and control-expressing mice during TMT exposure time. (Unpaired t test p= 0.1183, t=1.709).

h-j No differences can be found in rearing behavior between baseline and TMT exposure times, nor between eNpHR3.0-expressing mice and mCherry controls. (Unpaired t test baseline p= 0.3937, t=0.8914; Unpaired t test TMT p= 0.2558, t=1.205).

2.1.3.6 Deep brain Ca^{2+} imaging reveals two functionally distinct ensembles of NDNF neurons in BLA

To understand how BLA^{Ndnf} neurons participate in aversive behavior, we performed single-cell resolution *in vivo* Ca^{2+} imaging in freely behaving mice. We injected a Cre-dependent version of the genetically encoded calcium indicator GCaMP7s-eYFP virus unilaterally into the BLA of Ndnf-ires-cre-ERT2 animals to record NDNF neuronal activity using a head-mounted miniscope attached to a gradient-index relay (GRIN) lens (**Fig. 7a-b**). We tested animals both during CFC and odour-induced fear experiments following previously described experimental set ups (see material and methods). We analysed the activities of an average total of 60 cells and registered neuronal activity for all cells and where possible, tracked the same cells across different experimental conditions. Firstly, we calculated z-score calcium activity for each active cell in every condition. In our CFC experiments, we observed distinct activity changes among NDNF INs during freezing episodes, with each episode classified as freezing if it lasted longer than 2 seconds. A group of NDNF INs in day 1, exhibited decreased activity (z-scores < 0) during freezing episodes and foot shock presentations (**Fig. 7d**), while others showed increased activity (z-scores > 0) during the same events (**Fig. 7e**). Notably, these changes persisted across days, resulting in similar activity patterns in the same context and in the absence of salient stimuli on day 2. Some neurons showed decreased activity during freezing episodes (**Fig. 7f**) and others showing increased activity (**Fig. 7g**). To understand how BLA^{Ndnf} neurons participate in freezing and non-freezing behaviors we clustered the averaged z-scored calcium activity of all cells at all time points on both day 1 and day 2 (**Fig. 7h and i**). Clustering was performed by grouping BLA^{Ndnf} cells based on their activity relative to baseline: those with increased activity (z-scores > 0) and those with decreased activity (z-scores < 0). We found that on day 1, the averaged z-score activity decreased during freezing (**Fig. 7h**, dark orange column) and was significantly different than the averaged z-score with increased activity (**Fig. 7h**, light orange column). Interestingly,

on day 2, in the absence of foot shocks, BLA^{Ndnf} activity showed less variability, with most cells clustering close to baseline (**Fig. 7h**, blue columns). The z scores of the positive cells on day 1 were significantly higher than on day 2 (**Fig. 7h**, light blue column), and the reverse was true for the negative cells (**Fig. 7h**, dark blue column). BLA^{Ndnf} neuron activity during non-freezing (exploratory) events showed that on day 1, the z scores of the positive cells were significantly higher than those with negative activity (**Fig. 7i**, orange columns). However, on day 2, BLA^{Ndnf} activity remained close to baseline, with fewer cells showing activity changes (**Fig. 7i**, blue columns). We then compared the averaged z-scored activity of all cells on day 1 for three conditions: pre-stimuli, during stimuli (conditioning) and post stimuli (post conditioning), independent of the behavioural states. Averaged z-score activity was analysed over a period of 120 seconds for each condition (for a total of 360 seconds of CFC test). During day 1, NDNF INs activity was high during pre-stimuli, and progressively decreased throughout CFC, becoming significantly more negative during the post stimuli phase (**Fig. 7j**). This was a surprising finding considering the increased c-Fos expression post conditioning (**Fig. 3c**). The high NDNF INs activity seen during pre-stimuli might be related to the fact that no conditioning was happening during this phase and mice maintained a normal exploratory behavior, raising the possibility that NDNF INs might engage with non-freezing states. In summary, these data suggest that BLA^{Ndnf} neuron activity reflects the animal's behavior in the presence of an aversive stimulus (foot shocks). These cells are more active during exploratory or non-freezing states and less active when the animal is engaged in freezing. Moreover, the reduced variability and clustering of BLA^{Ndnf} neuron activity close to baseline on day 2 suggest an adaptation to a context that appears safer (no foot shocks) than on day 1.

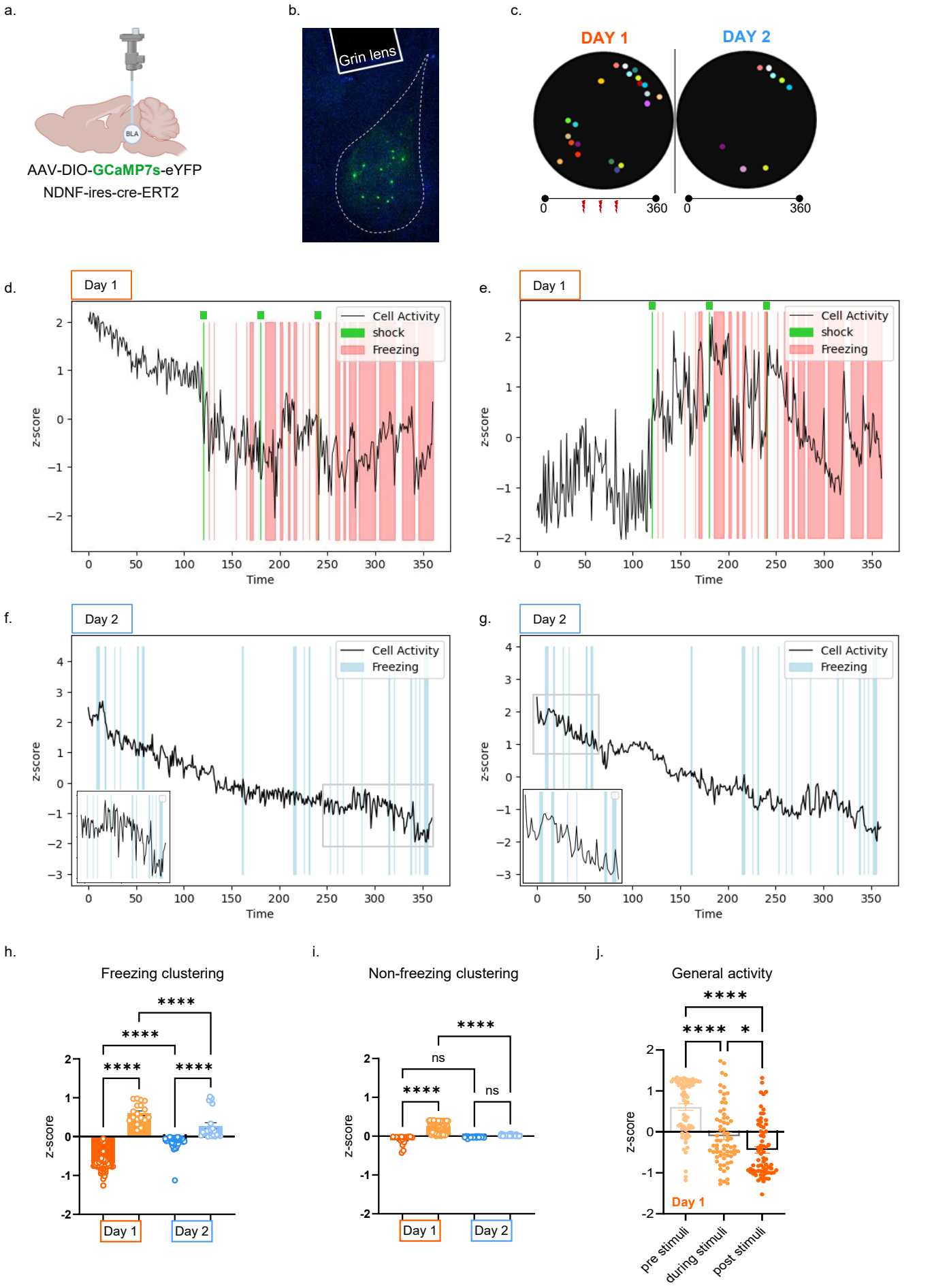
a.
BLA
AAV-DIO-GCaMP7s-eYFP
NDNF-ires-cre-ERT2
b.
Grin lens
c.
DAY 1
DAY 2
0
360
0
360
d.
Day 1
Cell Activity
shock
Freezing
z-score
Time
e.
Day 1
Cell Activity
shock
Freezing
z-score
Time
f.
Day 2
Cell Activity
Freezing
z-score
Time
g.
Day 2
Cell Activity
Freezing
z-score
Time
h.
Freezing clustering
****
****
****
****
z-score
Day 1
Day 2
i.
Non-freezing clustering
****
ns
****
ns
z-score
Day 1
Day 2
j.
General activity
****
****
*
z-score
Day 1
pre stimuli
during stimuli
post stimuli

Figure 7. Deep brain Ca^{2+} imaging reveals two NDNF cell clusters differentially modulated by freezing behavior

a. Scheme representing the AAV-DIO-GCaMP7s-eYFP virus injected unilaterally into the BLA of Ndnf-Cre mice together with GRIN-lens placement.

b. Representative AAV-DIO-GCaMP7s-eYFP expression in BLA^{Ndnf} neurons, with GRIN-lens track.

c. Example of miniscope field of view of NDNF cells recorded during day 1 and day 2 of CFC.

d. Representative NDNF cell activity trace showing decreased activity during freezing behavior (red) and footshocks (green) recorded during day 1 of CFC.

e. Representative NDNF cell activity trace showing increased activity during freezing behavior (red) and footshocks (green) recorded during day 1 of CFC.

f. Representative NDNF cell activity trace showing decreased activity during freezing behavior (blue) recorded during day 2 of CFC.

g. Representative NDNF cell activity trace showing increased activity during freezing behavior (blue) recorded during day 2 of CFC.

h. Averaged z-score Ca^{2+} activity of NDNF cells recorded during CFC (n=4 mice) grouped into freezing cluster. During freezing NDNF activity is either decreased or increased during day 1 and day 2 of CFC. Two-way ANOVA, ****P<0.0001.

i. Averaged z-score Ca^{2+} activity of NDNF cells recorded during CFC (n=4 mice) grouped into non-freezing cluster. During non-freezing NDNF activity is either decreased or increased during day 1 and day 2 of CFC, with significantly increased activity during day 1. Two-way ANOVA, ****P<0.0001.

j. Averaged z-score Ca^{2+} activity of NDNF cells recorded during pre-stimuli, during stimuli, post stimuli conditions of CFC (n=4 mice). NDNF cell activity is significantly more negative after foot shock exposure (Ordinary one-way ANOVA followed by Tukey's multiple comparison test ****p <0.0001, *p= 0.0141).

Next, we analysed the activity of cells that were consistently recorded across both days using longitudinal registration. We analysed activity changes between 'pre-stimuli' and exposure to foot shocks (experienced stimuli, day 1) and between recall and the period when the mice anticipated receiving footshocks (expected stimuli, day 2) (**Fig. 8a and b**). We found that cells whose z scores were positive during the pre-stimuli phase on day 1 showed a decrease in their activity during the experienced stimuli (**Fig. 8c and a**). Cells whose z scores were negative during the pre-stimuli phase on day 1 showed an increase in their activity during the experienced stimuli (**Fig. 8c and a**). This switch also occurred on day 2 when the animals were re-exposed to the same context (recall) and anticipated the stimulus (**Fig. 8b and d**). These data suggest that NDNF INs reflect

the animal's freezing behavior both positively (freezing-on) and negatively (freezing-off) during exposure to or anticipation of an aversive stimulus, consistent with a model in which NDNF INs participate in shaping the animal's response to threat. We provided more evidence for this hypothesis through correlation analysis between behaviour and NDNF neural activity, specifically on day 1 of CFC. Pearson correlations were performed assigning 1 to freezing events and 0 to non-freezing events across all 360 seconds of recordings. Neurons that significantly correlated to 1, showed either z-score > 0 (positive) or z-score < 0 (negative), whereas neurons that were not significantly correlated to freezing were termed neutral. Our data show ensembles of the BLA^{Ndnf} population whose activities correlated positively, negatively, or neutral across three time points including pre-stimuli, conditioning, and post-conditioning phases (**Fig. 9a**). We found that most neural activity states at pre-stimuli, before any fear conditioning, were neutral (44.6%) (**Fig. 9b**), suggesting that NDNF INs before foot shocks were presented did not significantly correlate with freezing behavior. During the fear conditioning phase, a considerable fraction of neurons shifted to a more negative state (40%), some of which persisted in the negative state post-conditioning (31.2%) while other cells shifted back to their original neutral state (39.5%) (**Fig. 9b**). These data are consistent with our finding that NDNF activity decreases in the presence of salient stimuli. Neurons that were neutral during the conditioning phase largely switched to the negative state (**Fig. 9a and b**). Moreover, a smaller proportion of cells that was negatively correlated (19.64%) or remained neutral (35.71%) during pre-stimuli shifted to either positive states or remained neutral throughout CFC (**Fig. 9a and b**). Correlation analysis also revealed that cells positively correlated with freezing during pre-stimuli (**Fig. 9c and d**) where significantly more likely to correlate negatively (**Fig. 9c**) or remain neutral (**Fig. 9d**) during conditioning, while remaining or shifting to a more negative state post-conditioning (**Fig. 9c and d**). These data show how NDNF INs ensembles participate in BLA network dynamics as the animal experiences and possibly learns to anticipate and adapt to the aversive stimuli.

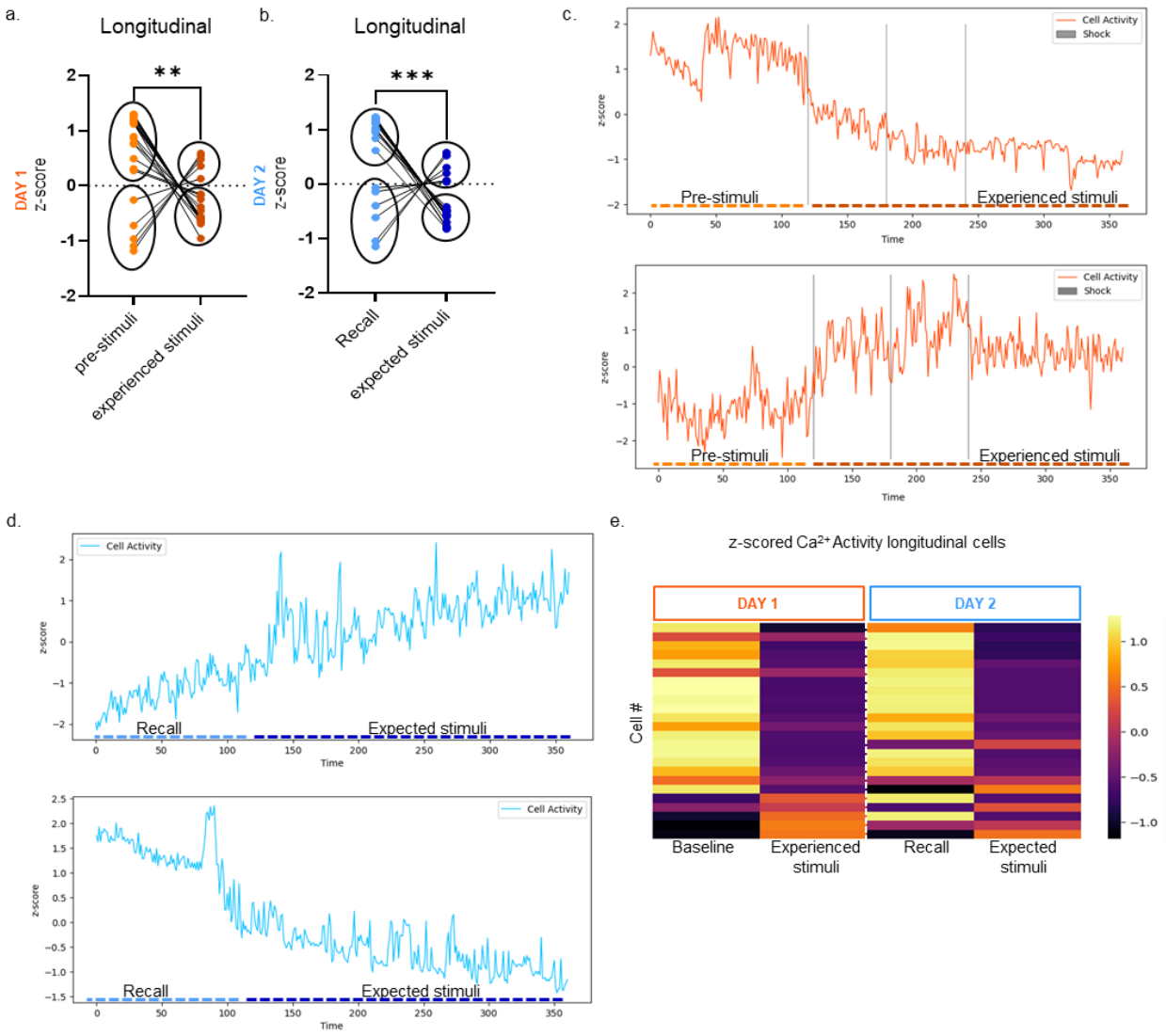

Figure 8. Deep brain Ca^{2+} imaging reveals two functionally different ensembles of NDNF neurons in BLA during CFC.

a. Averaged z-score activity of NDNF cells (day 1). Cell activity switch between positive and negative or viceversa can be seen between pre-stimuli and experienced stimuli time. Paired t test **p= 0.0012.

b. Averaged z-score activity of NDNF cells (day 2). Cell activity switch between positive and negative or viceversa can be seen between recall and expected stimuli time. Paired t test ***p= 0.0002.

c. Representative NDNF calcium activity cell trace during CFC day 1, the three vertical bars represent the time of foot shocks presentation (grey).

d. Representative NDNF calcium activity cell trace during CFC day 2.

e. Heatmap showing averaged z-score Ca^{2+} activity of longitudinal registered NDNF cells during day 1 (orange box) and day 2 (blue box) of CFC. Cell activity transition is plotted for both baseline/recall and experienced or expected stimuli.

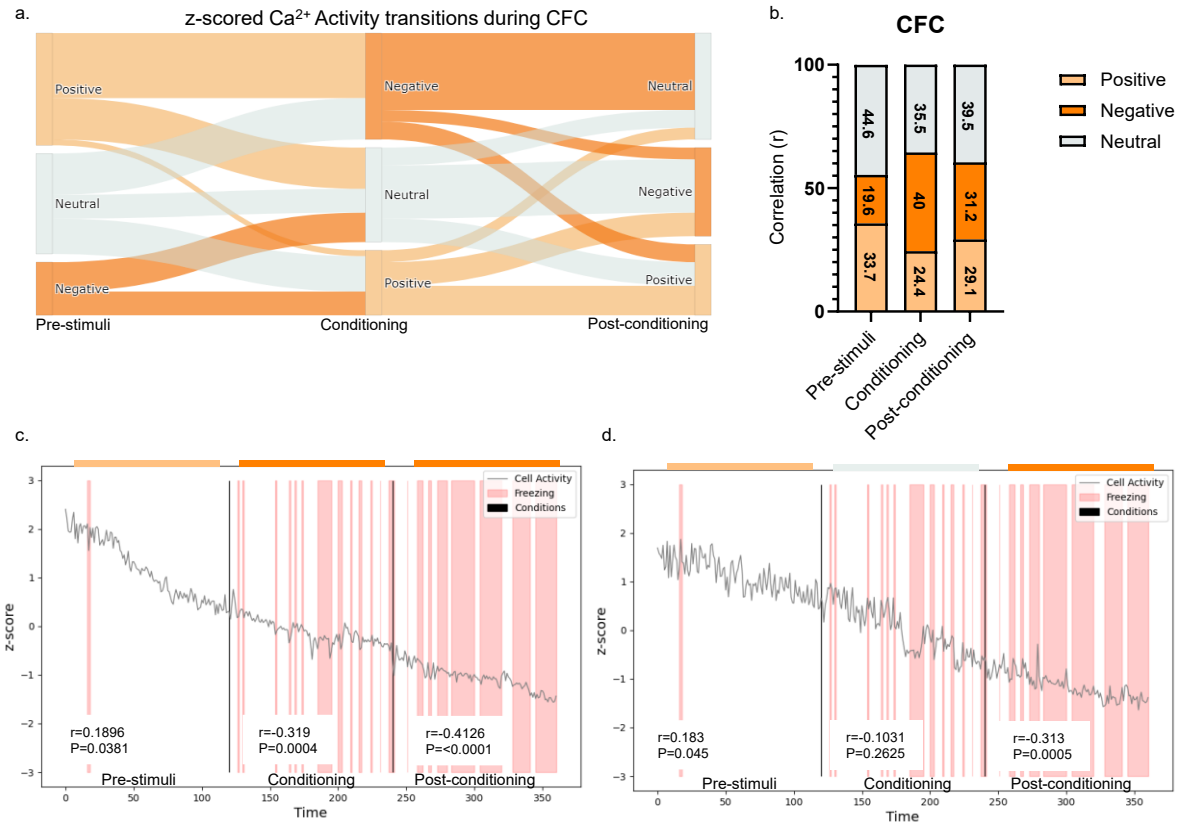

Figure 9. NDNF neuronal ensembles in BLA are negatively correlated to freezing behavior during CFC.

a. Alluvial plot of averaged z-score Ca^{2+} activity of NDNF cells correlated with freezing behavior. Transitions of cells activity are shown for positive (light orange), negative (dark orange) and neutral (light blue) combinations in pre-stimuli, conditioning and post-conditioning CFC behavioral conditions. The duration of each condition is 120s.

b. Percentages of NDNF cell activity during freezing behavior. Correlation (r) was analysed using the z-scored calcium activity of all cells registered in a total of 4 mice. Cells that showed a significance of $P > 0.05$, were considered as either positively (when $r > 0$, light orange), negatively (when $r < 0$, dark orange) correlated with freezing behavior. Cells that did not correlate with freezing were considered neutral (when P = ns, light blue).

c. Representative NDNF calcium activity trace during CFC. Pre-stimuli positive correlation with freezing (r=0.1896, P=0.0381), during conditioning negative correlation (r=-0.319, P=0.0004) as well as during post-conditioning (r=-0.4126, P<0.0001).

d. Representative NDNF calcium activity trace during CFC. Pre-stimuli it correlates positively with freezing (r=0.183, P=0.045), during conditioning it is neutral (ns) to then transition to a more negative state during post-conditioning (r=-0.313, P=0.0005).

Similar ensemble states could be detected during odour-induced fear experiments (**Fig. 10a and b**). Z-scored activities of longitudinally registered cells showed the presence of two ensembles. One ensemble of cells that had negative z scores during habituation and showed an increase in activity during TMT exposure (**Fig. 10a and b** (top)). A second ensemble of cells that had positive z scores during habituation and showed a decrease in activity during TMT exposure (**Fig. 10a and b** (bottom)). Within these ensembles, similarly to CFC, some cells correlated positively with freezing (**Fig. 10c**) behavior and others negatively (**Fig. 10d**). Cells whose activity could be detected exclusively during either habituation or during TMT exposure remained largely neutral and did not correlate with freezing behavior (**Fig. 10e and f**), suggesting a lack of selectivity between either state. Taken together, these data show the presence of two functionally different ensembles that may work cooperatively to regulate both conditioned and innate fear behaviors.

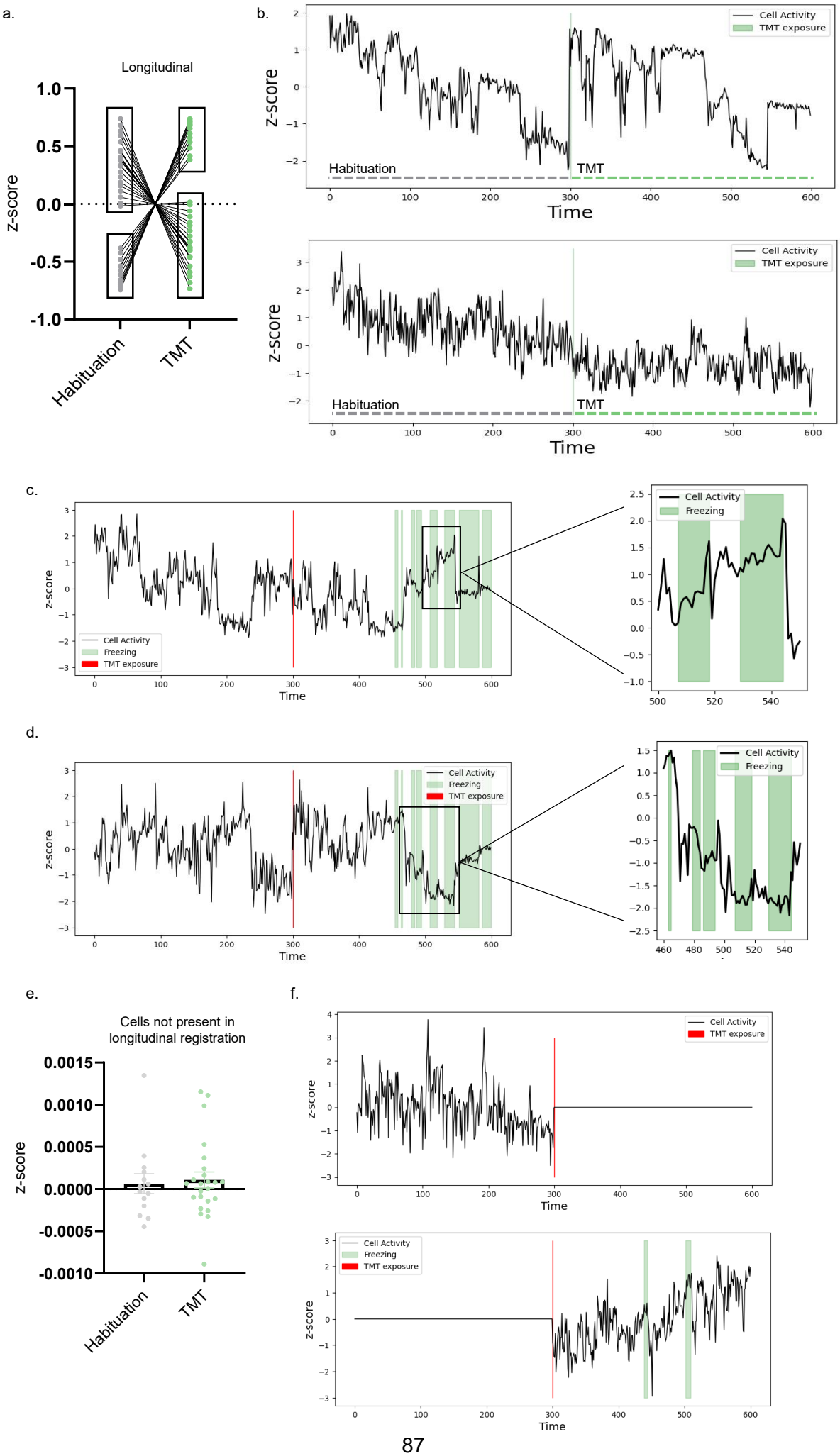
a.
Longitudinal
z-score
Habituation
TMT
b.
Cell Activity
TMT exposure
z-score
Habituation
TMT
Time
c.
Cell Activity
Freezing
TMT exposure
z-score
Time
d.
e.
Cells not present in longitudinal registration
z-score
Habituation
TMT
f.

Figure. 10 Deep brain Ca^{2+} imaging reveals two functionally distinct ensembles of NDNF neurons in BLA during innate threat behavior.

a. Averaged z-score activity of longitudinal registered NDNF cells during innate threat behavior reveals calcium activity switch between habituation and TMT exposure.

b. Representative z-score calcium activity trace showing activity change from negative cell state during habituation (grey) to positive cell state during TMT exposure (green) time (up panel). Representative z-score calcium activity trace showing activity change from positive cell state during habituation to negative cell state during TMT exposure time (bottom panel).

c. Representative z-score calcium activity trace showing increased activity during freezing behavior (green). Green bars represent freezing episodes and in right box the zoomed in calcium activity.

d. Representative z-score calcium activity trace showing decreased activity during freezing behavior (green). Green bars represent freezing episodes and in right box the zoomed in calcium activity.

e-f Averaged z-score activity of cells that are not present during longitudinal registration and are only active during either habituation or TMT exposure time (e). Representative z-score calcium activity trace showing NDNF cell active only during habituation (up panel), or during TMT exposure (bottom panel), (f).

2.1.3.7 BLA^{Ndnf} neurons receive inputs from brain regions associated with fear responses

To understand whether the behavior that NDNF INs mediate in the BLA might be influenced by the synaptic inputs that they receive, we employed brain wide monosynaptic rabies tracing. First, we unilaterally injected the helper virus AAV2/5-synP-DIO-sTpEpB-GFP into the BLA of Ndnf-ires-cre-ERT2 animals and 5 weeks later we injected an RV-N2C dG-mCherry virus into the same location (**Fig. 11a**). With this viral strategy, NDNF INs were labelled with GFP (green), cells that send inputs to NDNF INs were labelled with mCherry (red), and NDNF INs that receive these inputs (starter cells) appeared yellow (**Fig. 11b**). The majority of GFP$^+$ NDNF INs were located in the lateral amygdalar nucleus (LA) (43 ± 9%) and posterior BLA (BLAp, 51.5 ± 14.5%) (N=2 mice, **Fig. 11c**). GFP$^+$/mCherry$^+$ starter cells were evenly distributed between LA, anterior BLA (BLAa) and BLAp (18.2 ± 4%, 24.2 ± 8%, 27.2 ± 18%, respectively) (**Fig. 11d**). This variance could in part be due to differences in targeting injection sites during rabies injection. Interestingly, many of the monosynaptic mCherry$^+$ input cells that NDNF INs receive come from local regions, including the BLA itself, the piriform-amygdalar area, and the dorsal endopiriform nucleus. Fewer inputs were found coming from regions further away including the paraventricular nucleus of the thalamus and temporal association areas (layer 2/3). Major inputs were also present from regions such as the caudoputamen (CP) and the cortical amygdala area (plCoA) (**Fig. 11e and f**). The cortical amygdala area has long been studied for its involvement in innate olfactory valence, as it is one of the primary regions capable of mediating innate attraction or aversion to odors[66].Taken together, these data demonstrate that monosynaptic inputs to BLA^{Ndnf} neurons mostly come from local BLA neurons, however some long-range inputs exist.

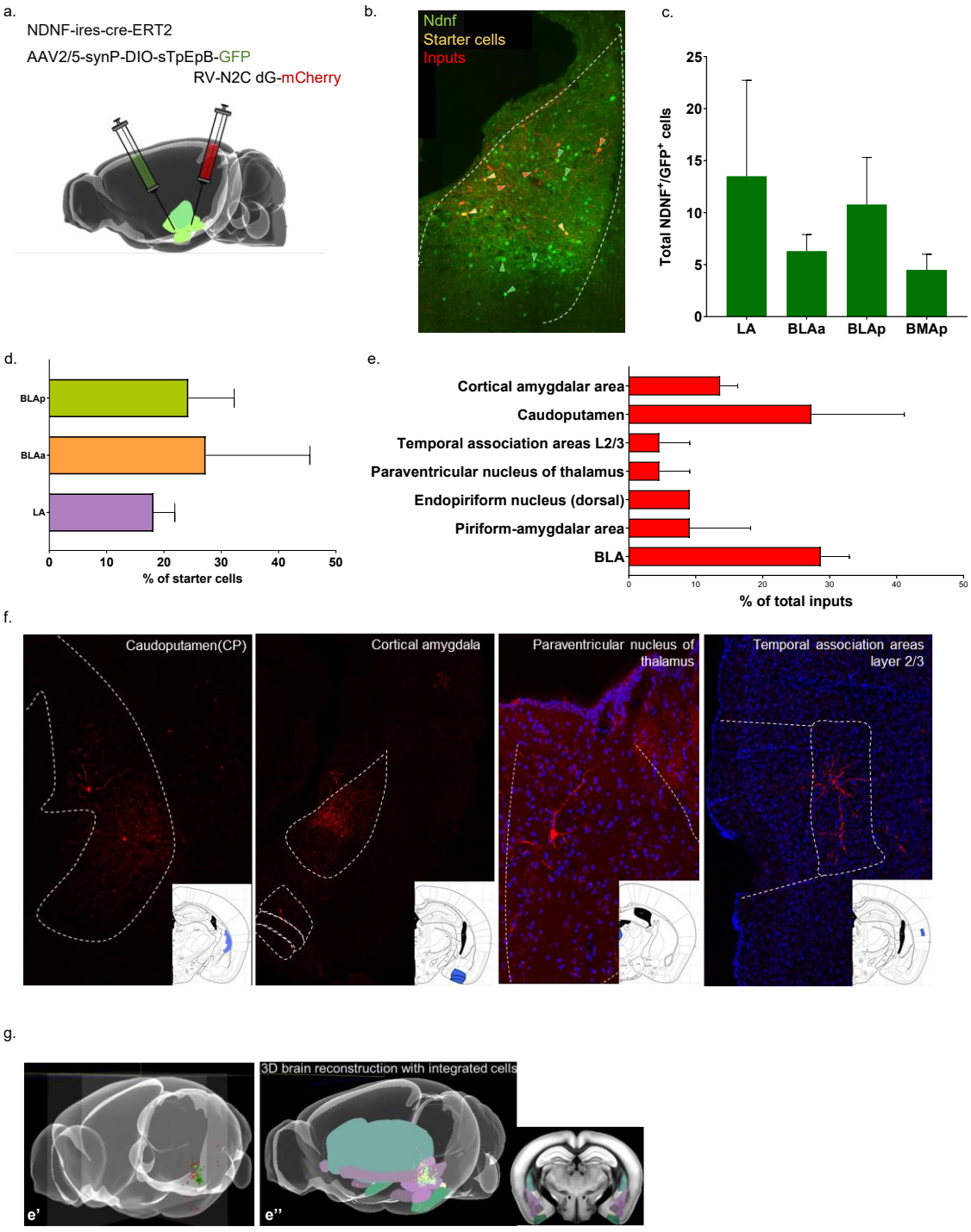
a.
NDNF-ires-cre-ERT2
AAV2/5-synP-DIO-sTpEpB-GFP
RV-N2C dG-mCherry
b.
Ndnf
Starter cells
Inputs
c.
Total NDNF+/GFP+ cells
25
20
15
10
5
0
LA
BLAa
BLAp
BMAp
d.
BLAp
BLAa
LA
0
10
20
30
40
50
% of starter cells
e.
Cortical amygdalar area
Caudoputamen
Temporal association areas L2/3
Paraventricular nucleus of thalamus
Endopiriform nucleus (dorsal)
Piriform-amygdalar area
BLA
0
10
20
30
40
50
% of total inputs
f.
Caudoputamen(CP)
Cortical amygdala
Paraventricular nucleus of thalamus
Temporal association areas layer 2/3
g.
3D brain reconstruction with integrated cells
e'
e''

Figure 11. BLA^{Ndnf} neurons receive inputs from brain regions associated with fear responses processing.

a. Scheme representing the combination of AAV2/5-synP-DIO-sTpEpB-GFP (helper virus) and RV-N2C-dG-mCherry (rabies virus) viruses injected unilaterally into the BLA (in green) of NDNF-Cre mice.

b. Representative image showing NDNF cells (green arrows) targeted by the helper virus, inputs cells targeted by the rabies virus (red arrows) and in yellow is the overlap between the two (starter cells, yellow arrows).

c. Percentage of total NDNF^{+}/GFP^{+} cells (n=2 mice), shows NDNF neuron localization distributed in the LA, BLAa, BLAp and BMAp.

d. Percentage of starter cells (%) localized in LA, BLAa and BLAp.

e. Main input regions projecting to NDNF neurons in the BLA, coming from BLA, piriform-amygdalar area, endopiriform nucleus (dorsal part), paraventricular nucleus of thalamus, temporal association areas L2/3, caudoputamen, cortical amygdala area.

f. Representative images showing input regions.

g. 3D brain reconstruction of inputs (red dots), NDNF cells (green dots) and starter cells (yellow dots) (e'). 3D brain reconstruction of all areas from which NDNF neurons receive inputs from with integrated cells (e'').

2.1.4 Discussion

In this report we have described a previously poorly understood BLA-IN population, shedding light on their functional role in BLA-related behaviors. Using a combination of c-Fos staining, optogenetics and *in vivo* calcium imaging in freely behaving Ndnf-cre mice, we found that BLA^{Ndnf} neurons represent a distinct population within the BLA, exerting unique modulatory effects during both fear acquisition and expression of innate fear behaviors. Specifically, BLA^{Ndnf} neurons are activated by aversive stimuli, such as foot shocks, and optogenetic inhibition revealed their role in promoting fear expression. Interestingly, *in vivo* calcium experiments identified two functionally different ensembles that display opposing activities in response to aversive stimuli.

The BLA has recently been the focus of investigation in single nucleus RNA-seq and multiplex *in situ* hybridization (mFISH) studies[13, 107, 108, 109], which revealed transcriptomic heterogeneity[108] with functionally and spatially defined subpopulations segregating differently in lateral and basal amygdala[13]. These studies also showed the presence of a subpopulation of Ndnf/Lamp5/Reln-expressing neurons within the BLA GABAergic clusters. Our RNA-FISH data revealed that 93.5 ± 3.3% of Ndnf^{+} cells co-localize with Gad1 (Fig. 1b) confirming the GABAergic nature of Ndnf^{+} cells in the BLA, in line with data reported in both neocortex and hippocampus[35,39,102]. Moreover, our data show that Ndnf^{+} cells highly express Reln and Npy (Fig. 1c and d) and do not overlap with other interneuron neurochemical markers such as Sst and Pvalb (Fig. 2c and d). These data are in line with findings from a recent study[36] which confirmed that BLA^{Ndnf} neurons co-express with both Reln and Npy, both of which are known to be expressed by NDNF INs in L1 of the cortex, showing no overlap with major IN classes[35,36,110]. Our data confirm the NGF identity of Ndnf^{+} cells and further reveal that they belong to the Reln/Lamp5 subclass, as they exhibit high Lamp5 expression (Fig. 1c).

Having confirmed and further characterized Ndnf marker-expression patterns in BLA, we sought to characterize BLA^{Ndnf} neuron activity dynamics in anxiety and fear related behaviors. Emotions, especially fear, are regulated by a complex neural circuitry involving various brain regions, including the amygdala, mPFC, EC, BNST, and hippocampus[96,49]. The BLA, central to these processes, integrates positive and negative stimuli where distinct neural ensembles respond to aversive or rewarding experiences, contributing to an animal's ability to appropriately evaluate and react to threats[59,58,13,100]. Our functional analysis is the first to suggest a role of BLA^{Ndnf} neurons in regulating fear acquisition. We find that BLA^{Ndnf} neurons are significantly activated

by foot shocks during the fear acquisition phase (day 1) but show no significant activation during fear recall (no shocks, day 2), raising the possibility that NDNF INs are primarily involved in the initial encoding of fear rather than in the retrieval of fear memories (Fig. 3c). This distinction emphasizes the potential function of BLA^{Ndnf} neurons in adapting an animal's behavior to immediate threats rather than recalling previously learned fear responses. Moreover, this aligns with findings from single-cell RNA-seq studies[107], which reveal that several interneuron types respond to learning and recall of fear memories following exposure to a tone-cued fear conditioning paradigm. Authors performed single cell RNA-seq sampling at 2h, 8h, 24h after conditioning and during a recall period characterized by the absence of footshocks. Among these IN types the authors included two BLA-$Reln^+$ populations: $Reln^+/Ndnf^+$ and $Reln^+/Crim1^+$. Specifically, they found that gene expression in the $Reln^+/Ndnf^+$ population correlated strongly with CFC-activated learning genes, with elevated expression levels at both 8h and 24h post-conditioning[107]. These results further suggest a specialized function of BLA^{Ndnf} neurons, where their activity and gene expression are tuned to facilitate initial encoding of fear behaviours.

Our study builds upon previous research that focused on other GABAergic INs, such as VIP, PV and SOM neurons, each of which has been shown to play distinct roles in associative fear learning and memory formation[35,101, 111] .Here, optogenetic manipulations targeting BLA^{Ndnf} neurons during a CFC paradigm[62] revealed that NDNF inhibition was sufficient to significantly reduce freezing behavior during fear acquisition, (Fig. 5e) suggesting that NDNF INs activity promotes fear expression during conditioning. Notably, PV-INs exhibit similar activity, promoting fear acquisition by disinhibiting PNs that are responsible for encoding fear[35,60,111]. It is known that $Ndnf^+$ neurons generate slow postsynaptic suppression on PNs axons[36,9], we could therefore speculate that inhibition of NDNF INs might contribute to disinhibition of PNs during fear acquisition, placing BLA^{Ndnf} neurons in an intricate inhibitory BLA microcircuit modulating fear responses together with other major IN classes. Furthermore, photoinhibition of BLA^{Ndnf} neurons during recall results in all animals retaining the memory of the aversive context experienced during fear acquisition (Fig. 5l), suggesting that NDNF INs are not involved in fear memory recall. This stands in contrast to the BLA's established role in memory recall and consolidation, suggesting that NDNF INs are unlikely to be part of the BLA's engram populations[100,112] . Further investigations that explore the effects of photoinhibition on both fear acquisition and recall might be necessary to further support the conclusion that NDNF INs are essential for the expression of fear but not memory recall, as based on our current data inhibiting

NDNF INs on both days would lead to a reduction in fear expression during acquisition, but preserve the animal's ability to recall the fear memory during recall.

While classical interneuron populations in the BLA have been extensively studied in the context of Pavlovian fear conditioning, their roles in mediating innate fear responses to predator odors remain poorly understood. Here, we show that photoinhibition of NDNF INs while animals were exposed to the predator odour, TMT, significantly reduced freezing behavior. This suppression suggests that NDNF INs neurons play a role in adapting animal's survival responses in the presence of innate threats. These findings align with the BLA's role in integrating innate olfactory responses to predators and emphasise the need for further research into how individual interneurons contribute to these behaviors. Interestingly, our data show that NDNF neurons selectively modulate freezing when presented with a salient stimulus as opposed to general anxiety-like behaviors, as shown by a stability in rearing behaviors (Fig. 6h). Whereas, in the absence of a salient stimulus (eg. foot shock or TMT), inhibition of BLA^{Ndnf} neurons during OF and EPM tests, promotes exploratory activity and reduces anxiety-like behavior, respectively. Typically, inhibitory activity of INs targeting specific PNs that project to the CeL is associated with suppression of anxiety-like states, while inhibition of the BLA-CeL pathway tends to increase such responses[113,114]. Thus, our finding that NDNF inhibition reduces anxiety-like behaviors may stem from the microcircuits they establish with specific PNs that do not preferentially connect to CeL neurons known to suppress anxiety. Further research is essential to explore these microcircuits in greater detail.

The optogenetic experiments are supported by *in vivo* calcium imaging data, indicating that BLA^{Ndnf} neurons differentially modulate aversive behaviors based on stimulus saliency. Specifically, our data show that NDNF INs activity patterns segregate depending on the animal's transitions between freezing and non-freezing states. BLA^{Ndnf} neurons recruited into the freezing ensemble displayed decreased activity during fear acquisition (Fig. 7h, dark orange column), whereas other cells remained highly active during freezing episodes (Fig. 7h, light orange column). The non-freezing ensemble showed consistent activity patterns across both days, with reduced variability compared to the freezing ensemble (Fig. 7i). However, during fear recall, NDNF neurons displayed higher activity levels during freezing, with a significant increase in comparison to less-active cells (Fig. 7h, blue columns). This aligns with our findings that in the absence of photoinhibition during recall mice freeze more as expected (Fig. 5e)

These calcium imaging data reveal two distinct functional ensembles within the NDNF INs population: a “freezing-on” group, where NDNF INs remain active during freezing episodes and a “freezing-off” group, where NDNF INs decrease activity during freezing and may become more active during non-freezing states. Additionally, longitudinal registration to identify the same NDNF cells over days, revealed that cells showing increased activity during “pre-stimuli” or “recall” phases exhibited decreased activity during conditioning (day 1) and during anticipation of a stimulus on day 2. Conversely, another subset displayed an opposite pattern, with increased activity during conditioning and stimulus expectation but decreased activity during pre-stimuli or recall (Fig. 8a and b).

How could these findings align with our optogenetic experiments? Recent studies have identified BLA PNs with opposing roles in fear learning and freezing. Rspo2^{+} PNs promote fear conditioning and freezing, whereas Lypd1^{+} PNs promote appetitive behavior and reduce freezing after fear learning[13]. Assuming that NDNF INs directly inhibit these PN subpopulations, freezing-on neurons would primarily inhibit Lypd1^{+} appetitive neurons, because inhibition of these PNs would favour freezing. During non-freezing episodes, the freezing-on neurons would be silent and allow Lypd1^{+} appetitive neurons to be active. Freezing-off NDNF INs would primarily inhibit Rspo2^{+} anxiogenic neurons, because during freezing the freezing-off neurons would be silent and allow Rspo2^{+} PNs to be active and promote freezing. During non-freezing episodes, the freezing-off neurons would be active and inhibition of these PNs would favour non-freezing. For the first time, our study suggests the presence of two functionally distinct BLA^{Ndnf} neuron populations that modulate freezing behaviors differentially in response to threat. Future studies should aim to disentangle these functional differences by specifically targeting each ensemble during aversive behaviors. Previous research has identified two types of NDNF INs in cortical L1: NDNF^{+}/NPY^{+} (NGF cells) and NDNF^{+}/NPY^{-} (canopy cells), each with unique molecular, morphological, and electrophysiological properties[110]. Based on our HCR dataset, approximately 80% of Ndnf cells in the BLA express Npy (Fig. 1f), suggesting that the remaining 20% may correspond to Ndnf^{+}/Npy^{-} cells. This observation leads us to speculate that the differential activity patterns seen in our calcium imaging data may be influenced by both NDNF^{+}/NPY^{+} and NDNF^{+}/NPY^{-} cells. Future research using an intersectional genetic approach (for example crossing Ndnf-cre mice to a Npy-hrGFP line[115]) could allow specific optogenetic manipulation of these two populations independently, enabling a deeper understanding of their distinct roles in aversive behaviors[116].

Our observations align with the notion that IN responses in the BLA vary depending on the stimuli they receive, modulating PNs responses in distinct ways[19]. Specifically, it has been shown that BLA-PNs projecting to the mPFC can influence either fear expression or extinction depending on whether INs are activated or inhibited during fear-related behaviors[19]. Given that disinhibition is considered an important mechanism for fear learning in BLA[35,117], we can further speculate that the NDNF INs activities observed in our calcium data may represent a disinhibitory mechanism of "fear-extinction" BLA-PNs, thereby reducing freezing behavior. Thus, further research is needed to better understand how photoinhibition of NDNF INs may disrupt IN-PNs interactions in the BLA, leading to reduced freezing behavior.

Correlation analysis revealed that when the stimulus is less salient (i.e. during pre-stimuli), one subset of NDNF INs shows positively correlated activity. However, under high-salience conditions (i.e. during foot shocks), a different subset of NDNF INs becomes active, exhibiting positive correlation specifically during conditioning. This suggests that separate groups of NDNF INs are selectively recruited based on the salience of the stimulus. Notably, the same neural activities were observed in odour-induced fear experiments. Similar findings were observed in cortical L1, where NDNF INs are specifically activated when a sensory stimulus becomes relevant to the animal and are suppressed in less salient conditions[35]. Dual-opsin optogenetic experiments will be essential to further clarify whether NDNF ensembles are actively involved in both suppressing and activating freezing responses during CFC or predator odours-related behaviors.

To further investigate how NDNF INs modulate fear expression, we focused on dissecting the macrocircuits they form with other brain regions. It is known that the BLA receives major inputs from areas coordinating fear behaviors, such as mPFC, EC, hippocampus, auditory and insular cortices and BNST[49]. Interestingly, our rabies tracing data revealed that NDNF INs receive major inputs from the CP and CoA (Fig. 11e and f). The cortical amygdala has been extensively studied for its role in innate olfactory valence and mediates natural attraction or aversion to specific odours[66], whereas the CP processes learned safety signals, adjusting threat responses based on past experiences[118,119]. Inputs from the plCoA are thought to be of glutamatergic nature as it has been shown that glutamatergic plCoA neurons send direct projections to BLA, NAc, BNST and MeA and encode for different odour stimuli[66]. Moreover, mice with chronically implanted electrodes in the CP were tested during safety conditioning and they observed an increase in the slope and amplitude of CS-evoked field potentials. This study shows how CP actively processes learned safety signals,

modulating threat responses based on learned experiences, allowing the animal to appropriately adjust its fear response when the threat is no longer present (i.e. after learning that a previously feared cue is safe)[118,119]. Therefore, our results add important work suggesting that CoA → BLA^{Ndnf} and CP → BLA^{Ndnf} pathways may regulate NDNF INs, enabling appropriate responses to either conditioned or innate aversive stimuli. Future studies involving optogenetic *in vivo* manipulations will be essential in uncovering the specific roles these inputs play in regulating fear-related behaviors.

In conclusion, this study presents, for the first time, a combined anatomical, behavioral, and functional characterization of BLA^{Ndnf} neurons. Our findings reveal that a subpopulation of NDNF INs is recruited during fear acquisition and TMT exposure, driving freezing behaviors. This response may rely on the disinhibitory actions of BLA^{Ndnf} neurons, which modulate specific PN projecting neurons. Additionally, NDNF INs display opposing shifts in activity in response to variations in stimulus salience, potentially regulated by downstream brain regions. This suggests that two molecularly distinct BLA^{Ndnf} ensembles may contribute to these response dynamics. Future research should aim to further elucidate these circuits, understanding how NDNF INs interact with other BLA INs to maintain a balanced E/I ratio and what occurs when this balance is disrupted. Such investigations could provide deeper insights into how BLA hyperexcitability in fear-related states contributes to the pathological mechanisms underlying disorders like anxiety and PTSD.

2.1.5 Materials and Methods

Animals

Experiments were performed in adult mice (> 8 weeks). The wild-type animals were from the C57BL/6NRj strain (Janvier Labs - http://www.janvier-labs.com). Ndnf-ires-cre-ERT2 (B6(Cg)-Ndnftm1.1(cre/ERT2)Ispgl/J) mice were acquired from the Jackson Laboratory (RRID: IMSR_JAX:034875)[35]. Td-Tomato Rosa26R mouse lines[120] were previously described using the Ai9lsl-tdTomato[B6.Cg-Gt(ROSA)26SorTM9.CAG-tdTomato/Hze/J][121,122].The transgenic Ndnf-IRES-CreERT2 mouse line was kept by backcrossing heterozygous transgenic mice with wild-type C57BL/6NRj mice (Janvier Labs). Animals used for optogenetic experiments and calcium imaging were handled and housed on a 12 h inverted light cycle for at least one week before the experiments. Mice had access to ad libitum food at all times. All behavioural tests were conducted during the dark phase of the cycle. Both male and female mice were used and all the experiments were performed following regulations from the government of Upper Bavaria.

Viral constructs

The following AAV viruses were purchased from Addgene: AAV-EF1a-double floxed-hChR2(H134R)-eYFP, AAV-hSyn-DIO-GFP, AAV-DIO-GCaMP7s-eYFP. The following were obtained from the University of North Carolina Vector Core (https://www.med.unc.edu/genetherapy/vectorcore): AAV-EFIa-DIO-eNpHR3.0-mCherry, AAV-EF1a-DIO-mCherry, AAV2/5-synP-DIO-sTpEpB-GFP. Rabies virus N2C-dG-mCherry (EnvA) was provided by Prof. Dr. Karl-Klaus Conzelmann (Gene Center - Max von Pettenkofer-Institute of Virology, Ludwig-Maximilians-Universität München).

In situ Hybridization Chain Reaction (HCR), tissue preparation

HCR RNA-FISH experiments, were performed using adult wild-type mice (≥8 weeks) of the C57BL/6NRj strain (Janvier Labs). After transcardial perfusion and post-fixation, brains were cryoprotected. Cryoprotection was achieved as follows: brains were submerged in a 10% sucrose (w/v) in RNAse-free DPBS, w/o MgCl2 and CaCl2, solution on a rotator at 4°C for ≥18 hours. Following this step, the same process was repeated with a 20% sucrose in DPBS (w/v) solution and with a 30% sucrose (w/v) solution. After cutting off the cerebellum, the cryoprotected brain tissue was oriented for coronal sectioning (Bregma -1.1 to -2.4) and embedded in a cryomold filled with O.C.T. The block was transferred onto dry ice. The block was placed onto a specimen

chuck and acclimated to -20°C for approx. 20 minutes inside the cryostat (CryoStar™ NX70). 20 µm-thick coronal sections were picked up with Superfrost® Plus slides and were ready for HCR™.

HCR-FISH Multiplexed, Quantitative, High-Resolution RNA Imaging

On the first day of the HCR protocol[104], the slices were post-fixed with 4% PFA (stock, 16% Formaldehyde sol. w/v, Thermo Fisher Scientific) in 1x DPBS (w/o MgCl2 and CaCl2, Sigma-Aldrich) for 15 min. at 4°C. The slides were moved into RNase-free 50%, 70%, and 100% ethanol (Ethanol absolute 99,8%, Sigma Aldrich) in distilled, RNase-free water for 5 minutes each at RT. This was followed by a final dehydration step in fresh 100% ethanol for 5 minutes. The slides were immersed twice in fresh, 1x DPBS at RT. Finally, the slices were carefully dried with a Kimwipe and the slice perimeter was traced 2-4 times with an Immedge® hydrophobic barrier pen to keep all reagents within this perimeter. Meanwhile, 150 µL per slide of 30% Probe Hybridization Buffer (HB; 30% formamide) and a humidified chamber were warmed to 37°C. Following the wash, the slices were incubated at RT in an RT-HB for 10 minutes. After this incubation, the excess HB was carefully removed with a Kimwipe. Finally, three pairs of probes of each probe set were added to the pre-warmed 30% HB from a stock concentration of [1 µM] for a working concentration of [16 nM]. The samples were covered with a coverslip and incubated at 37°C overnight in the humidified chamber. The following probes were purchased from Molecular Instruments: Cck – B1, Gad1– B2, Lamp5 – B1, Ndnf– B3 and B4, Npy – B1, Pvalb – B3, Reln – B2, Slc17a7 – B1, Sst – B1.

On the second day, the wash buffer (WB; 30% formamide) was preheated to 37°C in a water bath. After 10 minutes, the slices were briefly immersed in the warm wash buffer to float off the coverslip. Next, the probes were removed by soaking the slides in warm 75%/25%, 50%/50%, and 25%/75% of WB/5x SSCT, respectively, for 15 minutes each at 37°C. This was followed by a final 15-minute wash in 100% 5X SSCT at 37°C. The slides were then immersed in 5X SSCT for 5 minutes at RT. Afterward, the corresponding hairpins from a stock [c] of 3 µM for a working [c] of 60 nM, were placed separately into PCR tubes, to prevent h1 and h2 from interacting with each other before amplification. These were then heated in a Thermocycler at 95°C for 90 seconds and then snap-cooled for 30 minutes in the dark at RT. During this waiting period, the slides were dried with a Kimwipe, and 200 µL of amplification buffer was added on top of the samples, pre-amplifying them in a humidified chamber for 30 minutes at RT. After the waiting period, the snap-cooled hairpins were added together

into 150 µL per slide of warm amplification buffer, added on top of each sample, and covered with a coverslip. This was incubated overnight in a dark, humidified chamber at RT. Following this incubation, the sections were washed with fresh 5x SSCT twice for 30 minutes and once for 5 minutes. Directly after the wash, the slides were carefully dried with a Kimwipe. Hairpins were purchased from Molecular Instruments: B1-488nm, -647nm. B2-488 nm. B3 -546 nm, -647nm. B4- 488nm, -546 nm and -647nm. Finally, 1 drop of ProLong™ Diamond Antifade Mountant with NucBlue (DAPI) was added on top of each slice. The slices were covered with a coverslip and left to cure in the dark at RT for ≥ 2 hours. Amplification, hybridization and wash buffers were purchased from Molecular Instruments.

Stereotaxic surgeries

Mice were anesthetized using 1.5% isoflurane (Cp-pharma, Germany) and placed in a stereotaxic frame (model 1900, Kopf Instruments). Body temperature was maintained at 37°C using a heating pad. Carprofen (Rimadyl – Zoetis), (5 mg/kg body weight) was given via subcutaneous injection. Mice were bilaterally (unilaterally only for calcium imaging experiments and monosynaptic tracings) injected using glass pipettes (#708707, BLAUBRAND intraMARK) with 0.4µl of virus in the BLA by using the following coordinates calculated with respect to the bregma: -1.55 mm anteroposterior (AP), ±3.2 mm medial-lateral (ML), and −4.6 mm dorso-ventral (DV). After the injection, the pipette remained in the brain for 5 min to allow for the virus to spread in BLA and after surgery mice recovered in the home cage at a warm temperature. Virus was allowed to be expressed for a minimum duration of 3 weeks before histology or behavioural paradigms. For animals not undergoing implant surgery, the wound was closed with Vetbond (3M, USA).

Optic fiber implants

Mice used in optogenetic experiments were implanted with optic fibers (200-µm core, 0.50 NA, 1.25-mm ferrule - Thorlabs) above the BLA (−4.4 mm ventral from bregma) immediately after viral injection. The skull was first protected with a layer of histo-glue (Histoacryl, Braun), the optic-fibers were then fixed to the skull using UV light-curable glue (Loctite AA3491 - Henkel), and the exposed skull was covered with dental acrylic (Paladur - Heraeus).

GRIN lens implantation and baseplate fixation

Three weeks after GCaMP7s viral injection in the BLA, mice were implanted with a gradient index (GRIN) lens. At the same coordinates of the optic fibers implants, a small craniotomy was made and a 20G needle was slowly lowered into the brain to clear the path for the lens to a depth of -4.2 mm from bregma. After retraction of the needle, a GRIN lens (ProView lens; diameter, 0.5 mm; length, ~8.4 mm, Inscopix) was slowly implanted above the BLA and then fixed to the skull using UV light-curable glue (Loctite AA3491 - Henkel). The skull was first protected with histo glue (Histoacryl, Braun), and the implant fixed with dental acrylic (Paladur - Heraeus). 4 to 8 weeks after GRIN lens implantation, a baseplate was positioned above the GRIN lens. Briefly mice were placed in the stereotaxic setup and anesthetised, the baseplate (BPL-2; Inscopix) was positioned above the GRIN lens, adjusting the distance and the focal plane until neurons expressing GCaMP7s were visible. The baseplate was fixed using C&B Metabond (Parkell). A baseplate cap (BCP-2, Inscopix) was left in place to protect the lens.

Tamoxifen

Tamoxifen (solid) was prepared by dissolving 20mg tamoxifen in 100% ethanol to obtain a final concentration of 40 mg/ml. The solution was then diluted 1:1 with Kolliphor ® EL (Sigma). Heating and stirring the mixture allows for the ethanol to evaporate. After that, 100 µl aliquots were frozen until use. Before use, the stock solution was diluted with PBS to the desired concentration and the pH value of 7.4 was confirmed. Mice were injected with approximately 200 µl of tamoxifen solution (200 mg per kilogram of body weight) for three days every other day. The mice that underwent brain viral injection received the first injection the day after surgery.

Behavior paradigms

All mice were handled for a period of 4 days prior behavioral experiments. For optogenetic experiments mice were tethered to the optic-fiber patch cords (Plexon Inc) and habituated to them in a context different from the ones used during behaviors as all behavioral tests required novelty to the context for 10 to 15 minutes daily over 4 days. For calcium imaging experiments, the mini-scope and cable (Inscopix) were fixed on the head of mice and habituated to it in a context different from the ones used during behaviors for 15 minutes daily. The behavior arenas were housed inside a soundproof chamber equipped with houselights and video cameras (c920 webcam, Logitech).

Optogenetic manipulations

Mice were bilaterally attached to optic-fiber patch cords (Plexon Inc) connected to a 465-nm LED (for ChR2, photoactivation) via Optogenetic LED module (Plexon Inc) and mating sleeve (Thorlabs). Photostimulation was performed using 10 ms, 463-nm light pulses at 20 Hz and 10 mW. Photoinhibition was performed using a 620-nm LED light (eNpHR3.0-mCherry) constantly at 10 mW. The LED was triggered, and pulses were controlled via PlexBright 4 Channel Optogenetic Controller and with Radiant Software (Plexon Inc).

Open Field (OF) test

Mice with optic fiber patch cords were tethered and allowed to explore a square arena (40 cm × 40 cm × 25 cm) for 10 minutes. The photostimulation or photoinhibition was delivered for the entirety of the test. The spatial location and the movement of the mice were recorded and analysed using video tracking software Ethovision XT16 (Noldus Information Technologies).

Elevated plus maze (EPM) test

The EPM test was performed in a plus-shaped arena, made of two open arms (35 cm length each) and two closed arms (35 cm length each) with walls (15 cm high), 5 cm wide and extended from a central platform (5 × 5 cm) to allow mice to freely move across the arms of the setup. The maze is elevated 45 cm from the floor. Mice with optic fiber patch cords tethered were placed in the central zone with their heads toward the closed arm and were able to freely explore the arena for 10 minutes. The photoinhibition strategy was the same as in the OF test. The behavior of the mice was recorded with video cameras (c920 webcam, Logitech). Ethovision XT16 software (Noldus Information Technologies) was used to analyse behavioral parameters.

Contextual fear conditioning (CFC)

This paradigm was modified from a previous study [123]. On the first day of the experiment (fear acquisition, day 1), mice were introduced to the contextual fear conditioning chamber (Med Associates) 25 x 15 x 25 cm, with a grid floor from which they received three consecutive footshocks (2s each, 1.1mA) at 120, 180 and 240 seconds with 60-second intervals during a 360-second session. During day 1 all mice were bilaterally connected to optic fiber cables while photoinhibition was delivered at constant light of 620 nm (10 mW). On the following day (fear recall, day 2), mice were connected to optic fiber patch cables and placed in the fear conditioning chamber for 360s, and neither footshocks nor LED light was delivered. Freezing behavior, defined

as complete immobility at exception of breathing, was used as a proxy of fear response. Freezing was automatically quantified using the software ANYmaze 7.2 (Stoelting) as described previously[124]. Briefly, the software calculated a “freezing score” depending on the number of pixel changes between frames. If the freezing score lasted longer than 2 s, mice were considered to be freezing. Freezing behavior during recall was verified in the same way. We manually verified when resting was mistakenly counted as freezing behaviour. Animals were excluded from testing if they were able to jump out of the arena and no tests could be carried out further.

Predator odour fear conditioning

Mice were introduced into a custom-made Plexiglas arena (20 x 20 x 40 cm) modified with a lid to help concentrate the 2,3,5-trimethyl-3-thiazoline (TMT, Sigma-Aldrich) within the space, while ensuring that the optic fibers, connected to a rotary module above the arena, could move freely with the animal. A sliding door (15 x 15 cm) on the side of the apparatus allowed for TMT exposure without disturbing the mouse. The test began with a 5-minute "habituation" phase, during which the arena contained a piece of filter paper attached to the sliding door without odour and no photoinhibition was applied. This was followed by a 5-minute exposure period, during which 5 µL of TMT was pipetted onto the filter paper through the sliding door and photoinhibition was delivered at constant light of 620 nm (10 mW). Both steps occurred in a single recording session, with a brief automatic pause in the video-tracking system between phases to prevent data contamination during the introduction of TMT. Mice were recorded from a front view (to avoid interference with optic fibers, cables and lid). Freezing and rearing were automatically quantified using the software ANYmaze 7.2 (Stoelting).

***In vivo* calcium imaging of freely moving mice**

All *in vivo* imaging experiments were conducted on freely moving mice. GCaMP7s fluorescence signals were acquired using a miniature integrated fluorescence microscope system (nVoke – Inscopix) secured in the baseplate holder before each imaging session. Settings (20Hz, Gain 5, LED power 1.1, Focus 480-510) were kept constant within subjects and across imaging sessions. Image acquisition and behavior were synchronized using the data acquisition box of the nVoke Imaging System (Inscopix) triggered by a continuous train of TTL pulses sent from the ANYmaze 7.2 (Stoelting) software. We used the IDPS (Inscopix data processing software, version 1.8.0) for the acquisition of calcium image data, rigid motion correction, automatic

selection of neuro somata as the regions of interests (ROIs), and extraction of raw calcium traces.

Data analysis of multiplexed FISH

Images were analysed with Halo® (Indica Labs, version 3.6.4134) image analysis software with an added FISH-IF plug-in. This plug-in provided the total cell population, measured signal intensity, and assessed the colocalization of DAPI with multiple mRNA probes. Confocal images in lif format (Leica Image File) were imported into the Halo "studies" menu, where the BLA was manually delineated based on cytoarchitecture and co-localization of different probes was automatically analysed with visual and manual inspection when automatic detection was inaccurate.

Monosynaptic rabies tracings analysis

After transcardial perfusion and post-fixation, brains were sliced (50µm) using a Vibratome (VT1000S, Leica). All sections were then imaged and each image was processed using the HERBS (Histological E-data Registration in rodent Brain Spaces) software, as described previously[125]. Briefly, all slices were aligned to the Allen Mouse Brain Atlas and we obtained individual cell counts by colour coding starter cells (yellow), input cells (red), NDNF cells in green. For each cell counted, an automatic annotation of cellular location within the brain section was generated by HERBS and post-hoc analysed using Excel 2016 (Microsoft, USA).

Histology

Mice were anesthetized with ketamine/xylazine solution (Medistar and Serumwerk) (100 mg/kg and 16 mg/kg, respectively) and transcardially perfused with ice-cold phosphate-buffered saline (PBS), followed by 4% paraformaldehyde (PFA) (1004005, Merck) (w/v) in PBS. Brains were extracted and post-fixed overnight in 4% PFA in PBS at 4°C. For mice needed for FISH, the same protocol was followed, using only RNAse-free reagents. 50-100µm free-floating coronal sections were sliced using a Vibratome (VT1000S - Leica).

Immunohistochemistry

Brain sections were washed with 1xPBS $^{+}$ 0.3% Triton (Triton X-100, Carl Roth) (PBST) at RT on a shaker and blocked in 20% Normal Donkey Serum (NDS, Jackson ImmunoResearch-017-000-121) in 0.3% PBST for 2h at RT. Primary antibodies were left overnight (or weekend) at 4 °C diluted into 1% NDS $^{+}$ 0.1% PBST. Primary antibodies: goat anti-mCherry (1:1000) (Origene AB0040-200), rabbit anti-GFP-Alexa

FluorTM 488 conjugate (1:1000), (Invitrogen, A21311), rabbit anti-c-Fos (1:1000), (Cell signaling technology). Following washes with 0.3% PBST at RT, in order to remove unbound primary Ab, secondary antibodies were added in 1% NDS + 0.1% PBST and left overnight (or 4 hours) at 4 °C. Secondary antibodies: donkey anti-goat/rabbit 647/488, (1:1000) (Jackson). After washing with PBS, slices were stained for DAPI (Invitrogen™ NucBlue™ Fixed Cell ReadyProbes™ Reagent) for 15 to 20 mins at RT. Sections were then coverslipped using Daco mounting medium (Dako North America, Inc.) and borosilicate glass coverslips.

Microscopy and image processing

A Leica SP8 confocal microscope equipped with a 20×/0.75 IMM or 10x/0.30 FLUOTAR objective (Leica) was used to acquire fluorescence z-stack images. The tile scan and automated mosaic merge functions of Leica LAS X software was used. Images were minimally processed with FIJI ImageJ software (NIH) to adjust for brightness and contrast for optimal representation of the data. The same parameters were applied to all images throughout the analyses.

Statistical analysis

No statistical methods were used to pre-determine sample sizes. The numbers of samples in each group were based on those in previously published studies. Statistical analyses were performed with Prism 10.2.3 (GraphPad) and all statistics are indicated in the figure legends. Unless otherwise specified, T-tests, one-way ANOVA followed by Tukey's multiple comparison or two-way ANOVA with Bonferroni post-hoc tests were used for individual comparisons of normally distributed data. When normality was not assumed, Mann-Whitney U test was performed for individual comparisons. After the conclusion of experiments, virus-expression and implants placement were verified. Mice with very low or null virus expression were excluded from analysis.

2.2 NDNF interneurons activity is altered in a mouse model of Huntington's Disease

Manuscript 2: "**NDNF interneurons activity is altered in a mouse model of Huntington's Disease**"

Ylenia Mastrodicasa*, Sonja Blumenstock*, Dennis Feigenbutz, Irina Dudanova, Rüdiger Klein

YM, SB and RK conceptualized the study, DF performed and analysed snRNA-seq experiments, SB performed *in vivo* 2-photon experiments and analysed calcium and behavioral data, YM performed electrophysiological experiments *ex vivo*, collected and analysed whole-cell current- clamp and voltage-clamp recordings. YM and RK wrote the manuscript with the contribution of SB and DF. ID, provided support on the R6/2 mouse line, RK supervised and provided funding.

My contribution to this manuscript in detail:

For this study I designed, performed and analysed all electrophysiological experiments. I have performed stereotaxic injections of AAV9 cre-dependent GCaMP7f in the M1 of R6/2 and littermate control mice to be patched at 9 weeks of age. I performed immunohistochemistry and imaging of NDNF neurons filled with biocytin during *ex vivo* patch-clamp recordings.

NDNF interneurons activity is altered in a mouse model of Huntington's Disease

Ylenia Mastrodicasa *[1,2], Sonja Blumenstock *[1,3], Dennis Feigenbutz [1], Irina Dudanova [4], Rüdiger Klein [1,5]

[1]Department of Molecules – Signaling – Development, Max Planck Institute for Biological Intelligence, 82152 Martinsried, Germany

[2]Graduate School of Systemic Neurosciences, Ludwig-Maximilians-Universität München, 82152 Martinsried, Germany

[3]UC San Diego School of Biological Sciences Department of Neurobiology, La Jolla, USA

[4]Medical school, Center for Anatomy, University of Cologne, Cologne, Germany

[5]Lead contact

Correspondence: ruediger.klein@bi.mpg.de (R.K.)

2.2.1 Abstract

Huntington's disease (HD) is a hereditary neurodegenerative disorder resulting from the expansion of a CAG triplet repeat within the Huntingtin (HTT) gene. HD pathology is marked by progressive neurodegeneration, predominantly affecting the cortex and striatum, which manifests clinically with motor, cognitive, and psychiatric symptoms. While much research has focused on the degeneration of cortical glutamatergic pyramidal neurons and the disruption of excitation-inhibition balance in HD, the specific role of GABAergic interneurons (INs) in HD pathology and their contribution to local microcircuit disruptions remains largely unknown. In this study, we characterize the role of neuron-derived neurotrophic factor (NDNF)-positive neurons in primary motor cortex (M1) in the R6/2 mouse model of HD, providing insights into their potential impact on cortical network disruptions and disease pathophysiology. We use a combination of single-nuclei RNA sequencing (snRNA-seq) technique, head-fixed two-photon Ca^{2+} imaging and *ex vivo* patch clamp to understand how the Ndnf neuron transcriptome changes at different stages of HD progression and how this can affect both *in vivo* activity during behavior and intrinsic electrophysiological properties. Transcriptomic data reveal that expression of NDNF IN marker genes are downregulated in R6/2 mice compared to WT controls at advanced disease stages. Moreover, head-fixed two-photon calcium imaging reveals increased Ca^{2+} activity in NDNF INs at locomotion onset during a running wheel test. Patch-clamp recordings of NDNF INs in brain slices from the M1 of R6/2 mice show an increased action potential (AP) firing rate but normal synaptic transmission across different disease stages compared to littermate controls. These data suggest that NDNF INs play a role in the circuitry dysfunction seen in HD, affecting the M1 of the cortex due to their hyperexcitability and activity changes throughout HD disease progression in R6/2 mice.

2.2.2 Introduction

Huntington's disease (HD) is a severe, autosomal dominant neurodegenerative disorder for which no curative therapies currently exist [79,126, 127]. HD affects about 5-10 people per 10,000[74] with symptoms onset typically manifesting between 35 and 40 years old. Although rare, symptoms may also appear before the age of 21, a condition referred to as juvenile HD[75]. The disease is characterized by diverse clinical signs, spanning from psychiatric and cognitive symptoms, which usually are the first signs of HD disease progression[76], to involuntary movements, referred to as chorea, followed by bradykinesia, weight loss and dementia[76,80]. Typically, these symptoms are

ultimately fatal between 15 to 20 years after disease onset[76,80]. Although no effective cure is available for HD, it is known, that HD is caused by a pathological CAG triplet expansion, characterized by more than 35 repeats in the first exon of the Huntingtin gene (HTT), leading to the formation of a mutant HTT gene (mHTT)[76]. HD onset and severity are correlated with the length of CAG repeats; generally, the larger the CAG expansion, the earlier the onset of symptoms (2). The CAG repeats in mHTT lead to an expanded polyglutamine (polyQ) tract at the amino terminus of the HTT protein[76], resulting in the aggregation of mHTT, often referred to as inclusion bodies (IB)[80].

Neurodegeneration in HD patients can be predominantly noticed in two brain regions, the striatum and neocortex[128]. In the striatum, GABAergic spiny projection neurons (SPNs) are affected the most by progressive neuronal loss resulting in striatal atrophy[76]. The neocortex consists of two major neural populations: cortico-pyramidal neurons (CPNs), which make up approximately 80%, and GABAergic interneurons (INs), accounting for the remaining 20% [80, 129].Whilst studies have primarily focused on CPN degeneration, there is evidence that INs are also susceptible to neurodegeneration in HD[79], with a loss of calbindin-positive (CB^+) neurons shown in the M1 of patients predominantly suffering from motor symptoms[79,80].

Previous studies[80] done in R6/2 mice models of HD[82] demonstrated that major cortical IN populations such as somatostatin (SOM), parvalbumin (PV) and vasoactive intestinal peptide (VIP) INs undergo expression changes during the disease progression in HD model mice. Specifically, SOM and VIP INs show a loss of cell marker expression in R6/2 mice and present faster formation of IBs compared to PV-INs, which are characterized by a loss of perisomatic synaptic terminals they form with CPNs[80]. Moreover, electrophysiological studies[130,81] revealed impairments in intrinsic firing properties of INs in R6/2 mice at different stages of HD-like symptoms progression[76]. Dysfunctional activity of INs directly impacts overall activity levels of CPNs, which has been suggested as a potential cause of cortical degeneration, contributing to cortical pathogenesis in HD[81].

Considering the important roles that cortical INs play in maintaining cortical E/I balance and modulating CPN activity, disruptions to their function could possibly contribute to neural degeneration and abnormal behavioral deficits seen in HD. Despite studies available on PV-INs [131], the role that other IN populations play in HD-related cortical dysfunctions is still largely unknown. Here, we focus on neuron-derived neurotrophic factor (NDNF) neurons, a novel IN subclass recently identified in the layer 1 (L1) of the neocortex[35]. NDNF INs are known to provide top-down inhibition onto all other IN

subclasses in layer 2/3 of the cortex and modulate CPN activity synergistically with SOM-INs[73]. Moreover, NDNF protein have been shown to be important in the treatment of neurodegenerative diseases and could provide promising treatments for conditions involving neural degeneration and nerve damage[33]. However, no current available research has been conducted on NDNF INs in relation to neurodegenerative diseases, including HD.

The present study sheds light on the functional roles of NDNF INs in M1 of R6/2 mice during HD disease progression through a combination of snRNA-seq, *ex-vivo* patch clamp and chronic *in vivo* two-photon calcium recordings. We employed snRNA-seq to identify transcriptional changes in NDNF INs across HD disease stages, as this method provides high-resolution insight into molecular alterations underlying disease progression. *Ex vivo* patch clamp recordings were used to characterize intrinsic electrophysiological properties and synaptic transmission of these neurons, allowing for a detailed functional study at the cellular level. Chronic *in vivo* two-photon calcium imaging enabled monitoring of neuronal activity patterns during behavior, linking cellular changes to circuit function in awake, behaving animals. snRNA-seq studies reveal that $M1^{Ndnf}$ interneurons experience age-dependent downregulation of their marker genes, with these changes starting to occur before disease onset. Moreover, *ex vivo* patch clamp recordings reveal that $M1^{Ndnf}$ cell activity is increased in R6/2 mice compared to littermate controls, as shown by an increase in their AP firing rate and hyperexcitability. No substantial changes can be seen in their synaptic transmission across different disease stages. These findings are further supported by *in vivo* two-photon calcium experiments during a running wheel task. Here $M1^{Ndnf}$ activity is specifically increased during locomotion and at advanced ages in R6/2 mice. These results advance our understanding of M1 cortical network dynamics and behavioral changes during HD progression, suggesting a potentially important role of $M1^{Ndnf}$ neurons.

2.2.3 Results

2.2.3.1 $M1^{Ndnf}$ interneurons show downregulation of marker genes in R6/2 mice throughout HD–like disease progression

To investigate the impact of HD on cortical interneurons, we conducted longitudinal snRNA-seq studies in the M1 region of R6/2 mice across multiple time points, allowing us to compare transcriptomic changes between early and late stages of disease progression. The R6/2 mouse line expresses exon 1 of the human HTT gene and

contains about 150 CAG repeats[82]. This line is characterized by a fast progressing and aggressive disease phenotype with a short life span of only 3 to 5 months[76]. Our snRNA-seq experiments were conducted using R6/2 mice with a CAG repeat tract length of 204 ± 5.85, (Mean ± SD, N=7). Previously, scRNA-seq studies revealed that NDNF INs in the neocortex are part of the NGFC family[34], based on their expression of Reln and Lamp5[132]. This co-expression was further confirmed through in situ hybridization experiments, which revealed Ndnf enrichment in L1 of the neocortex[34, 35]. Our snRNA-seq data of nuclei from M1 of WT and R6/2 mice, were collected at three different ages: at 5 weeks, when no symptoms are present; at 8 weeks, shortly before motor symptoms onset; and at 12 weeks, when the R6/2 mice are fully symptomatic[34, 80]. Firstly, to understand the cellular composition in M1 of R6/2 mice compared to WT, we plotted a UMAP integrating datasets from both genotypes and all three time points. We found that GABAergic neurons formed two distinct groups, one consisting of Lamp5 and Vip neurons and the second of Sst and Pv neurons (**Fig. 1a**). We also found that Ndnf expression was highly enriched within the Lamp5 subclass and did not overlap with any of the other major GABAergic subclasses (**Fig. 1b**). This data further supported the previous finding that Ndnf is expressed within the Lamp5 subclass[132]. We then investigated whether Ndnf expression levels within the Lamp5 subclass are differentially expressed at a later disease stage (12 weeks) in R6/2 mice compared to WT controls. Our findings confirmed our hypothesis, showing that Ndnf gene expression is indeed downregulated in Lamp5 interneurons in R6/2 mice at 12 weeks of age compared to WT controls (**Fig. 1c**). To further evaluate whether these expression changes would actually occur at earlier disease stages, and affect a wider range of marker genes, we identified the top 100 marker genes of the Lamp5 subclass and calculated their mean expression change across all ages (**Fig. 1d**). At 5 weeks, marker expression in Lamp5 neurons of R6/2 mice showed minimal changes. However, by 8 weeks, we observed a significant reduction in marker genes expression in these neurons, which persisted to 12 weeks (**Fig. 1d**). These data further emphasize the impact that HD-like disease progression in R6/2 mice has on the molecular profile of Lamp5 interneurons, specifically on transcriptional changes that may contribute to cortical dysfunction seen in R6/2 mice[76]. Further, these findings advance prior research[80], which focused on downregulation patterns of Pv, Sst, and Vip proteins in R6/2 mice, by also including the Lamp5 subclass and Ndnf interneurons among the affected groups.

Previous studies have demonstrated that synaptic proteins are downregulated in both glutamatergic neurons and interneurons of R6/2 mice compared to WT controls. This

reduction has been associated with an imbalance in cortical E/I seen in HD mice[127]. Therefore, in order to understand whether we could see a similar effect in Lamp5 INs of R6/2 mice at 12 weeks of age we performed pathway analysis. We showed a significant downregulation of multiple pathways involved in synaptic transmission (**Fig. 1e**). Specifically, among the "GABAergic synapse" genes, we found that expression of GABA receptors such as gamma-aminobutyric acid (GABA) type A receptor ($GABA_AR$) subunit Beta2 (Gabrb2), GABA B receptor ($GABA_BR$) subunit 2 (Gabbr2) as well as genes encoding for Gad1, Gad2, Reln and Ndnf were downregulated (**Fig. 1f**). Moreover, expression changes can be seen in several other GABAergic synaptic genes within the Lamp5 interneurons across different ages (**Fig. 1g**). For example, the synaptic gene $GABA_AR$ subunit Gamma2 (Gabrg2) is downregulated at 8 and 12 weeks in R6/2 mice (**Fig. 1g**). Mutations in the Gabrg2 gene have been associated with the onset of various epilepsy syndromes[133].In conclusion, these findings suggest that the downregulation of marker genes of NDNF INs occurs before disease onset and the expression of GABAergic synaptic genes, including that of Ndnf, decreases with the progression of HD-like symptoms, potentially contributing to cortical E/I imbalance.

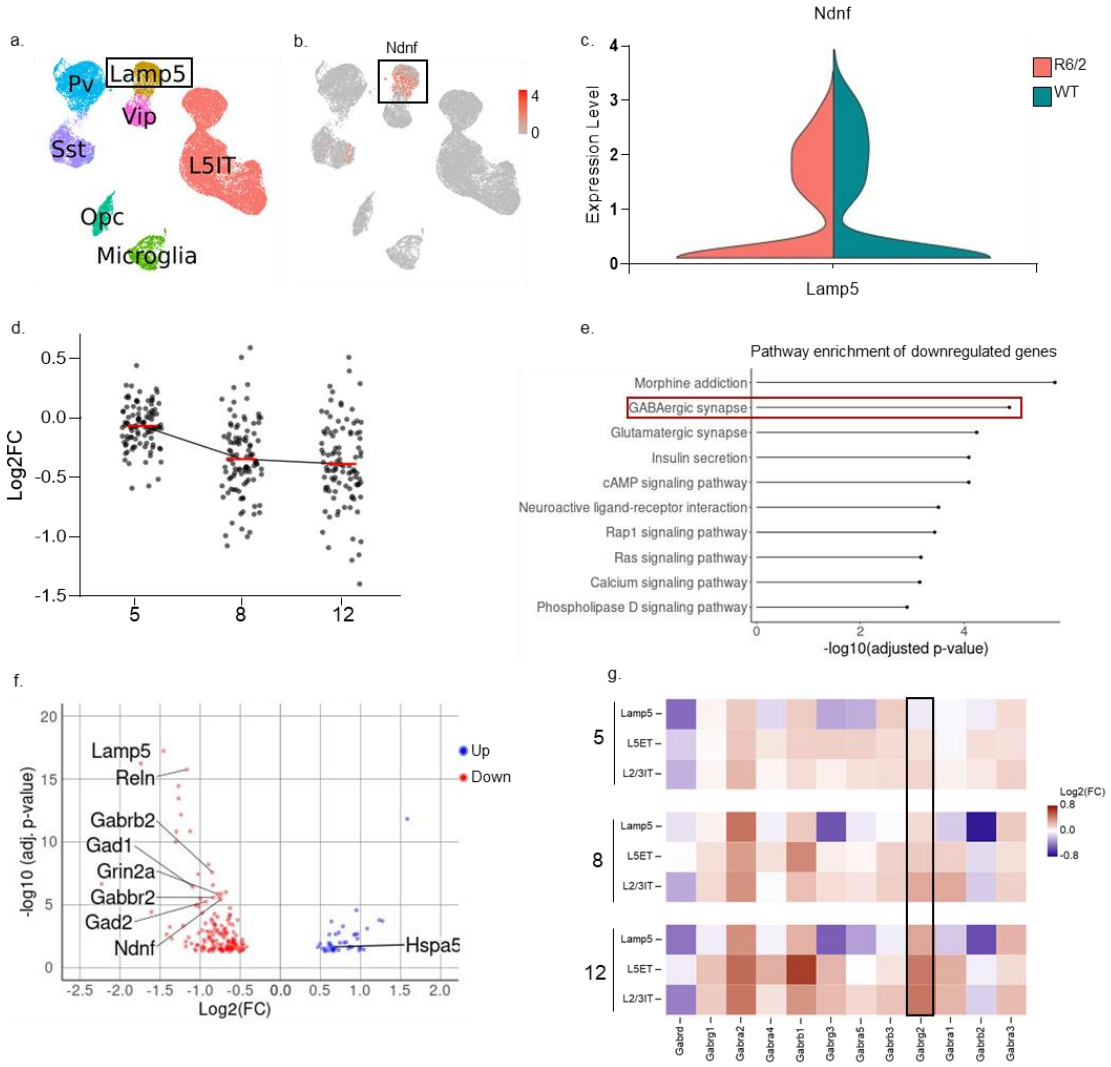

Figure 1

a. UMAP plot showing nuclei labelled by different cell subclass. The plot includes nuclei from WT and R6/2 mice at all three time points. Highlighted in the black box is the Lamp5 subclass of interest.

b. UMAP plot displaying the normalized expression of Ndnf within the Lamp5 subclass.

c. The expression level of Ndnf in Lamp5 interneurons is decreased in R6/2 mice compared to WT mice at 12 weeks of age.

d. The expression level of the top 100 marker genes in Lamp5 interneurons is reduced in R6/2 mice starting at 8 weeks. Each dot represents one gene from the top 100 marker list, with the red crossbar indicating the mean expression change.

e. Volcano plot highlighting the downregulation of multiple synaptic genes involved in GABAergic and glutamatergic signal transmission in Lamp5 interneurons of R6/2 mice at 12 weeks.

f. Pathway enrichment analysis of genes downregulated in Lamp5 interneurons of R6/2 mice at 12 weeks reveals significant downregulation of genes in pathways such as “GABAergic synapse” and “Glutamatergic synapse.”

g. Heatmap showing the log2 fold change (Log2FC) in expression of several synaptic genes in R6/2 mice across different ages.

Data generated and analysed by D.F.

2.2.3.2 M1^{Ndnf} interneurons are differentially modulated by locomotion

We next investigated whether NDNF neural activity in R6/2 mice, would show any changes throughout disease progression. For this reason, we performed head-fixed *in vivo* two-photon calcium imaging in the M1 of R6/2 :: Ndnf-cre mice and WT littermate controls, during a running wheel behavioral task. It is known that R6/2 mice start manifesting motor deficits, which include tremor, dyskinesia and balance impairments, starting between 9 to 11 weeks of age[81,127]. Motor deficit onset depends on CAG repeat length[127]. Due to their genetic instability, CAG repeats can increase overtime and this leads to an attenuation of the HD-like phenotype of R6/2 mice[85,127]. The CAG repeat length in our colony at the time when calcium recordings were performed was 284 ± 3 (Mean ± SD, N=6). Therefore, this cohort is characterized by a delayed onset. Despite the fact that the CAG repeat length in our colony was longer than ideal for robust HD-like behavioral phenotypes, we aimed to gain insights into potentially presymptomatic changes in NDNF activity associated with HD pathology. Therefore, we injected an adeno-associated virus (AAV9) containing a Cre-dependent version of the genetically encoded calcium indicator GCaMP7f, to be expressed in M1^{Ndnf} interneurons. During the same surgery, a cranial window was placed above the M1/M2 regions. After a training period (see materials and methods), we placed head-fixed mice on a freely rotating wheel and performed *in vivo* two-photon calcium imaging (**Fig. 2a**). Imaging was performed in three age groups (7-8, 9-10 and 11-12 weeks), which were selected following previous research on the progression of HD, its corresponding behavioral phenotype and our snRNA-seq dataset[76, 80, 83]. In order to classify the innate behaviours of the mice, we used a semi-supervised deep learning model (DeepEthogram) [134] and distinguished between a set of “active”, “quiet” and ‘stereotyped’ behaviors. Quiet periods were defined as intervals when the mice were resting or with lifted paws, while locomotion was classified as an active period (**Fig. 2b**) and stereotypical behavioral classes, included chewing, twitching, and grooming (**Fig. 2b**). We calculated the cumulative duration of the respective classified behavior (seconds/10mins) for both littermate controls and R6/2 mice. Our data indicate no significant differences across behaviors and timepoints when comparing R6/2 to littermate control mice (**Fig. 2c-g**), except for grooming periods which showed a significant difference at later stages (**Fig. 2h**).

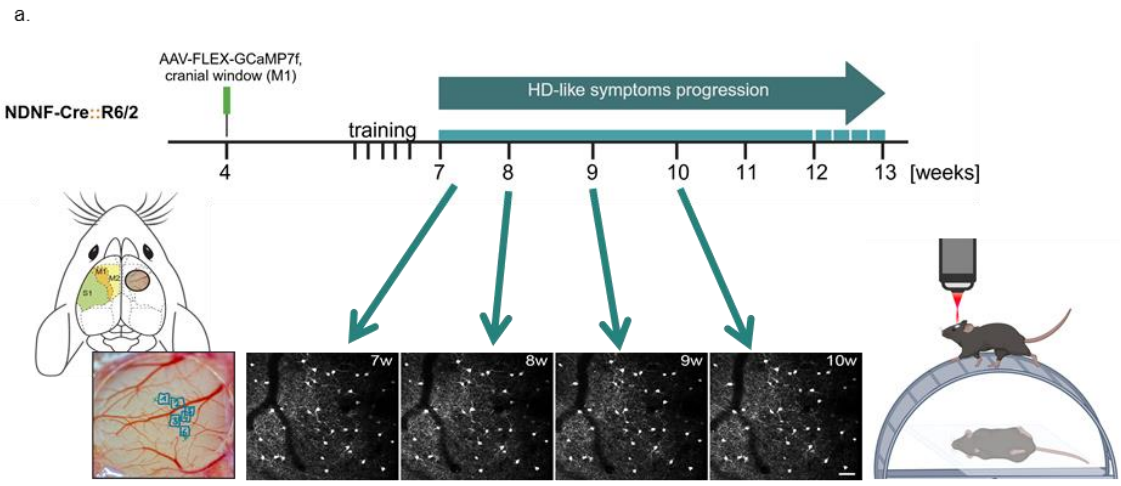
a.
AAV-FLEX-GCaMP7f,
cranial window (M1)
NDNF-Cre::R6/2
training
HD-like symptoms progression
4
7
8
9
10
11
12
13
[weeks]
7w
8w
9w
10w

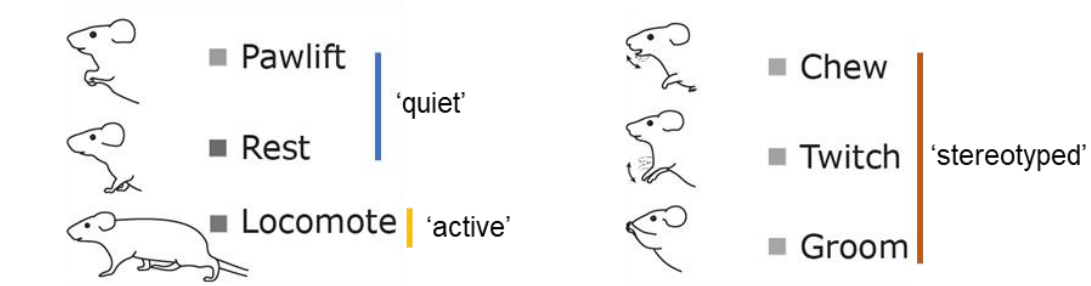
b.
Pawlift
Rest
Locomote
'quiet'
'active'
Chew
Twitch
Groom
'stereotyped'

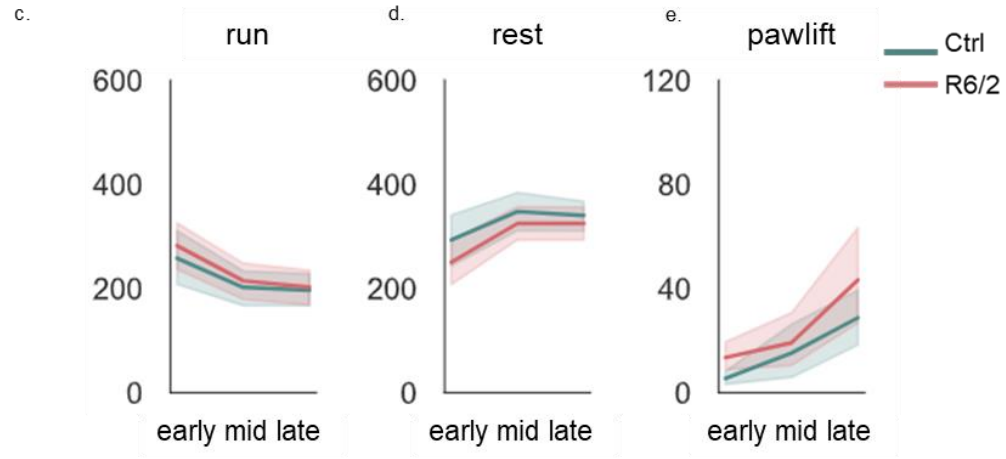
c.
run
d.
rest
e.
pawlift
Ctrl
R6/2
600
400
200
0
120
80
40
early mid late

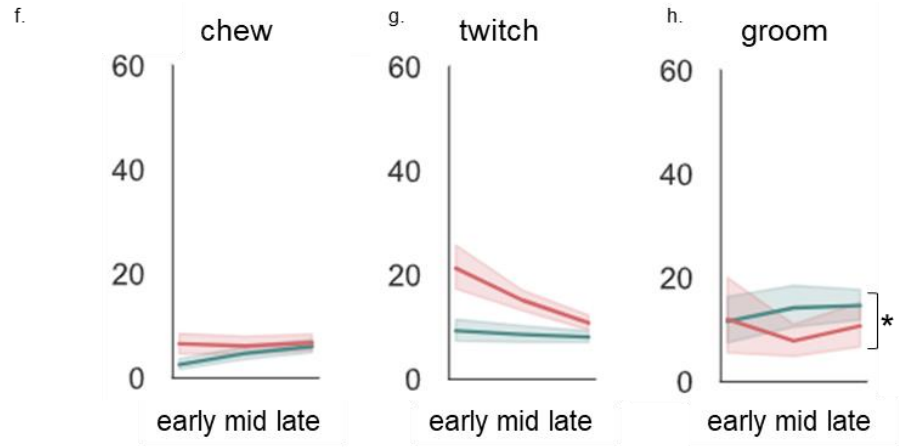
f.
chew
g.
twitch
h.
groom
60
40
20
0
*
early mid late

Figure 2.

a. Scheme depicting the experimental paradigm followed for two-photon *in vivo* experiments (up). From left to right (below): image showing different injection sites of AAV9-GCaMP7f between the M1 and M2 of the cortex. Images of same FOV imaged over the course of different weeks, starting from 7w until 10w. Scheme of head-fixed running wheel behavior set up during *in vivo* two-photo imaging.

b. Behavioural classifications, 'quiet' (pawlift and rest, blue line), 'active' (locomotion, yellow line) and 'stereotyped' (chew, twitch, groom, orange line).

c. Line plot showing no significant behavioral differences during 'run' between R6/2 (red) and Ctrl (green) across different ages (early, mid, late). Two-factor aligned rank transformed linear mixed model: ns.

d. Line plot showing no significant behavioral differences during 'rest' between R6/2 (red) and Ctrl (green) across different ages (early, mid, late). Two-factor aligned rank transformed linear mixed model: ns.

e. Line plot showing no significant behavioral differences during 'pawlift' between R6/2 (red) and Ctrl (green) across different ages (early, mid, late). Two-factor aligned rank transformed linear mixed model: ns.

f. Line plot showing no significant behavioral differences during 'chew' between R6/2 (red) and Ctrl (green) across different ages (early, mid, late). Two-factor aligned rank transformed linear mixed model: ns.

g. Line plot showing no significant behavioral differences during 'twitch' between R6/2 (red) and Ctrl (green) across different ages (early, mid, late). Two-factor aligned rank transformed linear mixed model: ns.

h. Line plot showing significant behavioral changes during 'groom' between R6/2 (red) and Ctrl (green) across mid and late stages. Two-factor aligned rank transformed linear mixed model: *P=0.1.

Data generated and analysed by S.B.

Moreover, in a representative (single mouse / session) control mouse at 8 weeks, we identified two distinct NDNF IN fluorescence dynamics associated with locomotion (**Fig. 3a**): one group of NDNF INs was positively correlated with locomotion, showing increased activity, while another group was more active during the resting state, displaying an anti-correlated pattern with locomotion events (**Fig. 3a and 3b**). Previous *in vivo* research has shown that the amplitude of calcium transients in M1 neurons is significantly reduced in R6/2 mice compared to WT during both motion and non-motion periods[135]. Additionally, in R6/2 mice, calcium transients were higher during non-motion periods than during motion. Building on these findings, we investigated whether

transitions between “active” (locomotion) and “quiet” states would influence calcium transients in NDNF INs within the M1 region of R6/2 mice and their littermate controls. We considered transitions between behavioural classes with a minimum of 3 seconds duration to avoid contamination of activity related to other movements. Each cells’ activity (ΔF/F0) was averaged across all individual transitions for each imaging session. Our results indicated that $M1^{Ndnf}$ neurons in R6/2 mice, both at 7-8 weeks and 11-12 weeks of age, showed a significantly increased ΔF/F at the onset of locomotion compared to controls (**Fig. 3c**). A reduction in $M1^{Ndnf}$ activity was observed at the transitions between locomotion to “quiet” states (**Fig. 3d**), however the activity of $M1^{Ndnf}$ neurons in R6/2 mice remains significantly higher during “quiet” periods relative to littermate controls (**Fig. 3d**). Notably, this is the first study that demonstrates the engagement of NDNF interneurons in locomotion activities within R6/2 mice as well as littermate controls, advancing our understanding of the role of NDNF INs in the M1. This is an interesting finding that highlights the potential role of NDNF INs in M1 cortical network dynamics, and together with other IN such as VIP, PV, and SST neurons, might regulate overall cortical E/I balance during locomotion. We demonstrated that $M1^{Ndnf}$ neurons in our R6/2 mice display early-stage alterations in calcium activity as soon as 9-10 weeks of age (**Fig. 3c and d**), even in the absence of overt HD-like symptoms. These functional changes, arising well before classical HD-like phenotypic behaviors, may signify early disruptions in cortical E/I balance, that could predispose the neural network to subsequent neurodegenerative processes[127]. This evidence aligns with preclinical human studies. Functional magnetic resonance imaging (fMRI) revealed cortical dysfunction in pre-symptomatic stages, supporting the notion that early, intrinsic cortical network changes could be instrumental in shaping the pathophysiology of HD well in advance of observable symptoms[136].

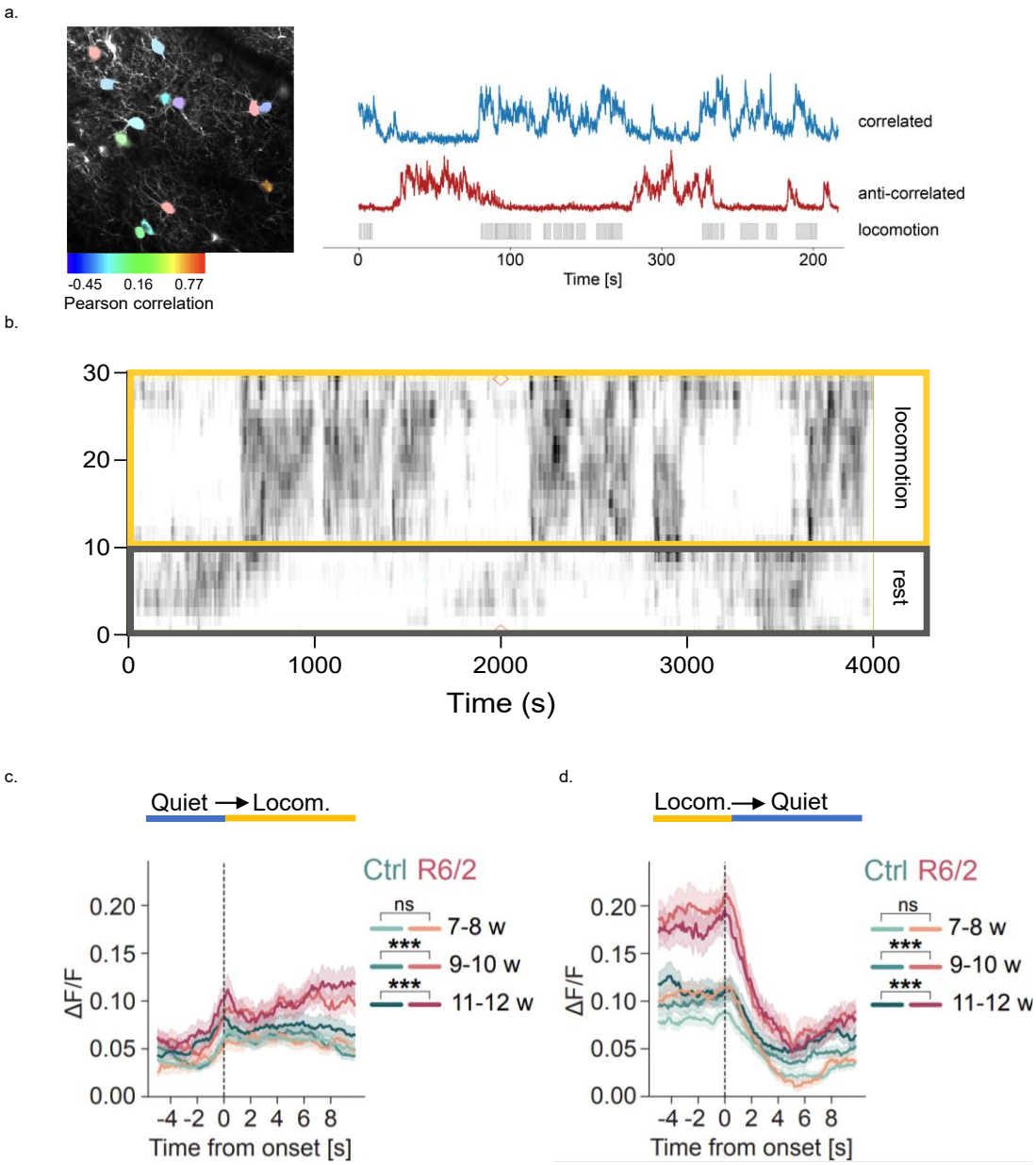

Figure 3.

a. Max—intensity projection of a FOV subset. Cells are colour coded according to their pairwise Pearson correlation (left image). Fluorescence dynamics of 2 representative neurons in a control mouse (8 w, right panel).

b. Rasterplot of all NDNF INs from one session (ctrl mouse, 8 w), showcasing two subpopulations positively and negatively correlated with locomotion.

c-d. (b) ΔF/F activity of NDNF interneurons aligned with the transition between quiet (rest) and locomotion and vice versa (c). NDNF IN activity is specifically increased during locomotion and at advanced ages in R6/2 mice. Two-factor aligned rank transformed linear mixed model: ***P < 0.001.

Data generated and analysed by S.B.

2.2.3.3 M1^{Ndnf} neurons display an increase in intrinsic excitability in R6/2 mice during different ages

The emergence of CPN hyperexcitability during disease progression is well characterized in mice models of HD[81], however the contribution of M1 inhibitory INs to the overall E/I imbalance in R6/2 mice during presymptomatic stages remains unclear. It is known that GABAergic neurotransmission is reduced in HD mice and in cortical motor and premotor areas and that INs undergo molecular and electrophysiological changes during HD-like symptoms progression[76,81,137]. To explore the role of cortical NDNF cells in HD circuit dysfunction, we performed whole-cell recordings in Ndnf-cre :: R6/2 brain slices, performing both voltage-clamp and current-clamp recordings of GCaMP7f-positive NDNF neurons in L1 (**Fig. 4a**). We analysed M1^{Ndnf} intrinsic excitability properties across two age groups (9-11 and 12 weeks) for R6/2 and littermate control mice, (**Fig. 4b**). At 9-10w, current clamp recordings revealed no significant changes in NDNF cell excitability (**Fig. 4c**). However, at 12w we found a significant increase in NDNF excitability in R6/2 versus control mice, as quantified by increased action potential generation in response to current step injections (**Fig. 4d**). Previous studies have correlated larger amplitudes of calcium transients with an increased number of action potentials (APs)[135]. Our findings are consistent with this, as the increased intrinsic excitability observed in M1^{Ndnf} cells supports our *in vivo* experiments, which demonstrated increased calcium activity of NDNF INs during locomotion periods. We found that age-related changes in intrinsic excitability also differed between genotypes across ages. In R6/2 mice, there was a significant increase in excitability between 9-10 weeks and 12 weeks of age (**Fig. 4e**), whereas the opposite trend was observed in littermate controls (**Fig. 4f**). Overall, these data suggest that presymptomatic HD mice exhibit altered intrinsic properties in M1^{Ndnf} cells, particularly during the later stages of HD-like progression, supporting the idea that cortical dysfunction arises prior to the onset of motor symptoms[127].

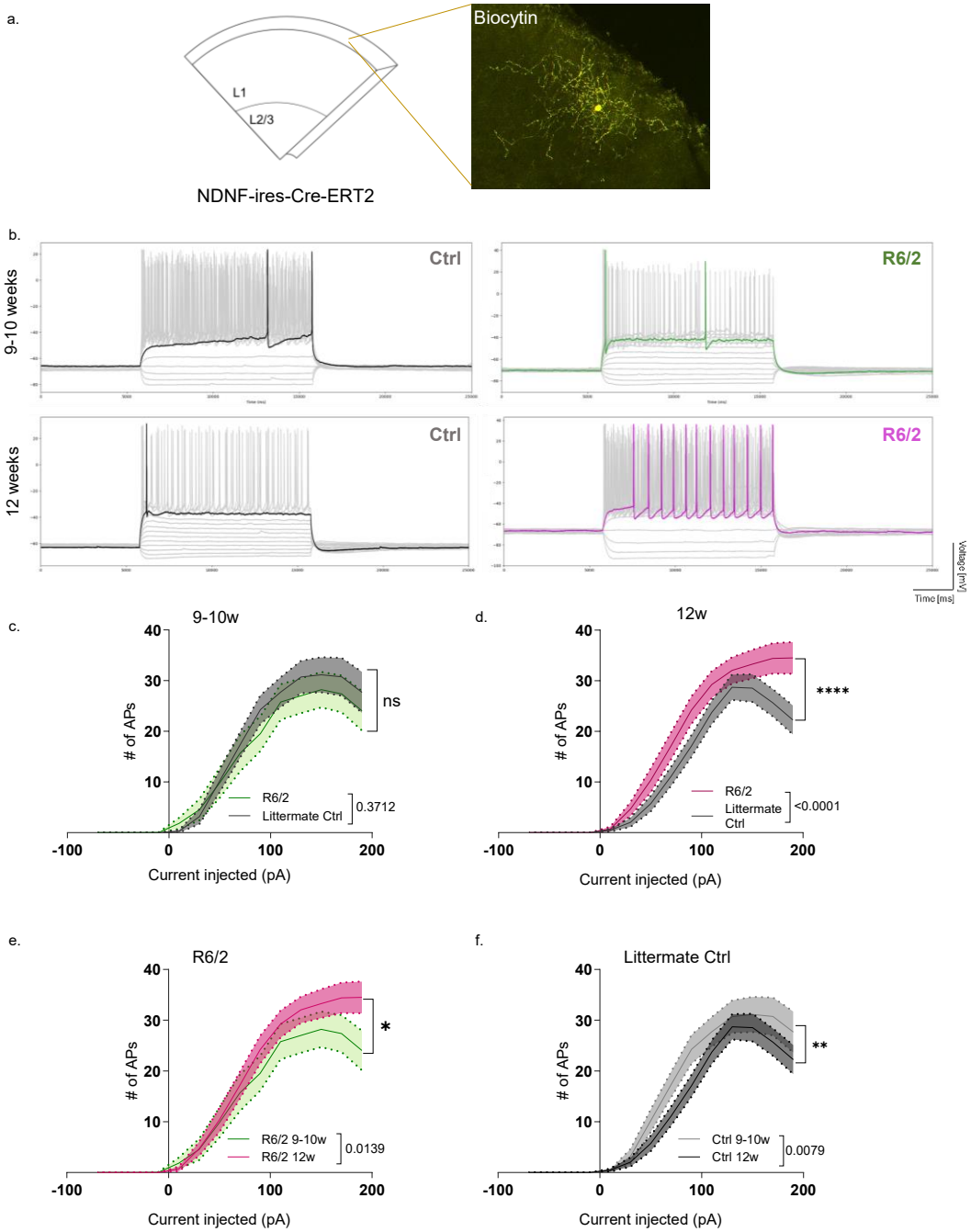

Figure 4.

a. From left to right: Scheme depicting the location of NDNF patched interneurons in the L1 of the primary motor cortex (M1); representative image of a biocytin-filled NDNF neuron patched in the M1.

b. Representative traces from whole-cell current-clamp recordings of NDNF IN in the M1 of R6/2 and littermate control mice at 9-10 weeks (ctrl, grey; R6/2 green) and at 12 weeks (ctrl, grey; R6/2 magenta) in response to currents steps injections of -20pA starting from -60pA up to +200pA.

c. Input-output curve for R6/2 (green) and littermate controls (grey) at 9-10 weeks of age show no significant changes in intrinsic NDNF IN excitability between groups (n=Ctrl [21]; n=R6/2 [18]). 2-way ANOVA, P=0.1558

d. Input-output curve for R6/2 (magenta) and littermate controls (grey) at 12 weeks of age show significant changes in intrinsic NDNF IN excitability between groups (n=Ctrl [34]; n=R6/2 [34]). 2-way ANOVA, P **** <0.0001.

e. Input-output curve for R6/2 at 12w (magenta) and at 9-10w (green) of age show significant changes in intrinsic NDNF IN excitability between ages (n=R6/2, 9-10w [18]; n=R6/2, 12w [34]). 2-way ANOVA, P= **0.005.

f. Input-output curve for Littermate Ctrl at 12w (dark grey) and 9-10w (light grey) of age show significant changes in intrinsic WT NDNF IN excitability between ages (n=ctrl, 9-10w [21]; n=ctrl, 12w [34]). 2-way ANOVA, P= ***0.0008.

Data generated and analysed by Y.M.

In addition to intrinsic excitability, we also sought to understand whether the increase in NDNF neuron activity we observed *in vivo* was due to changes in the properties of synaptic inputs received by NDNF neurons. Whole-cell voltage clamp recordings were performed in order to record both spontaneous excitatory and inhibitory post synaptic currents (sEPSC and sIPSC, respectively). We analysed spontaneous current amplitude (pA) in $M1^{Ndnf}$ neurons of both R6/2 and littermate controls. Our data were derived by calculating peak amplitude of each detected current, then calculating the mean amplitude for each cell for both sEPSC and sIPSC. We found that the distribution of current amplitudes showed no significant differences for sIPSC (**Fig. 5a**). However, changes in frequency distribution of amplitude were significantly different for sEPSC at 12 weeks, with sEPSC amplitudes in NDNF INs in R6/2 mice displaying a leftward shift in distribution compared to littermate controls (**Fig. 5b**). At 12 weeks sEPSC and sIPSC frequencies (Hz) were not altered between the two genotypes (**Fig. 5 c and d**) nor were the mean peak amplitudes for each cell for both conditions (**Fig. 5e and f**). These data suggest that $M1^{Ndnf}$ cells receive weaker excitatory postsynaptic inputs, as shown in Fig. 5b. Given their increased intrinsic excitability, this may reflect a failed compensatory attempt by the cortical network to restore balance.

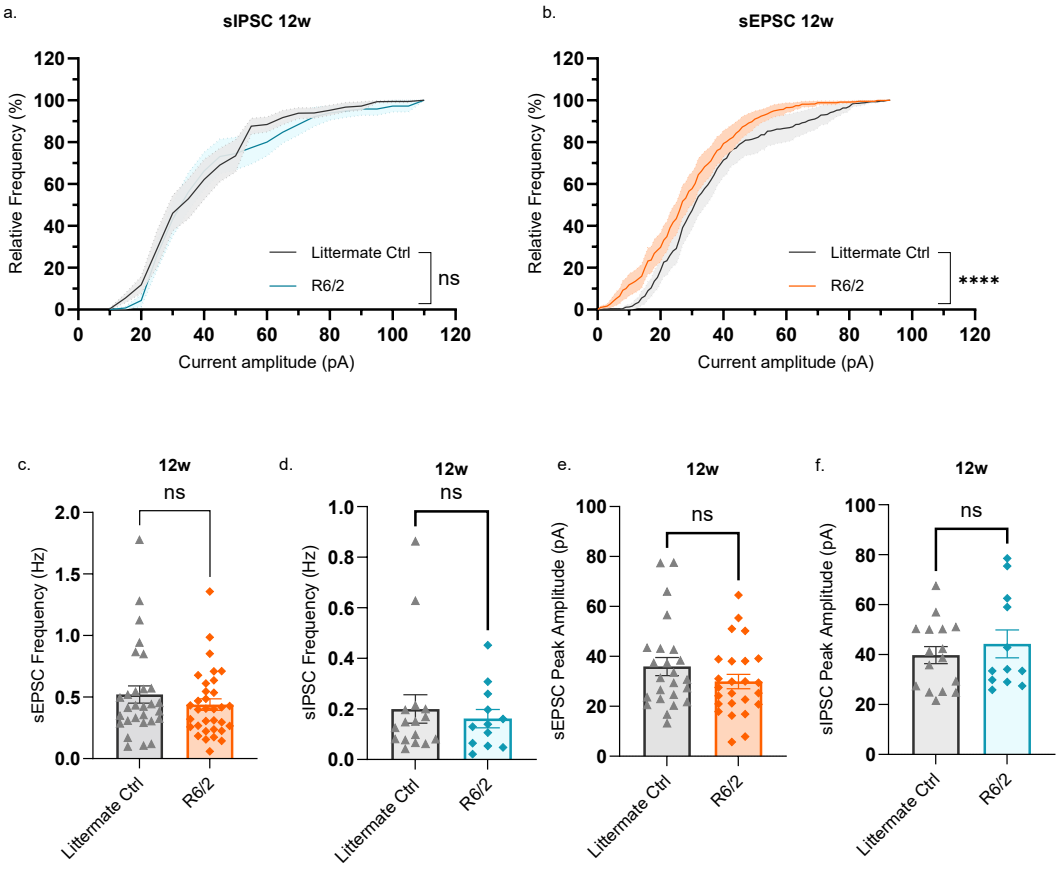

Figure 5.

a. Distribution of sIPSC amplitudes recorded during voltage-clamp experiments, show no significant difference in mean current at 12 weeks of age between R6/2 and littermate controls NDNF cells. (n=Ctrl [16]; n=R6/2 [18]). 2-way ANOVA, P=0.1420.

b. Distribution of sEPSC amplitudes recorded during voltage-clamp experiments, show significant differences in mean current at 12 weeks of age between R6/2 and littermate controls NDNF cells. (n=Ctrl [24]; n=R6/2 [25]). 2-way ANOVA, P **** <0.0001

c. Frequency of sEPSCs detected at 12 weeks of age for both R6/2 an littermate control cells. No significant differences on mean frequency are noted. (n=Ctrl [25]; n=R6/2 [27]). Unpaired t-test, P=0.4582

d. Frequency of sIPSCs detected at 12 weeks of age for both R6/2 an littermate control cells. No significant differences on mean frequency are noted. (n=Ctrl [16]; n=R6/2 [18]). Unpaired t-test, P= 0.8178.

e. Peak amplitude of sEPSCs detected at 12 weeks of age for both R6/2 an littermate control cells. No significant differences on mean peak amplitude are noted. (n=Ctrl [25]; n=R6/2 [27]). Unpaired t-test, P= 0.5315.

f. Peak amplitude of sIPSCs detected at 12 weeks of age for both R6/2 an littermate control cells. No significant differences on mean peak amplitude are noted. (n=Ctrl [16]; n=R6/2 [18]). Unpaired t-test, P= 0.6351.

Data generated and analysed by Y.M.

2.2.4 Discussion

Mechanisms underlying cortical hyperexcitability in HD have been previously identified in layer 2/3 of both M1 and the prefrontal cortex (PFC). In HD models, electrophysiology recordings and *in vivo* studies have shown an overall increase in cell activity and impairments in interneuron function in these regions[127,130,138]. In the present study, we demonstrate for the first time that $M1^{Ndnf}$ IN in layer 1 of the neocortex exhibit a significant increase in excitability in the R6/2 mouse model of HD. *In vivo*, $M1^{Ndnf}$ neurons play a role in modulating transitions between "quiet" and "locomotion" states, as demonstrated by rapid shifts in calcium activity. Specifically, an increase in NDNF neuron calcium activity was detected at locomotion onset, with a reduction in activity seen when mice transition to "quiet" states, during which NDNF IN maintain higher activities compared to littermate controls. Our data show that $M1^{Ndnf}$ neurons undergo functional changes prior to the onset of HD symptoms. Therefore, we hypothesise a possible mechanism by which NDNF INs are involved in cortical activity modulation by acting synergistically together with other INs. In normal conditions, VIP^+ INs are activated by locomotion, displaying increased firing rates *in vivo* during locomotion[139]. This increase suppresses SST^+ activity, possibly increasing the overall excitatory responses of CPNs[139]. Our data suggests an additional level of complexity that may be added to this mechanism. NDNF INs are more active at locomotion onset in R6/2 mice, thus other INs in lower cortical layers may become more inhibited, causing disinhibition of CPNs somata potentially intensifying the cortical hyperexcitability previously reported in HD[127]. However, previous studies showed that together with this somatic disinhibition, L1 NDNF IN provide direct and long-lasting inhibition to the apical dendrites of the CPNs[140]. It is possible that cortical hyperexcitability is likely not a generalizable state in the HD cortex. Further *in vivo* investigations are needed to understand how other INs might operate together with NDNF IN and how their activity changes during locomotion in R6/2 mice.

For instance, studying the activity of SST, PV, and VIP interneurons in head-fixed mice during locomotion will be crucial for understanding how the dual inhibition provided by L1 NDNF INs affects the activity of other cortical neurons. Studies conducted in the L1 of the visual cortex have shown that NDNF INs disinhibit CPNs by directly inhibiting PV INs at the somatic level[140]. Therefore, exploring how this inhibition could affect locomotion-induced changes in PV IN activity could provide valuable insights.

Additionally, we identified two distinct ensembles of NDNF neurons, distinguished by opposing correlations with locomotion or 'active' state: an ensemble correlated with locomotion and another which is anti-correlated. This intriguing finding may relate to

functional subdivisions of NDNF INs in the neocortex, as NDNF IN have been described as NPY^+ (NGF cells) and NPY^- (canopy cells), each characterized by distinct molecular, morphological, and electrophysiological properties[110]. However, more recent studies called for caution[73] in dividing NDNF in two groups based on co-expression of NPY, as this was shown to be age- and brain region-dependent. Therefore, further in situ hybridization experiments should explore expression patterns of key molecular markers between different age groups in $M1^{Ndnf}$ neurons to elucidate whether the ensembles that we see *in vivo* might correspond to distinct subpopulations of NDNF INs, defined by expression of different molecular markers. Further studies are needed to dissect the specific role of both ensembles in regulating M1 cortical network activity during locomotion in HD mice during advanced disease stages.

In the neocortex, NDNF IN not only co-express with NPY but also with other key molecular markers. Interestingly, studies using scRNA-seq analysis revealed that L1 NDNF IN co-express markers such as Reln and Lamp5, further identifying them as NGF cells[132]. Our snRNA-seq data confirm that NDNF IN are part of the Lamp5 population. Further, Ndnf expression is downregulated in Lamp5 interneurons in R6/2 mice starting at 8 weeks of age. Moreover, the top 100 marker genes (including Ndnf) of Lamp5 interneurons showed a reduced expression in R6/2 mice starting from 8 weeks. These findings emphasise that the broader molecular profile of Lamp5 interneurons changes with HD-like disease progression in R6/2 mice. However, how these transcriptional changes might relate to cortical dysfunction seen in HD, remain unexplored. Here, we advance our understanding of the downregulation patterns seen in previous studies focused on PV, SST and VIP protein expression changes[80], by including the Lamp5 subclass and NDNF INs among the affected groups in HD mice.

Importantly, NDNF IN in the neocortex and other brain areas such as the basolateral amygdala and hippocampus[35,36,39] demonstrated a powerful and atypical form of inhibition. This is mediated by both GABAA and GABAB receptors, in part due to the release of large amounts of GABA via volume, rather than synaptic, transmission[39]. Interestingly our snRNA-seq data show that among the “GABAergic synapse” genes both GABAA and GABAB receptor’s genes were downregulated across ages within the Lamp5 subgroups of R6/2 mice. We could therefore hypothesize that the downregulation of GABA receptors may relate to the increase in activity in NDNF INs seen by our calcium imaging *in vivo.* This downregulation of inhibitory receptors could exacerbate the increase in intrinsic excitability we have demonstrated in NDNF INs.

Considering their hyperactivity during presymptomatic stages of HD, it is important to consider the wider role that NDNF INs play in cortical microcircuits. L1 NDNF INs provide top-down inhibition onto lower layers 2/3 of the neocortex, regulating the

activity of all other major INs subclasses and CPNs [73]. Therefore, further research is needed to clarify how the hyperexcitability of NDNF IN in HD mice relates to and influences the activity of other interneurons and CPNs. Given our *in vivo* data, which show an increased calcium activity in NDNF interneurons and the onset of locomotion, behavioral experiments in symptomatic HD mice will be crucial for understanding how this hyperexcitability evolves with the appearance of motor symptoms.

Although the functional changes of other INs during locomotion in R6/2 mice remain to be explored, histological changes in INs have been reported in previous studies[80]. Specifically, PV, SST and VIP INs show morphological alterations in R6/2 mice, suggesting that mHTT influences these changes. Moreover, although VIP and SST INs develop mHTT inclusions at a faster rate compared to PV INs, all IN populations are affected by mHTT[80]. We hypothesize that NDNF INs might also be affected by mHTT and would further investigate how mHTT influences the functional changes reported in this study. Similar histological experiments should therefore be conducted to assess the development of mHTT inclusions in NDNF INs across different disease time points in HD disease models to further confirm our hypothesis.

In conclusion, we report for the first time that $M1^{Ndnf}$ neurons in R6/2 mice undergo early transcriptomic changes, followed by alterations in calcium activity across different behavioral states (i.e. “quiet”, “active”), and also demonstrate that $M1^{Ndnf}$ neurons are intrinsically hyperexcitable when assessed using *ex vivo* electrophysiology. These findings advance our understanding of the key classes of interneurons involved in the disrupted cortical excitatory/inhibitory balance seen in HD, with NDNF INs likely playing a significant role in the cortical circuit dysfunction observed in mouse models of HD.

2.2.5 Materials and Methods

Animals

R6/2 mice[82] transgenic for the 5′ end of the human huntingtin gene were maintained by crossing R6/2 males to F1 C57Bl6/CBA females. Animals were kept in a specific pathogen-free animal facility with free access to food and water. The presence of the transgene was verified by PCR with the following primers: forward, 5′CCGCTCAGGTTCTGCTTTTA-3′, reverse, 5′-TGGAAGGACTTGAGGGACTC-3′. CAG repeat length was determined by Laragen. After surgery, mice were kept in an inverted 14–10 h light-dark cycle. All animal experiments were approved by the Government of Upper Bavaria (animal protocols 55.2-1-54-2532-168-2014, ROB-55.2-2532.Vet_ 02-20-05), and all the methods were performed in accordance with the relevant guidelines and regulations.

Tissue dissection

Tissue was harvested from R6/2 and WT mice as previously described at 5, 8 and 12 weeks. Mice were anaesthetised by intra-peritoneal injections of 200 mg/kg Ketamine and 40 mg/kg Xylazine. Mice were perfused by intra cardiac injection of ice-cold cutting buffer (110 mM NaCl, 2.5 mM KCl, 10 mM HEPES, 7.5 mM MgCl2, 25 mM Glucose, 75 mM Sucrose, pH 7.4). All following procedures were performed at 4°C. The brain was extracted, transferred into cutting buffer and the fresh brain was cut at a thickness of 300 µM in cutting buffer on a Leica VT 1200S vibratome at 0.2 mm/s. Brain slices were transferred into dissection buffer (82 mM Na2SO4, 30 mM K2SO4, 10 mM HEPES, 10 mM glucose and 5 mM MgCl2), and the primary motor cortex was dissected.

Nuclei isolation and snRNA-seq

The protocol and buffers for nuclei isolation were adapted from Mathys et al. (2019)[141] and Wertz et al. (2020)[142] for detailed protocol and analysis information refer to “Temporally resolved single-nucleus RNA-sequencing profiling of the cortex reveals mechanisms of neuronal vulnerability in Huntington’s disease”, Dennis Feigenbutz-LMU[143].

Surgery

For *in vivo* calcium imaging, an adeno-associated virus (AAV9) containing a Cre-dependent version of the genetically encoded calcium indicator GCaMP7f was

expressed in cortical interneurons. Intracerebral injections of AAV and cranial window implantation were performed within the same surgery in 3.5-week-old mice deeply anesthetized with an intraperitoneal (i.p.) injection of ketamine/xylazine (130 and 10 mg kg−1 body weight, respectively). The analgesic carprofen (5 mg kg−1 body weight, subcutaneously) and the anti-inflammatory drug dexamethasone (10 mg kg−1, i.p.) were administered shortly before surgery. During surgery, the AAV (titer: ~10^{12} infecting units per ml) was injected into the motor cortex (3 injection sites with stepwise 200 nl injections at 150 and 200 µm depth). A cranial window was implanted over the left cortical hemisphere as previously described[144]. Briefly, a circular piece of skull (4 mm in diameter) was removed over the fore- and hindlimb area of M1 / M2 (position: 1.5 mm lateral and 1.0 mm anterior to bregma) using a dental drill. A round coverslip (VWR; d = 4 mm) was glued to the skull using histoacryl glue (B.Braun) and dental acrylic cement (Tetric Evoflow A1 / Paladur). After surgery, mice received a subcutaneous injection of the antibiotic enrofloxacin (5 mg kg−1) and were placed in a warm environment for recovery. A small custom-made metal bar (1 cm × 3 cm; 0.06 g) with a round opening was glued onto the coverslip with dental acrylic cement to allow for stable head fixation under the objective and repeated repositioning of mice during subsequent imaging sessions. Imaging began after a 21-day resting period after surgery.

Behavior

Handling and training

At the age of 5 weeks, mice were handled on 5 consecutive days for 10 min until they were familiarized with the trainer and routinely ran from hand to hand. In the subsequent behavior task training, mice got adjusted to the experimental setup and head fixation. Training sessions (30 min each, 4 consecutive days) were set in the dark with an IR light source.

Wheel task

Head-fixed mice were placed onto a freely rotating wheel (d = 19 cm, continuous surface)[145] and were free to behave according to their innate motivations. Mice typically showed alternating running and resting behaviors. Mouse behavior was tracked at 60 Hz with an IR-sensitive video camera (USB 2.0, 1/3″CMOS, 744 × 480 pixel; 8 mm M0814MP2 1.4–16 C, 2/3″, megapixel c-mount objective; TIS) and custom software (Input Controller, TIS). Running wheel motion was captured by a rotary

encoder (1000 CPR, 60 Hz sampling rate), speed and directionality were decoded online using a Tensy 3.2 processor board custom written Arduino code.

In vivo two-photon imaging

Imaging was performed using a commercial two-photon microscope (B-Scope, ThorLabs) equipped with a ×16/0.8-NA objective (Nikon) and a InsightDS^{+} laser (Newport Spectra Physics) tuned to 920 nm. Image acquisition was controlled through ThorImage software. Images (768 × 768 pixels) were recorded at ~10 Hz for the duration of the behavioral session. Frame times were recorded and synchronized with behavioral recordings using the ThorSync software.

Image analysis

A combination of Suite2P[146] and Cellpose[147] software was used to generate regions of interest (ROIs) corresponding to individual neurons and to extract their fluorescence. ROI classifications by the automatic classifier were further refined by manual inspection. A fluorescence trace's time-varying baseline (F0) was estimated by smoothing inactive portions of the trace using a previously described iterative procedure[147]. Briefly, this process identified the trace's active and inactive portions, removing active portions and using the LOESS-smoothed inactive portions (interpolated across active periods) to estimate the time-varying baseline. The normalized ΔF/F0 trace was then calculated, where ΔF was found by subtracting the baseline trace from the raw trace, and F0 is the calculated time-varying baseline.

Video analysis

We used supervised, deep-learning models to extract bodypart movement trajectories from behavior videos [148]. For classification of innate behaviors, we used semi-supervised deep-learning models[134].

Behavior-related activity onset

To estimate the activity of individual neurons at the transition between behaviors, each neuron's activity (ΔF/F0) was aligned to the transition between behavior classes. We only considered transitions between classes with a minimum of 3s duration to avoid contamination of activity related to other movements. Each neuron's activity was averaged across all individual transitions.

Acute brain slice preparation and electrophysiological recordings

Mice were deeply anesthetized with isoflurane and decapitated. The brain was placed in an ice-cold cutting solution saturated with a mixture of 95% O2 and 5% CO2 containing 30 mM NaCl, 4.5 mM KCl, 1 mM MgCl2, 26 mM NaHCO3, 1.2 mM NaH2PO4, 10 mM glucose, and 194 mM sucrose. Typically, 4–5 300 µm thick M1 cortical slices were obtained. After slicing the brain at a thickness of 300 µm on a vibratome (Leica VT1000S, Germany), the slices were transferred into an artificial cerebrospinal fluid (aCSF) solution containing 124 mM NaCl, 4.5 mM KCl, 1 mM MgCl2, 26 mM NaHCO3, 1.2 mM NaH2PO4, 10 mM glucose, and 2 mM CaCl2 (310 to 320 mOsm), saturated with 95% O_2/5% CO_2. Slices were then placed into a carbogen-bubbled holding chamber, heated to ~32 °C via water bath, for 1 hour. The holding chamber was then left at room temperature (22–24 °C) for a minimum of 1 h prior to experimentation. Last, the brain slices were transferred to a recording chamber continuously perfused with aCSF solution saturated with 95% O_2/5% CO_2.

Whole-cell patch clamp recordings from the M1 of Ndnf-Cre::R6/2 and littermate control (Ndnf-Cre^+/R6/2-) were performed on brain slices with a MultiClamp 700B amplifier, a Digidata 1550digitizer (Molecular Devices) and a Hum Bug 50/60 Hz Noise Eliminator (Quest scientific). Patch pipettes were prepared from filament containing borosilicate micropipettes (World Precision Instruments) using a P-1000 micropipette puller (Sutter Instruments), with a resistance of 3–7 MΩ. The intracellular solution for current and voltage clamp recordings contained 130 mM potassium gluconate, 10 mM KCl, 2 mM MgCl2, 10 Mm HEPES, 2 mM Na-ATP, 0.2 mM Na2GTP and biocytin (0.5%) pH7.35, and 290mOsm. Slices were visualized with a fluorescence microscope equipped with IR–DIC optics (Olympus BX51) and a DAGE-MTI camera (IR-2000). The holding potential for voltage-clamp recordings was -70 mV in EPSC experiments and 0 mV in IPSC. Data were acquired using Clampex 10.3 (Molecular Devices). Recordings were made between 2–9 h after killing. Data were sampled at 10 kHz, filtered at 2 kHz and analysed with Clampfit (Molecular Devices) and Stimfit 0.5.

Immunohistochemistry

Biocytin-filled coronal slices were fixed overnight in 4% PFA in PBS at 4°C, then were incubated in 0.3% TPBS with a streptavidin conjugate (647nm; 1:1000, BioLegend) for 3 hrs at RT. Next, the slices were briefly washed three times with PBS and cleared with TDE 67% for 1-2 hr at RT. Finally, the slices were mounted with a drop of TDE 67% and Dako (Dako North America, Inc.) mounting medium, using a spacer and covered with a coverslip.

Microscopy and image processing

Epifluorescence images were obtained with an upright epifluorescence microscope (Zeiss) with 10×/0.3 objectives (Zeiss).

Statistics

snRNA-seq analysis:

Differences were considered statistically significant at a p-value < 0.05 and in cases of multiple comparisons at an adjusted p-value < 0.05. The method for calculating p-values is indicated in the figure caption of plots.

In vivo two-photon analysis:

Statistical tests were selected based on data distributions and significance was set at $p < 0.05$. All evaluated datasets were tested for normality and non-parametric tests were used where appropriate. No statistical methods were used to pre-determine sample sizes, but our sample sizes are similar to those reported in previous publications[127,149]. To compare two or more groups (i.e. genotypes, disease stage, time before and after behavior onset), mixed-effects models were used to account for the nested structure of the data and minimize effects introduced by inter-animal variability, unless otherwise stated. For statistical estimation of non-normally distributed datasets, we used an Aligned Rank Transform (ART) variant of mixed-effects models using the ARTools packaged from R, which allows for nonparametric mixed-effects model testing. Multiple comparisons were corrected using the two-stage False Discovery Rate (FDR) method. Two-factor mixed-effects models for comparing population average activity aligned to behavior transitions were constructed as follows:

$$y \sim genotype + time\_bin + genotype{:}\,time\_bin + (1\,|\,animal)$$

With fixed main effect terms for genotype (ctrl, R6/2) and 2s time bins in aligned behavior transitions (starting at -4, -2, 0, 2, 4, 6, 8) seconds relative to movement onset), the interaction term between genotype and time bin, and a random effect term grouped by animal. If a significant interaction was detected, posthoc pairwise Mann-Whitney U tests were performed between groups for each disease stage.

Ex vivo recordings analysis:

All statistical analysis was performed using Prism 10.2.3 (GraphPad) and all statistics are indicated in the figure legends. Unless otherwise specified, Paired t-tests, 2-way

analysis of variance ANOVA were performed with initial data handling and processing performed using a Microsoft Excel. For all datasets, significance was defined as a p-value less than 0.05. Unless stated otherwise, all datapoints are displayed as mean ± standard error of the mean (SEM).

3. DISCUSSION

This thesis set out to provide novel insights into the role of NDNF interneurons in both fear-related behaviour and neurodegenerative pathology.

3.1 Characterization of NDNF-expressing interneurons in the BLA

Firstly, in order to identify and localize Ndnf-expressing IN, as well as other markers they may possess, we employed hairpin chain reaction (HCR) high-resolution RNA fluorescence *in situ* hybridization (HCR™ RNA-FISH)[104]. Previous studies performed in layer 1 of the neocortex and in the hippocampus used a combination of *in situ* hybridization and IHC strategies to investigate a range of Ndnf markers, revealing strong co-expression with Gad1, Reln, Npy and nNos [35,39,34,102]. These markers were consistently expressed in NGFC, firmly establishing their classification as a subclass of NDNF interneuron[34,150]. Notably, the properties of NDNF L1-INs distinguish them from other well-characterized cortical interneuron populations, such as PV-, SOM-, or VIP-expressing interneurons[35]. We demonstrate that Ndnf^{+} cells are sparsely distributed in the BLA and provide strong evidence for their GABAergic nature, as a substantial proportion co-localizes with Gad1. This finding aligns with recent studies on NDNF IN in the BLA, which used a combination of viral strategies and IHC techniques to reveal that these cells are GABAergic and express Reln and Npy[36]. Our data confirm these findings using *in situ* hybridization, further establishing that Ndnf^{+} cells belong to the NGFC family, characterized by high co-expression of Reln, Npy, and nNos, with minimal overlap with other major interneuron markers such as Sst and Pvalb. Furthermore, in the BLA, we confirm previous data from our lab classifying

Ndnf^{+} cells within the Reln/Lamp5 subclass[13], as evidenced by their strong co-expression with Lamp5.

3.2 Decoding the role of NDNF interneurons in anxiety and fear responses

After confirming and further characterizing the expression patterns of Ndnf markers in the BLA, I aimed to investigate the dynamics of BLA^{Ndnf} IN in relation to anxiety and fear-related behaviors. Considering the well-established roles of PNs and major INs in the BLA in modulating anxiety- and fear-related behaviors, we hypothesised that BLA^{Ndnf} IN may contribute to the fine-tuning of aversive stimuli and contribute to the modulation of these intricate microcircuits underlying fear behaviors in the BLA.

Therefore, we decided to explore the role BLA^{Ndnf} IN in regulating fear acquisition during a CFC paradigm. Unlike paradigms involving auditory or visual conditioned stimuli (CS), this approach associates the aversive stimulus with the context itself [62] (see paragraph 1.2.2). Our results suggest that NDNF neuron activity is not required for expression of fear memory during fear recall. Moreover, an increased immobility (marked by stillness with occasional head movements) and a significantly reduced locomotor activity during day 2 compared to day 1, further supported our findings. To further understand whether NDNF neuron activity influences the expression of fear memory on day 2, I employed the same CFC paradigm as previously described, but this time I photoinhibited NDNF INs exclusively on day 2, leaving day 1 unaffected. As expected, control mice showed a typical response, with significantly increased freezing on day 1. Similarly, NDNF mice when not photoinhibited, learned the

fear conditioning paradigm and displayed a significant increase in freezing behavior. NDNF neuron-inhibited mice, however, did not show significant differences in freezing or immobility between day 1 (no photoinhibition) and day 2 (with photoinhibition). Photoinhibition on day 2 also resulted in decreased exploratory behavior, suggesting that all mice retained a memory of the aversive context experienced during fear acquisition. Collectively, these results indicate that BLA^{Ndnf} neurons are essential for fear expression during conditioning but are not required for fear memory recall. Notably, PV IN exhibit similar activity, promoting fear acquisition by disinhibiting PNs[45,60,111]. NDNF IN in the BLA are known to induce slow postsynaptic suppression on PN axons[9,36] and disinhibition is considered to be an important mechanism for fear learning in BLA[35, 117], therefore we can hypothesise that inhibiting NDNF INs could lead to disinhibition of PNs during fear acquisition. This places BLA^{Ndnf} neurons as part of a complex inhibitory microcircuit in the BLA that modulates fear responses alongside other major IN classes described previously.

To further define the role of NDNF INs in fear memories, it would be valuable to investigate the effects of photoinhibition of NDNF INs during both fear acquisition and recall. Since photoinhibition during recall alone does not affect freezing behavior, we would hypothesize that photoinhibition across both phases would result in reduced freezing during acquisition but might not produce any significant changes during recall. This would align with our findings, which demonstrate that NDNF INs are not involved in fear recall. Performing such an experiment would provide additional support for this hypothesis.

In support of these findings, our studies using early immediate gene c-Fos expression revealed that NDNF INs are more active during fear acquisition but not during recall. These findings are further corroborated by single-nucleus RNA sequencing data, which showed that several interneuron subtypes in the BLA respond to learning and recall of fear memories following exposure to a tone-cued fear conditioning paradigm. Among these, the $Reln^{+}/Ndnf^{+}$ population exhibited gene expression patterns that strongly correlated with CFC-activated learning genes, with elevated expression levels at 8 hours and 24 hours post-conditioning[107]. These results collectively suggest a specialized role for BLA^{Ndnf} neurons in the initial encoding of fear behaviors, with their activity and gene expression tuned to facilitate learning during the acquisition phase of fear conditioning.

In this study, we also investigated the effects of optogenetic inactivation of NDNF interneurons in the BLA during a behavioral task involving exposure to the predator odour TMT. Using this paradigm, we have demonstrated that photoinhibition of NDNF INs during exposure to the predator odour significantly reduced freezing behavior. This finding indicates that BLA^{Ndnf} neurons contribute to the ability of animals to adapt their survival responses when exposed to innate threats. These results align with the established role of the BLA in integrating innate olfactory responses to predators and emphasise the importance of further investigating the contributions of specific interneurons to such behaviors.

As discussed previously, the behavioral response to positive or negative stimuli depends on the saliency of the stimuli. Our data reveal that NDNF INs selectively modulate freezing responses to salient stimuli, such as foot shocks

or predator odors, without influencing general anxiety-like behaviors, as indicated by stable rearing behavior during exposure to TMT. Conversely, in the absence of a salient stimulus, such as during open field (OF) and elevated plus maze (EPM) tests, photoinhibition of BLA^{Ndnf} neurons promotes exploratory activity and reduces anxiety-like behavior.

These contrasting effects suggest that NDNF INs establish microcircuits with PNs that differ in their connectivity to the CeL. Typically, inhibitory inputs to PNs projecting to the CeL are associated with reduced anxiety-like states, while inhibiting the BLA-CeL pathway tends to increase such responses[113,114]. Our findings that NDNF inhibition reduces anxiety-like behaviors may indicate that these neurons preferentially modulate PNs that are not strongly connected to CeL neurons implicated in anxiety suppression. Further research is necessary to elucidate the specific microcircuits and downstream targets of BLA^{Ndnf} neurons to better understand their diverse roles in modulating fear and anxiety-like behaviors. To investigate the microcircuits formed by BLA^{Ndnf} neurons and subsequentially their downstream targets based on already existing literature, we propose conducting patch sequencing experiments. For instance, using an AAV Cre-dependent ChR2 virus to photoactivate NDNF INs in brain slices while recording from neighbouring neurons could provide insights into the primary connections established by NDNF INs within the BLA. Simultaneously collecting the transcriptomic profiles of the responsive cells would enable a detailed molecular analysis of the specific neuronal populations interconnected with NDNF INs.

Furthermore, it would be valuable to examine how the intrinsic properties of NDNF INs are altered following CFC. For example, exposing mice to footshocks

and performing patch-clamp recordings after different timepoints could help identify any changes in the intrinsic electrophysiological properties of NDNF INs *ex vivo*. These experiments could provide comprehensive insights into the changes in NDNF excitability and how these changes may relate to our behavioral findings. Previous studies have reported that neurons in the LA exhibit increased excitability in response to fear conditioning, with changes primarily occurring 24 hours after exposure to the aversive stimulus, rather than within the first hour[151]. This finding suggests that the modulation of intrinsic neuronal excitability may be time-dependent, potentially driven by the recruitment of local brain circuits. This long-lasting modulation of excitability may involve mechanisms such as distinct protein synthesis pathways and alterations in GABAergic and glutamatergic receptor dynamics[152].

3.3 Functional subgroups of NDNF interneurons in freezing and non-freezing states

In order to determine whether the NDNF population responds uniformly to both conditioned and innate stimuli or, alternatively, exhibits a more heterogeneous activity pattern we performed *in vivo* calcium imaging experiments following the same behavioral tests described above for both CFC and TMT exposure behavioural paradigms. This approach was motivated by previous studies[45,53,60,61,64,101] that highlighted the diverse response patterns among BLA cells.

Our calcium recordings show that BLA^{Ndnf} neurons modulate aversive behaviors in a stimulus-specific manner based on saliency. Specifically, our data indicate that the activity patterns of NDNF neurons shift depending on whether the animal is in a freezing or non-freezing state. For instance, within the population of BLA^{Ndnf} neurons, a distinct "freezing ensemble" was recruited during freezing behavior: some neurons within this group showed a reduced activity during fear acquisition, while others maintained elevated activity during freezing episodes. By contrast, the "non-freezing ensemble" displayed stable activity across both days, with less variability compared to the freezing ensemble. During the fear recall phase, NDNF INs showed increased activity during freezing of the most active cells, which is consistent with what we observed during recall when in the absence of photoinhibition mice showed increase in freezing behaviors.

These imaging data thus reveal two distinct functional subgroups within the NDNF neuron population: a "freezing-on" subgroup, where NDNF INs maintain activity during freezing episodes, and a "freezing-off" subgroup, where NDNF

neuron activity decreases during freezing but increases during non-freezing states.

3.4 Longitudinal analysis of NDNF neuronal activity

In order to quantify changes in BLA^{Ndnf} neural activity under different experimental conditions across sessions or days, we employed a longitudinal registration analysis. Identifying the same cells across different imaging sessions can be challenging, particularly when using a one-photon head-mounted calcium imaging microscope compared to a two-photon setup. This difficulty arises from phenomena such as light scattering and the lack of optical sectioning in one-photon imaging, which increase the potential for crosstalk between adjacent cells in the same field of view (FOV). As a result, distinguishing the same cells across days becomes more difficult, as it is harder to separate individual cells from others within the FOV[153]. The number of behavioral sessions, as well as the timing of recordings, and whether they are conducted across consecutive days or spread over weeks, are also important considerations. These factors can influence cell identification consistency, particularly when the same FOV contains a high number of detected cells[153].

In our calcium imaging sessions, we carefully monitored the number of cells detected across sessions, such as between habituation and TMT exposure, and across consecutive days during CFC experiments. The number of detected $NDNF^{+}$ interneurons per FOV was 17 cells on average (n = 4 mice), allowing us to track and analyse the same activity of the same cells with better precision. Additionally, our experiments were conducted over a maximum of two days, which facilitated cell activity tracking without complications. This cell count was expected considering the relatively low number of GABAergic cells in the BLA

(~20% of total BLA neurons) and our HCR analysis, which showed an average of 13 Ndnf^{+} cells/20 µm BLA slice.

In both the CFC and TMT experiments, we successfully tracked the same cells and observed distinct activity patterns within specific cell subsets. Notably, some cells showed increased activity during pre-stimulus and recall phases, with reduced activity during the conditioning phase (day1) and stimulus anticipation (day 2). Conversely, another subset displayed the opposite trend, with increased activity during conditioning and anticipation phases, yet lower activity during pre-stimulus and recall phases. We had the same activities patterns during predator odour behaviour. These results suggest that distinct NDNF IN subsets might contribute differently to aversive stimuli, providing valuable insights into the dynamic role of NDNF neurons in the BLA.

3.5 BLA^{Ndnf} macro and microcircuitry in fear and anxiety modulation

Recent research has identified that distinct BLA PNs play opposing roles in fear learning and freezing behavior: Rspo2^{+} PNs facilitate fear conditioning and freezing, while Lypd1^{+} PNs support appetitive behavior and decrease freezing following fear learning[13]. Based on this model, it is plausible that NDNF neurons exert direct inhibitory control over these PN subpopulations. "Freezing-on" NDNF neurons might primarily inhibit Lypd1^{+} PNs, whose inhibition promotes freezing behavior. During non-freezing episodes, however, the activity of "freezing-on" neurons would decrease, allowing Lypd1^{+} PNs to facilitate non-freezing behaviors. In contrast, "freezing-off" NDNF neurons likely inhibit Rspo2^{+} PNs; when "freezing-off" neurons are active during non-freezing

episodes, Rspo2^{+} PNs are inhibited, thereby reducing freezing. During freezing episodes, the suppression of "freezing-off" neurons would allow Rspo2^{+} PNs to promote freezing behavior (**Fig. 10**). This model provides a cohesive framework linking specific BLA^{Ndnf} ensembles to distinct functional roles in modulating freezing and non-freezing states.

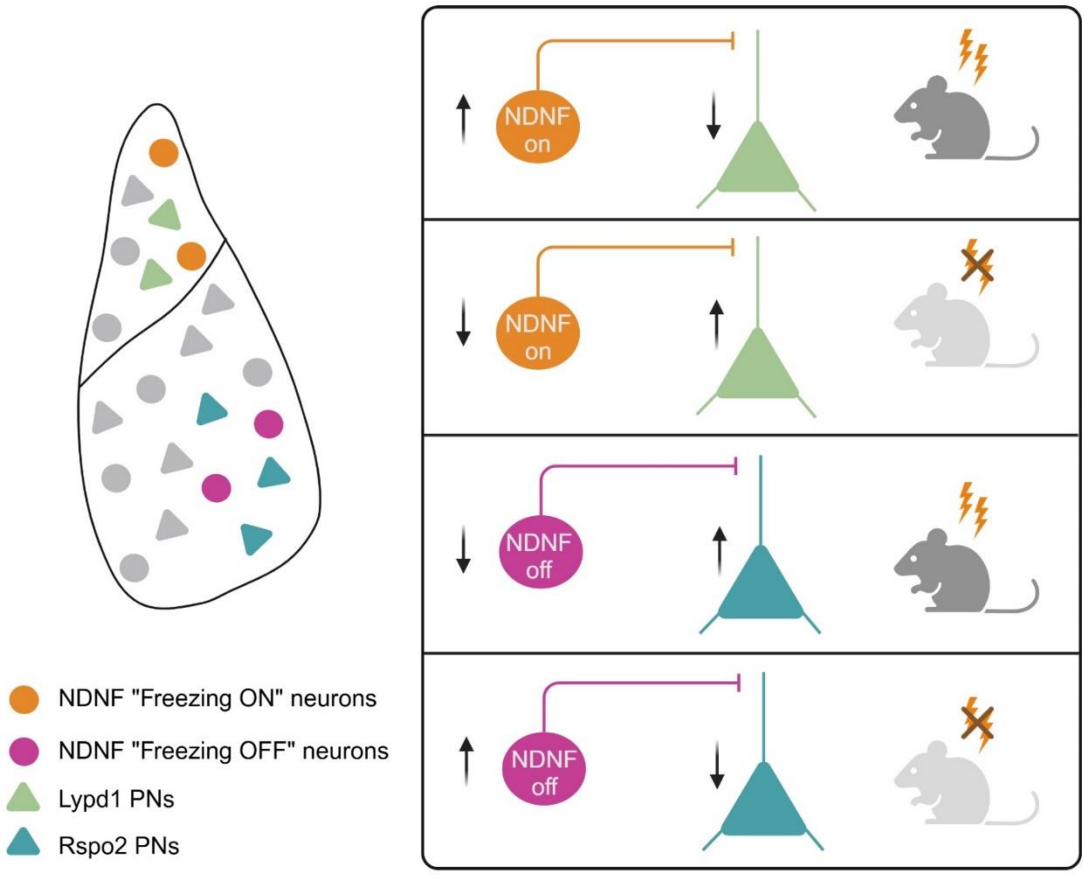

Fig. 10 – Fear microcircuit of NDNF "ON" and "OFF" neurons.
The NDNF microcircuit involved in freezing behaviors is depicted with color-coded neurons: NDNF "freezing-on" neurons are shown in orange, NDNF "freezing-off" neurons in purple, Lypd1^{+} PNs in green, and Rspo2^{+} PNs in blue. From top to bottom: an active NDNF "ON" neuron inhibits Lypd1^{+} PNs, promoting freezing; a less active NDNF "ON" neuron disinhibits Lypd1^{+} PNs, promoting non-freezing behavior; a less active NDNF "OFF" neuron disinhibits Rspo2^{+} PNs, promoting freezing; and an active NDNF "OFF" neuron inhibits Rspo2^{+} PNs, promoting non-freezing behavior.

Our primary hypothesis in order to better understand the nature of these two ensembles, was formulated based on our HCR data set. In our analysis, approximately 80% of Ndnf cells in the BLA express Npy, leaving the remaining 20% to be $Ndnf^{+}/Npy^{-}$ cells. This is in line with previous studies[73] which identified two types of NDNF IN in cortical layer 1: $NDNF^{+}/NPY^{+}$ (NGF cells) and $NDNF^{+}/NPY^{-}$ (canopy cells), which are characterized by different molecular, morphological, and electrophysiological properties[110]. Therefore, we might speculate that the distinct activity patterns observed in our calcium imaging data could be shaped in different and opposite ways by both $NDNF^{+}/NPY^{+}$ and $NDNF^{+}/NPY^{-}$ cell populations.

To gather compelling evidence in support of this model, future experiments could employ transgenic mouse lines and advanced imaging techniques to dissect the roles of $NDNF^{+}/NPY^{+}$ and $NDNF^{+}/NPY^{-}$ subpopulations in modulating aversive behaviors. A valuable step would involve the use of Flp recombinase enzymes to develop new mouse lines such as Lypd1-Flp and Rspo2-Flp, which would allow for the selective manipulation of $Lypd1^{+}$ and $Rspo2^{+}$ PNs populations within the BLA. Combined with NDNF-Cre or NPY-Cre driver lines, this approach would enable precise targeting of specific neuron subtypes to study how NDNF INs engage with these two populations.

For instance, crossing NDNF-Cre with an NPY-Flp line could facilitate selective optogenetic activation or inhibition of $NDNF^{+}/NPY^{+}$ cells while sparing $NDNF^{+}/NPY^{-}$ cells. Conversely, an NDNF-Cre line combined with a viral Cre-off system strategy, could target $NDNF^{+}/NPY^{-}$ cells selectively[154]. By using *in vivo* calcium imaging and optogenetic manipulations in these lines, we could

measure specific behavioral and neuronal responses to both conditioned and unconditioned stimuli.

Additionally, *ex vivo* patch-clamp recordings in brain slices would provide valuable insights into how NDNF^{+}/NPY^{+} and NDNF^{+}/NPY^{-} cells interact with Rspo2^{+} and Lypd1^{+} PNs. This approach could clarify whether NDNF^{+}/NPY^{+} cells preferentially inhibit Lypd1^{+} neurons to support freezing, while NDNF^{+}/NPY^{-} cells modulate Rspo2^{+} neurons to influence non-freezing behaviors, or viceversa. Finally, transcriptomic profiling of activity-specific neurons using scRNA-seq could identify molecular markers that further differentiate these subpopulations, shedding light on potential synaptic pathways involved in their differential roles in fear and anxiety regulation.

The opposite roles of BLA^{Ndnf} neurons in conditioned and innate behaviors might provide insights into the microcircuitry of the BLA. However, it is also important to consider the diversity of inputs received by NDNF IN. Classically, the mPFC, EC, BNST, AC and hippocampus have been described as substrates for the acquisition and extinction of fear memories and anxiety-related behaviors, including social interactions, providing the primary flow of information to the BLA[31,49,96]. The recruitment of these brain regions can vary depending on the saliency and type of stimulus (conditioned, unconditioned, or innate), hormonal responses to potential threats, neurotransmitter release, and the animal's internal state[98,99]. Previous studies took advantage of monosynaptic rabies tracing approach to identify specific brain-wide inputs to VIP, SST, and PV IN[45]. This work delineates an intriguing macrocircuit, revealing inputs from regions such as the insular cortex, basal forebrain, thalamus, and auditory cortex, which

might contribute to the already known role of these INs in regulating associative fear learning[45].

Following a similar logic, we used a combination of AAV2/5-synP-DIO-sTpEpB-GFP and RV-N2C dG-mCherry viruses to perform monosynaptic rabies tracing to target the specific inputs that NDNF INs receive in the BLA. Our findings reveal that NDNF INs in the BLA receive prominent inputs from the CP and the plCoA. This distinct input pattern suggests that NDNF INs are part of a separate macrocircuit from other BLA INs types. The CP, previously implicated in safety signal processing, is known to support adaptive responses to aversive stimuli based on learned experiences, allowing mice to accurately respond to contexts that are no longer threatening[118,119]. Inputs from olfactory regions have been characterized in studies examining NDNF INs inputs in the MeA, showing a different connectivity profile from that of SST neurons within the same region[155]. Given the role of the CoA in mediating olfactory valence, influencing attraction or aversion to specific odors[66], our data suggest that NDNF IN could modulate behavioral responses in contexts involving aversive olfactory cues, as seen in our TMT experiments. This unique macrocircuitry highlights the role of NDNF neurons in integrating inputs related to safety and olfactory valence, distinguishing them from other BLA INs types.

3.6 NDNF neuron dynamics in the motor cortex: hyperexcitability and implications for HD pathogenesis

This study advances our understanding of cortical hyperexcitability mechanisms in HD by demonstrating, for the first time, that M1 NDNF INs in layer 1 of the neocortex display increased excitability in R6/2 mice. While previous work identified hyperactivity and disrupted interneuron function in layers 2/3 of motor (M1) and prefrontal (PFC) cortices, we show that M1 NDNF INs actively modulate transitions between different behavioral states with age dependent changes. In particular, our 2-photon *in vivo* experiments show that $M1^{Ndnf}$ IN display an increase in calcium activity at locomotion onset (or active state), with reduced activity during transitions to “quiet” states, while maintaining an overall increased activity in R6/2 mice compared to littermate controls. Interestingly, $M1^{Ndnf}$ IN in R6/2 mice display altered excitability already during pre-symptomatic stages. These alterations may disrupt cortical E/I balance, potentially enhancing the cortical hyperexcitability associated with HD. Our findings further suggest that NDNF INs work alongside other interneurons, such as VIP^{+} INs, which are activated by locomotion, to regulate the activity of CPNs. Specifically, increased activity in NDNF INs at locomotion onset in R6/2 mice may contribute to the disinhibition of CPN somata in deeper cortical layers. Additionally, NDNF INs are known to provide sustained inhibition to the apical dendrites[73,140] of CPNs, adding a layer of complexity to cortical hyperexcitability in HD that calls for caution before further exploration of how different IN subtypes influence network dynamics. Previous studies have not aligned neural activity changes with behavior, nor have they examined different behavioral classifications as we did in this study. Further research should investigate the

role of other interneurons during behavioral paradigms, such as wheel running, to help construct a potential mechanism that could explain the cortical alterations commonly observed in HD.

In a representative case, we also identified two functionally distinct ensembles of NDNF INs: one associated with locomotion and another that is anti-correlated with locomotion. This subdivision may correspond to molecularly distinct NDNF subtypes, potentially linked to NPY co-expression, though further investigation is required to clarify these the relation between functional and cellular identity.

Transcriptomic analysis confirmed that NDNF INs in the R6/2 model, classified within the broader Lamp5 interneuron population, display a significant downregulation of Ndnf and GABAergic receptor genes, beginning at 8 weeks of age. This finding complements earlier research[80] that demonstrated protein expression changes in PV, SST, and VIP INs, highlighting NDNF IN as another population affected by HD. The downregulation of inhibitory GABAergic receptors in NDNF cells may partly explain the increased calcium excitability observed in NDNF INs *in vivo*. Importantly, in other neurodegenerative diseases such as AD, a study using scRNA transcriptomic profiling of the adult PFC in AD patients[156] revealed a significant reduction in the $Reln^{+}/Lamp5^{+}$ that was associated with poorer cognitive and memory scores during cognitive resilience testing, suggesting that these interneurons play a role in maintaining cognitive function, particularly in aging[156]. This finding raises intriguing questions about the potential role of NDNF IN in both AD and HD, especially in the context of learning and memory. Given their involvement in modulating cortical circuits, it would be interesting to investigate how NDNF INs contribute to cognitive decline in AD and HD. Specifically, studying how changes in NDNF

interneuron activity may impact synaptic plasticity and memory-related behaviors could provide valuable insights into the mechanisms of cognitive dysfunction in these diseases.

Given the intrinsic hyperactivity of NDNF INs in early HD, further research is needed to clarify how this hyperexcitability impacts other IN classes and CPNs. Behavioral studies in symptomatic HD mice will help determine how NDNF hyperexcitability evolves as motor symptoms appear. Additionally, investigating mHTT inclusion formation in NDNF INs could help confirm their involvement in HD pathogenesis, as other interneuron types (PV, SST, VIP) are known to develop mHTT inclusions. For instance, markers for mHTT, such as the EM48 antibody, could provide further insights into the development of mHTT inclusions in NDNF INs, potentially revealing similarities with other major IN classes. Previous studies[80] have shown that mHTT inclusions develop more frequently and are larger in CPNs compared to interneurons; however, by 8 weeks of age, mHTT inclusions have also been observed in R6/2 interneurons.

It is also important to acknowledge the limitations of our study. Although we were able to demonstrate changes in NDNF IN activity during the presymptomatic stages of HD, before the onset of motor symptoms, further *in vivo* and electrophysiological studies are needed in fully symptomatic R6/2 mice. Such studies would help clarify the causal relationship between NDNF hyperexcitability during locomotion and motor deficits in the later stages of HD-like symptom progression. Will this hyperexcitability persist, intensify, or be offset by compensatory mechanisms? These are compelling questions that future research should aim to address.

3.7 Scientific perspective and research outlook

The present work identifies NDNF INs as important regulators of both fear and motor-related behaviors, with potential implications for understanding pathological processes in anxiety, PTSD, and HD. However, several questions remain open and may define important directions for future research.

Although originally described in the L1 of the neocortex as key regulators of long-range and modulatory inputs[35,110], in the present study, NDNF INs emerge as important neuronal subclass not only in shaping fear-related responses in the BLA but also in motor function within the M1 of an HD mouse model. Previous studies in cortical L1[110] identified two types of NDN INs: $NDNF^{+}/NPY^{+}$ (neurogliaform cells) and $NDNF^{+}/NPY^{-}$ (canopy cells), which can be distinguished by their molecular, morphological, and electrophysiological profiles. Our HCR dataset suggests a similar division in the BLA, with approximately 80% of $Ndnf^{+}$ cells co-expressing Npy. We hypothesize that the distinct calcium dynamics observed in our *in vivo* experiments, may reflect the presence of these two functionally different populations. However, recent studies in cortical L1[73] caution against using NPY expression alone to define functionally distinct NDNF subclasses in adult brains. While NPY co-expression is useful to distinguish NDNF subtypes in the juvenile cortex, this specificity appears to diminish with age due to broader NPY expression and limited physiological or connectivity differences between NPY^{+} and NPY^{-} cells. Whether similar expression pattern occurs in the BLA remains unknown. Given the anatomical and developmental distinctions of this region, future studies should explore whether NPY continues to delineate meaningful subpopulations

of NDNF INs in the adult BLA. This could involve intersectional genetics, transcriptomic profiling, and *in vivo* optogenetics approaches.

For example, intersectional genetic tools (i.e., NDNF-Cre x NPY-Flp or Cre-off viral strategies) could be employed to selectively manipulate $NDNF^{+}/NPY^{+}$ and $NDNF^{+}/NPY^{-}$ populations. Similarly, combining NDNF-Cre drivers with novel Flp mouse lines targeting BLA projection neurons, such as Lypd1-Flp or Rspo2-Flp, could reveal how NDNF INs modulate specific fear-related downstream pathways.

The intrinsic and *in vivo* activities change of NDNF INs in the early stages of HD, before evident motor symptoms appear, highlights their involvement into pathophysiological changes and their potential contribution to HD onset.

Further studies in symptomatic R6/2 mice are needed to determine whether these changes persist and evolve. Does NDNF IN hyperactivity drive later disease stages motor dysfunction, or is it counterbalanced by compensatory mechanisms? *In vivo* electrophysiology and behavioral assays in later stages of disease progression of R6/2 animals will be required to approach this open yet important question. Lastly, our findings emphasise the dynamic role of NDNF INs across behavioral domains, from regulating fear expression to maintaining motor control. Future work should continue to investigate how state-dependent changes in NDNF INs activity shape neural circuit functions.

3.8 Conclusions

The aim of this study was to investigate the molecular characteristics and organization of NDNF INs within the BLA, examine their potential role in fear- and anxiety-related behaviors, and determine how *in vivo* NDNF activity might reveal their modulatory influence. Their unique form of inhibition, previously studied in the neocortical layer 1, prompted us to explore the role of NDNF INs in the microcircuits of the HD cortical network. Through a combination of *in situ* hybridization, behavioral analysis, diverse viral techniques, *in vivo* calcium imaging (both one-photon and two-photon approaches), and electrophysiology, we made substantial contributions to understanding the role of NDNF INs and the mechanisms by which they modulate fear behaviors and locomotion in presymptomatic HD mice.

In conclusion, this study provides the first comprehensive molecular, behavioral, and functional characterization of NDNF INs, revealing their critical involvement across two distinct brain regions and behavioral contexts. In the BLA, NDNF INs are actively recruited during fear acquisition and exposure to TMT, driving freezing responses. This behavior may rely on the disinhibitory actions of BLA^{Ndnf} neurons, which influence specific projection neurons within the BLA and potentially interact with downstream regions to modulate responses based on stimulus salience. Our findings suggest that two molecularly distinct NDNF INs ensembles may contribute to flexible response dynamics in fear and anxiety states, with implications for disorders such as anxiety and PTSD. Further research would allow us to understand the molecular profile of these two functionally different NDNF IN in the BLA and how they cooperatively or antagonistically modulate fear behaviours.

Additionally, in the M1 cortex of HD models, we demonstrate that NDNF INs undergo early molecular and functional changes, preceding motor symptoms onset. Our results indicate that these changes may disrupt cortical E/I balance, contributing to early cortical circuit dysfunction in HD. The role of NDNF INs appears to shift across behavioral states, highlighting their importance in maintaining neural stability and adapting network responses to animal's behaviour. Taken together, this work emphasises the central role of NDNF INs in modulating both fear and motor-related behaviors, laying the groundwork for future studies to further clarify how disruptions in NDNF circuits could contribute to neurological and psychiatric conditions.

4. APPENDIX

4.1 Affidavit

Herewith I confirm that I wrote the accompanying PhD Thesis / Admission thesis myself:

Title: Characterization of NDNF neurons in the mouse basolateral amygdala and in the primary motor cortex of a Huntington's disease model

In the thesis no other sources and aids have been used than those indicated.

The passages of the thesis that are taken in wording or meaning from other sources have been marked with an indication of the sources (including the World Wide Web and other electronic text and data collections).

Furthermore, all parts of the thesis that were *de novo* generated with the help of artificial intelligence tools were identified by footnotes/annotations at the appropriate places and the artificial intelligence tools used were listed. The prompts used were listed in the appendix. This statement applies to all text, graphics, drawings, sketch maps, and pictorial representations contained in the Work.

X (Native speaker) Proof-reading of the work otherwise written without outside help

Munich, 26/11/2024

(Location/date)

YLENIA MASTRODICASA

(First and last name in block letters)

Ylenia, Mastrodicasa

(Signature)

4.2 Declaration of author contribution

Manuscript 1: "**Conditioned and Innate Fear responses are mediated by Basolateral Amygdala Ndnf-expressing neurons**"

Ylenia Mastrodicasa*, Federica Fermani, Maria Fernanda Frutos Marquez, Rüdiger Klein

YM and RK conceptualized the study and designed the experiments. YM performed most of the experiments. FF supported with *in vivo* calcium recording experiments and analysis, MFFM performed and analysed *in situ* hybridization experiments and assisted with immunohistochemistry, histology, microscopy, and image processing. YM and RK wrote the manuscript with inputs form all authors. RK supervised and provided funding.

My contribution to this manuscript in detail:

- For this study I participated in designing the experiments, performing experiments, data analysis, image processing, creating graphs and visuals for experimental paradigms, wrote and edited the manuscript.
- I performed stereotaxic injections and procedures, including optic fibers implants and participated in GRIN lens and baseplate implants.
- I performed and analysed behavioral experiments, including cFos experiments.
- I collected and analysed monosynaptic rabies tracings data.
- I designed and supervised *in situ* hybridization experiments and analysis.

Manuscript 2: “**NDNF interneurons activity is altered in a mouse model of Huntington's Disease**”

Ylenia Mastrodicasa*, Sonja Blumenstock*, Dennis Feigenbutz, Irina Dudanova, Rüdiger Klein

YM, SB and RK conceptualized the study, DF performed and analysed snRNA-seq experiments, SB performed *in vivo* 2-photon experiments and analysed calcium and behavioral data, YM performed electrophysiological experiments *ex vivo*, collected and analysed whole-cell current- clamp and voltage-clamp recordings. YM and RK wrote the manuscript with the contribution of SB and DF. ID, provided support on the R6/2 mouse line, RK supervised and provided funding.

My contribution to this manuscript in detail:

For this study I designed, performed and analysed all electrophysiological experiments. I have performed stereotaxic injections of AAV9 cre-dependent GCaMP7f in the M1 of R6/2 and littermate control mice to be patched at 9 weeks of age. I performed immunohistochemistry and imaging of NDNF neurons filled with biocytin during *ex vivo* patch-clamp recordings.

Ylenia Mastrodicasa

Sonja Blumenstock

Prof. Dr. Ruediger Klein

5. BIBLIOGRAPHY

Disclaimer: In the process of writing this thesis, AI language model provided by OpenAI, such as ChatGPT (https://chatgpt.com/) was used for different parts of chapters 1, 2 and 3.

---

[1] Anna Beyeler and Joanna Dabrowska, 'Neuronal Diversity of the Amygdala and the Bed Nucleus of the Stria Terminalis', Handbook of Behavioral Neuroscience, 26 (2020), pp. 63–100, doi:10.1016/b978-0-12-815134-1.00003-9.

[2] P. Sah and others, 'The Amygdaloid Complex: Anatomy and Physiology', *Physiological Reviews*, 83.3 (2003), pp. 803–34, doi:10.1152/physrev.00002.2003.

[3] Michele Pignatelli and Anna Beyeler, 'Valence Coding in Amygdala Circuits', Current Opinion in Behavioral Sciences, 26 (2019), pp. 97–106, doi:10.1016/j.cobeha.2018.10.010.

[4] Asla Pitkänen, Vesa Savander, and Joseph E. LeDoux, 'Organization of Intra-Amygdaloid Circuitries in the Rat: An Emerging Framework for Understanding Functions of the Amygdala', Trends in Neurosciences, 20.11 (1997), pp. 517–23, doi:10.1016/S0166-2236(97)01125-9.

[5] Tania Aerts and Eve Seuntjens, 'Novel Perspectives on the Development of the Amygdala in Rodents', Frontiers in Neuroanatomy, 15 (2021), doi:10.3389/fnana.2021.786679.

[6] Jacqueline Giovanniello and others, 'A Central Amygdala-Globus Pallidus Circuit Conveys Unconditioned Stimulus-Related Information and Controls Fear Learning', The Journal of Neuroscience, 40.47 (2020), pp. 9043–54, doi:10.1523/JNEUROSCI.2090-20.2020.

[7] Kenneth M. McCullough and others, 'Quantified Coexpression Analysis of Central Amygdala Subpopulations', *eNeuro*, 5.1 (2018), doi:10.1523/ENEURO.0010-18.2018.

[8] Jay F. Muller, Franco Mascagni, and Alexander J. McDonald, 'Postsynaptic Targets of Somatostatin-Containing Interneurons in the Rat Basolateral Amygdala', Journal of Comparative Neurology, 500.3 (2007), pp. 513–29, doi:10.1002/cne.21185.

[9] Norbert Hájos, 'Interneuron Types and Their Circuits in the Basolateral Amygdala', Frontiers in Neural Circuits, 15 (2021), doi:10.3389/fncir.2021.687257.

[10] Viktória K. Vereczki and others, 'Total Number and Ratio of GABAergic Neuron Types in the Mouse Lateral and Basal Amygdala', Journal of Neuroscience, 41.21 (2021), pp. 4575–95, doi:10.1523/JNEUROSCI.2700-20.2021.

[11] Euiseok J. Kim and others, 'Extraction of Distinct Neuronal Cell Types from within a Genetically Continuous Population', Neuron, 107.2 (2020), pp. 274-282.e6, doi:10.1016/j.neuron.2020.04.018.

[12] Houri Hintiryan and Hong-Wei Dong, 'Brain Networks of Connectionally Unique Basolateral Amygdala Cell Types', Neuroscience Insights, 17 (2022), p. 26331055221080175, doi:10.1177/26331055221080175.

[13] Hansol Lim and others, 'Genetically- and Spatially-Defined Basolateral Amygdala Neurons Control Food Consumption and Social Interaction', *Nature Communications*, 15.1 (2024), p. 6868, doi:10.1038/s41467-024-50889-7.

[14] Aaron M. Jasnow and others, 'Thy1-Expressing Neurons in the Basolateral Amygdala May Mediate Fear Inhibition', *The Journal of Neuroscience*, 33.25 (2013), pp. 10396–404, doi:10.1523/JNEUROSCI.5539-12.2013.

[15] Kenneth M. McCullough and others, 'Molecular Characterization of Thy1 Expressing Fear-Inhibiting Neurons within the Basolateral Amygdala', *Nature Communications*, 7.1 (2016), p. 13149, doi:10.1038/ncomms13149.

[16] Kasra Manoocheri and Adam G Carter, 'Rostral and Caudal Basolateral Amygdala Engage Distinct Circuits in the Prelimbic and Infralimbic Prefrontal Cortex', ed. by John R Huguenard, *eLife*, 11 (2022), p. e82688, doi:10.7554/eLife.82688.

[17] Alexander J. McDonald, 'Neurons of the Lateral and Basolateral Amygdaloid Nuclei: A Golgi Study in the Rat', The Journal of Comparative Neurology, 212.3 (1982), pp. 293–312, doi:10.1002/cne.902120307.

[18] Samuli Kemppainen and Asla Pitkänen, 'Distribution of Parvalbumin, Calretinin, and Calbindin-D28k Immunoreactivity in the Rat Amygdaloid Complex and Colocalization with γ-Aminobutyric Acid', Journal of Comparative Neurology, 426.3 (2000), pp. 441–67, doi:10.1002/1096-9861(20001023)426:3<441::AID-CNE8>3.0.CO;2-7.

[19] Sabine Krabbe, Jan Gründemann, and Andreas Lüthi, 'Amygdala Inhibitory Circuits Regulate Associative Fear Conditioning', *Biological Psychiatry*, Molecular Signatures of Stress and Posttraumatic Stress Disorder, 83.10 (2018), pp. 800–09, doi:10.1016/j.biopsych.2017.10.006.

[20] A. J McDonald and F Mascagni, 'Colocalization of Calcium-Binding Proteins and GABA in Neurons of the Rat Basolateral Amygdala', Neuroscience, 105.3 (2001), pp. 681–93, doi:10.1016/S0306-4522(01)00214-7.

[21] Donald Gordon Rainnie and others, 'Physiological and Morphological Characterization of Parvalbumin-Containing Interneurons of the Rat Basolateral Amygdala', Journal of Comparative Neurology, 498.1 (2006), pp. 142–61, doi:10.1002/cne.21049.

[22] Alexander J McDonald and Franco Mascagni, 'Immunohistochemical Characterization of Somatostatin Containing Interneurons in the Rat Basolateral Amygdala', Brain Research, 943.2 (2002), pp. 237–44, doi:10.1016/S0006-8993(02)02650-1.

[23] E Mae Guthman and others, 'Cell-Type-Specific Control of Basolateral Amygdala Neuronal Circuits via Entorhinal Cortex-Driven Feedforward Inhibition', eLife, 9 (2020), p. e50601, doi:10.7554/eLife.50601.

[24] Ludmila Sosulina, Stéphanie Graebenitz, and Hans-Christian Pape, 'GABAergic Interneurons in the Mouse Lateral Amygdala: A Classification Study', Journal of Neurophysiology, 104.2 (2010), pp. 617–26, doi:10.1152/jn.00207.2010.

[25] Aaron M. Jasnow and others, 'Distinct Subtypes of Cholecystokinin (CCK)-Containing Interneurons of the Basolateral Amygdala Identified Using a CCK Promoter-Specific Lentivirus', *Journal of Neurophysiology*, 101.3 (2009), pp. 1494–506, doi:10.1152/jn.91149.2008.

[26] István Katona and others, 'Distribution of CB1 Cannabinoid Receptors in the Amygdala and Their Role in the Control of GABAergic Transmission', Journal of Neuroscience, 21.23 (2001), pp. 9506–18, doi:10.1523/JNEUROSCI.21-23-09506.2001.

[27] F. Mascagni and A. J. McDonald, 'A Novel Subpopulation of 5-HT Type 3A Receptor Subunit Immunoreactive Interneurons in the Rat Basolateral Amygdala', Neuroscience, 144.3 (2007), pp. 1015–24, doi:10.1016/j.neuroscience.2006.10.044.

[28] Franco Mascagni and Alexander J. McDonald, 'Immunohistochemical Characterization of Cholecystokinin Containing Neurons in the Rat Basolateral Amygdala', Brain Research, 976.2 (2003), pp. 171–84, doi:10.1016/S0006-8993(03)02625-8.

[29] Thomas Rhomberg and others, 'Vasoactive Intestinal Polypeptide-Immunoreactive Interneurons within Circuits of the Mouse Basolateral Amygdala', The Journal of Neuroscience, 38.31 (2018), pp. 6983–7003, doi:10.1523/JNEUROSCI.2063-17.2018.

[30] Indira Nederpelt and others, 'Kinetic Profile of Neuropeptide–Receptor Interactions', Trends in Neurosciences, 39.12 (2016), pp. 830–39, doi:10.1016/j.tins.2016.09.008.

[31] Maria Bompolaki and others, 'Activation of NPY Receptors in the BLA Inhibits Projections to the Bed Nucleus of the Stria Terminalis and Buffers Stress-Induced Decreases in Social Interaction in Male Rats', *Journal of Neuroscience*, 44.34 (2024), doi:10.1523/JNEUROSCI.0228-24.2024.

[32] Randy J. Leitermann, Amanda B. Rostkowski, and Janice H. Urban, 'Neuropeptide Y Input to the Rat Basolateral Amygdala Complex and Modulation by Conditioned Fear', Journal of Comparative Neurology, 524.12 (2016), pp. 2418–39, doi:10.1002/cne.23960.

[33] Xiu-Li Kuang and others, 'Spatio-Temporal Expression of a Novel Neuron-Derived Neurotrophic Factor (NDNF) in Mouse Brains during Development', *BMC Neuroscience*, 11.1 (2010), p. 137, doi:10.1186/1471-2202-11-137.

[34] Bosiljka Tasic and others, 'Adult Mouse Cortical Cell Taxonomy Revealed by Single Cell Transcriptomics', *Nature NEUROSCIENCE*, 19.2 (2016), p. 18.

[35] Elisabeth Abs and others, 'Learning-Related Plasticity in Dendrite-Targeting Layer 1 Interneurons', *Neuron*, 100.3 (2018), pp. 684-699.e6, doi:10.1016/j.neuron.2018.09.001.

[36] Attila Ozsvár and others, 'A Combinatory Genetic Strategy for Targeting Neurogliaform Neurons in the Mouse Basolateral Amygdala', *Frontiers in Cellular Neuroscience*, 18 (2024), p. 1254460, doi:10.3389/fncel.2024.1254460.

[37] Miho TERUNUMA, 'Diversity of Structure and Function of GABAB Receptors: A Complexity of GABAB-Mediated Signaling', *Proceedings of the Japan Academy. Series B, Physical and Biological Sciences*, 94.10 (2018), pp. 390–411, doi:10.2183/pjab.94.026.

[38] Eric M. Prager and others, 'The Basolateral Amygdala Γ-aminobutyric Acidergic System in Health and Disease', Journal of Neuroscience Research, 94.6 (2016), pp. 548–67, doi:10.1002/jnr.23690.

[39] Marion S. Mercier and others, *Long-Term Potentiation in Neurogliaform Cells Modulates Excitation-Inhibition Balance in the Temporoammonic Pathway* (Neuroscience, 27 January 2019), doi:10.1101/531822.

[40] Caren Armstrong, Esther Krook-Magnuson, and Ivan Soltesz, 'Neurogliaform and Ivy Cells: A Major Family of nNOS Expressing GABAergic Neurons', *Frontiers in Neural Circuits*, 6 (2012), doi:10.3389/fncir.2012.00023.

[41] Yi-Ting Hsu, Ya-Gin Chang, and Yijuang Chern, 'Insights into GABAAergic System Alteration in Huntington's Disease', *Open Biology*, 8.12 (2018), p. 180165, doi:10.1098/rsob.180165.

[42] Alessandra P. Princivalle, 'GABAB Receptors in Neurodegeneration', in *Behavioral Neurobiology of GABAB Receptor Function*, ed. by Styliani Vlachou and Kevin Wickman (Springer International Publishing, 2022), pp. 267–90, doi:10.1007/7854_2021_222.

[43] Jai S. Polepalli, Helen Gooch, and Pankaj Sah, 'Diversity of Interneurons in the Lateral and Basal Amygdala', Npj Science of Learning, 5.1 (2020), p. 10, doi:10.1038/s41539-020-0071-z.

[44] Boglárka Barsy and others, 'Different Output Properties of Perisomatic Region-Targeting Interneurons in the Basal Amygdala', European Journal of Neuroscience, 45.4 (2017), pp. 548–58, doi:10.1111/ejn.13498.

[45] Sabine Krabbe and others, 'Adaptive Disinhibitory Gating by VIP Interneurons Permits Associative Learning', Nature Neuroscience, 22.11 (2019), pp. 1834–43, doi:10.1038/s41593-019-0508-y.

[46] Marco Capogna, 'GABAergic Cell Type Diversity in the Basolateral Amygdala', Current Opinion in Neurobiology, 26 (2014), pp. 110–16, doi:10.1016/j.conb.2014.01.006.

[47] Patricia H. Janak and Kay M. Tye, 'From Circuits to Behaviour in the Amygdala', Nature, 517.7534 (2015), pp. 284–92, doi:10.1038/nature14188.

[48] Wen-Hua Zhang and others, 'Amygdala Circuit Substrates for Stress Adaptation and Adversity', *Biological Psychiatry*, Stress Vulnerability and Moderators of Stress Response, 89.9 (2021), pp. 847–56, doi:10.1016/j.biopsych.2020.12.026.

[49] Eduardo E. Benarroch, 'The Amygdala', *Neurology*, 84.3 (2015), pp. 313–24, doi:10.1212/WNL.0000000000001171.

[50] Kerry J. Ressler, 'Amygdala Activity, Fear, and Anxiety: Modulation by Stress', *Biological Psychiatry*, 67.12 (2010), pp. 1117–19, doi:10.1016/j.biopsych.2010.04.027.

[51] Jing Liu and others, 'Differential Efferent Projections of GABAergic Neurons in the Basolateral and Central Nucleus of Amygdala in Mice', *Neuroscience Letters*, 745 (2021), p. 135621, doi:10.1016/j.neulet.2020.135621.

[52] Nowrin Ahmed and Denis Paré, 'The Basolateral Amygdala Sends a Mixed (GABAergic and Glutamatergic) Projection to the Mediodorsal Thalamic Nucleus', *Journal of Neuroscience*, 43.12 (2023), pp. 2104–15, doi:10.1523/JNEUROSCI.1924-22.2022.

[53] Joshua Kim and others, 'Antagonistic Negative and Positive Neurons of the Basolateral Amygdala', *Nature Neuroscience*, 19.12 (2016), pp. 1636–46, doi:10.1038/nn.4414.

[54] Wei Tang and others, 'A VTA to Basal Amygdala Dopamine Projection Contributes to Signal Salient Somatosensory Events during Fear Learning', *Journal of Neuroscience*, 40.20 (2020), pp. 3969–80, doi:10.1523/JNEUROSCI.1796-19.2020.

[55] Anthony Burgos-Robles and others, 'Amygdala Inputs to Prefrontal Cortex Guide Behavior amid Conflicting Cues of Reward and Punishment', *Nature Neuroscience*, 20.6 (2017), pp. 824–35, doi:10.1038/nn.4553.

[56] David E. Moorman and Gary Aston-Jones, 'Prefrontal Neurons Encode Context-Based Response Execution and Inhibition in Reward Seeking and Extinction', *Proceedings of the National Academy of Sciences*, 112.30 (2015), pp. 9472–77, doi:10.1073/pnas.1507611112.

[57] Dana M. Smith and Mary M. Torregrossa, 'Valence Encoding in the Amygdala Influences Motivated Behavior', *Behavioural Brain Research*, 411 (2021), p. 113370, doi:10.1016/j.bbr.2021.113370.

[58] Yajie Sun, Helen Gooch, and Pankaj Sah, 'Fear Conditioning and the Basolateral Amygdala', *F1000Research*, 9 (2020), p. F1000 Faculty Rev-53, doi:10.12688/f1000research.21201.1.

[59] Jeansok J. Kim and Min Whan Jung, 'Neural Circuits and Mechanisms Involved in Pavlovian Fear Conditioning: A Critical Review', *Neuroscience and Biobehavioral Reviews*, 30.2 (2006), pp. 188–202, doi:10.1016/j.neubiorev.2005.06.005.

[60] Anna Cattani and others, 'Basolateral Amygdala Oscillations Enable Fear Learning in a Biophysical Model', *bioRxiv*, 2024, p. 2023.04.28.538604, doi:10.1101/2023.04.28.538604.

[61] Elizabeth K. Lucas and Roger L. Clem, 'GABAergic Interneurons: The Orchestra or the Conductor in Fear Learning and Memory?', *Brain Research Bulletin*, 141 (2018), pp. 13–19, doi:10.1016/j.brainresbull.2017.11.016.

[62] Peter Curzon, Nathan R. Rustay, and Kaitlin E. Browman, 'Cued and Contextual Fear Conditioning for Rodents', in *Methods of Behavior Analysis in Neuroscience*, ed. by Jerry J. Buccafusco, Frontiers in Neuroscience, 2nd edn (CRC Press/Taylor & Francis, 2009).

[63] Phillip L. W. Colmers and others, 'Loss of PV Interneurons in the BLA Contributes to Altered Network and Behavioral States in Chronically Epileptic Mice' (bioRxiv, 7 December 2023), p. 2023.12.05.570112, doi:10.1101/2023.12.05.570112.

[64] Joanna Oi-Yue Yau and others, 'The Roles of Basolateral Amygdala Parvalbumin Neurons in Fear Learning', *The Journal of Neuroscience*, 41.44 (2021), pp. 9223–34, doi:10.1523/JNEUROSCI.2461-20.2021.

[65] Cory M. Root and others, 'The Participation of Cortical Amygdala in Innate, Odour-Driven Behaviour', *Nature*, 515.7526 (2014), pp. 269–73, doi:10.1038/nature13897.

[66] James R. Howe and others, 'Control of Innate Olfactory Valence by Segregated Cortical Amygdala Circuits', *bioRxiv*, 2024, p. 2024.06.26.600895, doi:10.1101/2024.06.26.600895.

[67] Valentina Khalil and others, 'Subcortico-Amygdala Pathway Processes Innate and Learned Threats', ed. by Mario A Penzo and Kate M Wassum, *eLife*, 12 (2023), p. e85459, doi:10.7554/eLife.85459.

[68] Gwendolyn G. Calhoon and Kay M. Tye, 'Resolving the Neural Circuits of Anxiety', *Nature Neuroscience*, 18.10 (2015), pp. 1394–404, doi:10.1038/nn.4101.

[69] Fan Jie and others, 'Stress in Regulation of GABA Amygdala System and Relevance to Neuropsychiatric Diseases', *Frontiers in Neuroscience*, 12 (2018), p. 562, doi:10.3389/fnins.2018.00562.

[70] Thomas Prévot and Etienne Sibille, 'Altered GABA-Mediated Information Processing and Cognitive Dysfunctions in Depression and Other Brain Disorders', *Molecular Psychiatry*, 26.1 (2021), pp. 151–67, doi:10.1038/s41380-020-0727-3.

[71] Janaina M. Zanoveli and others, 'Extracellular Serotonin Level in the Basolateral Nucleus of the Amygdala and Dorsal Periaqueductal Gray under Unconditioned and Conditioned Fear States: An *in Vivo* Microdialysis Study', *Brain Research*, 1294 (2009), pp. 106–15, doi:10.1016/j.brainres.2009.07.074.

[72] Jonas Waider and others, 'Serotonin Deficiency Increases Context-Dependent Fear Learning Through Modulation of Hippocampal Activity', *Frontiers in Neuroscience*, 13 (2019), doi:10.3389/fnins.2019.00245.

[73] Jan Hartung and others, 'Layer 1 NDNF Interneurons Are Specialized Top-down Master Regulators of Cortical Circuits', *Cell Reports*, 43.5 (2024), doi:10.1016/j.celrep.2024.114212.

[74] Alex Medina and others, 'Prevalence and Incidence of Huntington's Disease: An Updated Systematic Review and Meta-Analysis', *Movement Disorders*, 37.12 (2022), pp. 2327–35, doi:10.1002/mds.29228.

[75] Hannah S. Bakels and others, 'Juvenile-Onset Huntington Disease Pathophysiology and Neurodevelopment: A Review', *Movement Disorders*, 37.1 (2022), pp. 16–24, doi:10.1002/mds.28823.

[76] Sonja Blumenstock and Irina Dudanova, 'Cortical and Striatal Circuits in Huntington's Disease', *Frontiers in Neuroscience*, 14 (2020), doi:10.3389/fnins.2020.00082.

[77] John Labbadia and Richard I. Morimoto, 'Huntington's Disease: Underlying Molecular Mechanisms and Emerging Concepts', *Trends in Biochemical Sciences*, 38.8 (2013), pp. 378–85, doi:10.1016/j.tibs.2013.05.003.

[78] Aislinn J. Williams and Henry L. Paulson, 'Polyglutamine Neurodegeneration: Protein Misfolding Revisited', *Trends in Neurosciences*, 31.10 (2008), p. 521, doi:10.1016/j.tins.2008.07.004.

[79] Eric H. Kim and others, 'Cortical Interneuron Loss and Symptom Heterogeneity in Huntington Disease', *Annals of Neurology*, 75.5 (2014), pp. 717–27, doi:10.1002/ana.24162.

[80] Kerstin Voelkl and others, 'Distinct Histological Alterations of Cortical Interneuron Types in Mouse Models of Huntington's Disease', *Frontiers in Neuroscience*, 16 (2022), doi:10.3389/fnins.2022.1022251.

[81] Xiaofeng Gu and others, 'Pathological Cell-Cell Interactions Elicited by a Neuropathogenic Form of Mutant Huntingtin Contribute to Cortical Pathogenesis in HD Mice', *Neuron*, 46.3 (2005), pp. 433–44, doi:10.1016/j.neuron.2005.03.025.

[82] Laura Mangiarini and others, 'Exon 1 of the HD Gene with an Expanded CAG Repeat Is Sufficient to Cause a Progressive Neurological Phenotype in Transgenic Mice', *Cell*, 87.3 (1996), pp. 493–506, doi:10.1016/S0092-8674(00)81369-0.

[83] Liliana Menalled and others, 'Systematic Behavioral Evaluation of Huntington's Disease Transgenic and Knock-in Mouse Models', *Neurobiology of Disease*, 35.3 (2009), pp. 319–36, doi:10.1016/j.nbd.2009.05.007.

[84] Jia Yi Li, Natalija Popovic, and Patrik Brundin, 'The Use of the R6 Transgenic Mouse Models of Huntington's Disease in Attempts to Develop Novel Therapeutic Strategies', *NeuroRx*, 2.3 (2005), pp. 447–64.

[85] I. Dragatsis and others, 'CAG Repeat Lengths ≥335 Attenuate the Phenotype in the R6/2 Huntington's Disease Transgenic Mouse', *Neurobiology of Disease*, 33.3 (2009), p. 315, doi:10.1016/j.nbd.2008.10.009.

[86] Marcy E. MacDonald and others, 'A Novel Gene Containing a Trinucleotide Repeat That Is Expanded and Unstable on Huntington's Disease Chromosomes', *Cell*, 72.6 (1993), pp. 971–83, doi:10.1016/0092-8674(93)90585-E.

[87] Edward C. Stack and others, 'Chronology of Behavioral Symptoms and Neuropathological Sequela in R6/2 Huntington's Disease Transgenic Mice', *Journal of Comparative Neurology*, 490.4 (2005), pp. 354–70, doi:10.1002/cne.20680.

[88] Brian Y. Chow and others, 'High-Performance Genetically Targetable Optical Neural Silencing by Light-Driven Proton Pumps', *Nature*, 463.7277 (2010), pp. 98–102, doi:10.1038/nature08652.

[89] Valentina Emiliani and others, 'Optogenetics for Light Control of Biological Systems', *Nature Reviews Methods Primers*, 2.1 (2022), pp. 1–25, doi:10.1038/s43586-022-00136-4.

[90] Amy S. Chuong and others, 'Noninvasive Optical Inhibition with a Red-Shifted Microbial Rhodopsin', *Nature Neuroscience*, 17.8 (2014), pp. 1123–29, doi:10.1038/nn.3752.

[91] Georg Nagel and others, 'Channelrhodopsin-2, a Directly Light-Gated Cation-Selective Membrane Channel', *Proceedings of the National Academy of Sciences*, 100.24 (2003), pp. 13940–45, doi:10.1073/pnas.1936192100.

[92] Tsai-Wen Chen and others, 'Ultrasensitive Fluorescent Proteins for Imaging Neuronal Activity', *Nature*, 499.7458 (2013), pp. 295–300, doi:10.1038/nature12354.

[93] Karel Svoboda and Ryohei Yasuda, 'Principles of Two-Photon Excitation Microscopy and Its Applications to Neuroscience', *Neuron*, 50.6 (2006), pp. 823–39, doi:10.1016/j.neuron.2006.05.019.

[94] Yaniv Ziv and others, 'Long-Term Dynamics of CA1 Hippocampal Place Codes', *Nature Neuroscience*, 16.3 (2013), pp. 264–66, doi:10.1038/nn.3329.

[95] Guohong Cui and others, 'Deep Brain Optical Measurements of Cell Type–Specific Neural Activity in Behaving Mice', *Nature Protocols*, 9.6 (2014), pp. 1213–28, doi:10.1038/nprot.2014.080.

[96] Meryl Malezieux, Alexandra S. Klein, and Nadine Gogolla, 'Neural Circuits for Emotion', *Annual Review of Neuroscience*, 46.1 (2023), p. null, doi:10.1146/annurev-neuro-111020-103314.

[97] Robert W. Levenson, 'Blood, Sweat, and Fears', *Annals of the New York Academy of Sciences*, 1000.1 (2003), pp. 348–66, doi:10.1196/annals.1280.016.

[98] Travis D Goode and others, 'Bed Nucleus of the Stria Terminalis Regulates Fear to Unpredictable Threat Signals', ed. by Geoffrey Schoenbaum, Catherine Dulac, and Geoffrey Schoenbaum, *eLife*, 8 (2019), p. e46525, doi:10.7554/eLife.46525.

[99] Philippe Nuss, 'Anxiety Disorders and GABA Neurotransmission: A Disturbance of Modulation', *Neuropsychiatric Disease and Treatment*, 11 (2015), pp. 165–75, doi:10.2147/NDT.S58841.

[100] Cristina Mazuski and John O'Keefe, 'Representation of Ethological Events by Basolateral Amygdala Neurons', *Cell Reports*, 39.10 (2022), p. 110921, doi:10.1016/j.celrep.2022.110921.

[101] TaeHyun Kim and others, 'Activated Somatostatin Interneurons Orchestrate Memory Microcircuits', *Neuron*, 112.2 (2024), pp. 201-208.e4, doi:10.1016/j.neuron.2023.10.013.

[102] Jun Guo and others, *Stratum Lacunosum-Moleculare Interneurons of the Hippocampus Coordinate Memory Encoding and Retrieval* (Neuroscience, 12 June 2021), doi:10.1101/2021.06.11.448103.

[103] Linda Overstreet-Wadiche and Chris J. McBain, 'Neurogliaform Cells in Cortical Circuits', *Nature Reviews. Neuroscience*, 16.8 (2015), pp. 458–68, doi:10.1038/nrn3969.

[104] 'MI-Protocol-RNAFISH-FrozenTissue-Rev4.Pdf' <https://files.molecularinstruments.com/MI-Protocol-RNAFISH-FrozenTissue-Rev4.pdf

[105] Muhammad Asim and others, 'Basolateral Amygdala Parvalbumin and Cholecystokinin-Expressing GABAergic Neurons Modulate Depressive and Anxiety-like Behaviors', *Translational Psychiatry*, 14.1 (2024), p. 418, doi:10.1038/s41398-024-03135-z.

[106] C. Lever, S. Burton, and J. O'Keefe, 'Rearing on Hind Legs, Environmental Novelty, and the Hippocampal Formation', *Reviews in the Neurosciences*, 17.1–2 (2006), pp. 111–34, doi:10.1515/REVNEURO.2006.17.1-2.111.

[107] Hannah Hochgerner and others, 'Neuronal Types in the Mouse Amygdala and Their Transcriptional Response to Fear Conditioning', *Nature Neuroscience*, 26.12 (2023), pp. 2237–49, doi:10.1038/s41593-023-01469-3.

[108] Timothy P O'Leary and others, 'Extensive and Spatially Variable Within-Cell-Type Heterogeneity across the Basolateral Amygdala', *eLife*, 9 (2020), p. e59003, doi:10.7554/eLife.59003.

[109] Bin Yu and others, 'Molecular and Cellular Evolution of the Amygdala across Species Analyzed by Single-Nucleus Transcriptome Profiling', *Cell Discovery*, 9.1 (2023), pp. 1–22, doi:10.1038/s41421-022-00506-y.

[110] Benjamin Schuman and others, 'Four Unique Interneuron Populations Reside in Neocortical Layer 1', *The Journal of Neuroscience*, 39.1 (2019), pp. 125–39, doi:10.1523/JNEUROSCI.1613-18.2018.

[111] Joseph M. Stujenske and others, 'Prelimbic Cortex Drives Discrimination of Non-Aversion via Amygdala Somatostatin Interneurons', *Neuron*, 110.14 (2022), pp. 2258-2267.e11, doi:10.1016/j.neuron.2022.03.020.

[112] James L. McGaugh, 'THE AMYGDALA MODULATES THE CONSOLIDATION OF MEMORIES OF EMOTIONALLY AROUSING EXPERIENCES', *Annual Review of Neuroscience*, 27.1 (2004), pp. 1–28, doi:10.1146/annurev.neuro.27.070203.144157.

[113] Olga Babaev, Carolina Piletti Chatain, and Dilja Krueger-Burg, 'Inhibition in the Amygdala Anxiety Circuitry', *Experimental & Molecular Medicine*, 50.4 (2018), pp. 1–16, doi:10.1038/s12276-018-0063-8.

[114] Kay M. Tye and others, 'Amygdala Circuitry Mediating Reversible and Bidirectional Control of Anxiety', *Nature*, 471.7338 (2011), pp. 358–62, doi:10.1038/nature09820.

[115] Anthony N. van den Pol and others, 'Neuromedin B and Gastrin-Releasing Peptide Excite Arcuate Nucleus Neuropeptide Y Neurons in a Novel Transgenic Mouse Expressing Strong Renilla Green Fluorescent Protein in NPY Neurons', *Journal of Neuroscience*, 29.14 (2009), pp. 4622–39, doi:10.1523/JNEUROSCI.3249-08.2009.

[116] Lief E. Fenno and others, 'Targeting Cells with Single Vectors Using Multiple-Feature Boolean Logic', *Nature Methods*, 11.7 (2014), pp. 763–72, doi:10.1038/nmeth.2996.

[117] Steffen B. E. Wolff and others, 'Amygdala Interneuron Subtypes Control Fear Learning through Disinhibition', *Nature*, 509.7501 (2014), pp. 453–58, doi:10.1038/nature13258.

[118] Michael T. Rogan and others, 'Distinct Neural Signatures for Safety and Danger in the Amygdala and Striatum of the Mouse', *Neuron*, 46.2 (2005), pp. 309–20, doi:10.1016/j.neuron.2005.02.017.

[119] Eryan Kong and others, 'Learning Not to Fear: Neural Correlates of Learned Safety', *Neuropsychopharmacology*, 39.3 (2014), pp. 515–27, doi:10.1038/npp.2013.191.

[120] Philippe Soriano, 'Generalized lacZ Expression with the ROSA26 Cre Reporter Strain', *Nature Genetics*, 21.1 (1999), pp. 70–71, doi:10.1038/5007.

[121] Linda Madisen and others, 'A Robust and High-Throughput Cre Reporting and Characterization System for the Whole Mouse Brain', *Nature Neuroscience*, 13.1 (2010), pp. 133–40, doi:10.1038/nn.2467.

[122] Tobias Ruff and others, 'FLRT3 Marks Direction-Selective Retinal Ganglion Cells That Project to the Medial Terminal Nucleus', *Frontiers in Molecular Neuroscience*, 14 (2021), doi:10.3389/fnmol.2021.790466.

[123] Rebecca L. Suthard and others, 'Basolateral Amygdala Astrocytes Are Engaged by the Acquisition and Expression of a Contextual Fear Memory', *Journal of Neuroscience*, 43.27 (2023), pp. 4997–5013, doi:10.1523/JNEUROSCI.1775-22.2023.

[124] Alexandra S. Klein and others, 'Fear Balance Is Maintained by Bodily Feedback to the Insular Cortex in Mice', *Science*, 374.6570 (2021), pp. 1010–15, doi:10.1126/science.abj8817.

[125] Jingyi Guo Fuglstad and others, 'Histological E-Data Registration in Rodent Brain Spaces', ed. by Mathieu Wolff, Laura L Colgin, and Mathieu Wolff, *eLife*, 12 (2023), p. e83496, doi:10.7554/eLife.83496.

[126] Kendra D. Bunner and George V. Rebec, 'Corticostriatal Dysfunction in Huntington's Disease: The Basics', *Frontiers in Human Neuroscience*, 10 (2016), doi:10.3389/fnhum.2016.00317.

[127] Johanna Burgold and others, 'Cortical Circuit Alterations Precede Motor Impairments in Huntington's Disease Mice', *Scientific Reports*, 9.1 (2019), p. 6634, doi:10.1038/s41598-019-43024-w.

[128] L.A. Raymond and others, 'Pathophysiology of Huntington's Disease: Time-Dependent Alterations in Synaptic and Receptor Function', *Neuroscience*, 198 (2011), pp. 252–73, doi:10.1016/j.neuroscience.2011.08.052.

[129] Javier DeFelipe, Lidia Alonso-Nanclares, and Jon I. Arellano, 'Microstructure of the Neocortex: Comparative Aspects', *Journal of Neurocytology*, 31.3–5 (2002), pp. 299–316, doi:10.1023/a:1024130211265.

[130] Damian M. Cummings and others, 'Alterations in Cortical Excitation and Inhibition in Genetic Mouse Models of Huntington's Disease', *Journal of Neuroscience*, 29.33 (2009), pp. 10371–86, doi:10.1523/JNEUROSCI.1592-09.2009.

[131] S. E. Dougherty and others, 'Hyperactivity and Cortical Disinhibition in Mice with Restricted Expression of Mutant Huntingtin to Parvalbumin-Positive Cells', *Neurobiology of Disease*, 62 (2014), pp. 160–71, doi:10.1016/j.nbd.2013.10.002.

[132] Bosiljka Tasic and others, 'Shared and Distinct Transcriptomic Cell Types across Neocortical Areas', *Nature*, 563.7729 (2018), pp. 72–78, doi:10.1038/s41586-018-0654-5.

[133] Jing-Qiong Kang and Robert L. Macdonald, 'Molecular Pathogenic Basis for *GABRG2* Mutations Associated With a Spectrum of Epilepsy Syndromes, From Generalized Absence Epilepsy to Dravet Syndrome', *JAMA Neurology*, 73.8 (2016), p. 1009, doi:10.1001/jamaneurol.2016.0449.

[134] James P Bohnslav and others, 'DeepEthogram, a Machine Learning Pipeline for Supervised Behavior Classification from Raw Pixels', ed. by Mackenzie W Mathis and others, *eLife*, 10 (2021), p. e63377, doi:10.7554/eLife.63377.

[135] Elissa J Donzis and others, 'Cortical Network Dynamics Is Altered in Mouse Models of Huntington's Disease', *Cerebral Cortex*, 30.4 (2020), pp. 2372–88, doi:10.1093/cercor/bhz245.

[136] Sarah A. J. Reading and others, 'Functional Brain Changes in Presymptomatic Huntington's Disease', *Annals of Neurology*, 55.6 (2004), pp. 879–83, doi:10.1002/ana.20121.

[137] J. Spampanato and others, 'Progressive Synaptic Pathology of Motor Cortical Neurons in a BAC Transgenic Mouse Model of Huntington's Disease', *Neuroscience*, 157.3 (2008), pp. 606–20, doi:10.1016/j.neuroscience.2008.09.020.

[138] Adam G. Walker and others, 'Altered Information Processing in the Prefrontal Cortex of Huntington's Disease Mouse Models', *Journal of Neuroscience*, 28.36 (2008), pp. 8973–82, doi:10.1523/JNEUROSCI.2804-08.2008.

[139] Katie A. Ferguson and Jessica A. Cardin, 'Mechanisms Underlying Gain Modulation in the Cortex', *Nature Reviews Neuroscience*, 21.2 (2020), pp. 80–92, doi:10.1038/s41583-019-0253-y.

[140] Katayun Cohen-Kashi Malina and others, 'NDNF Interneurons in Layer 1 Gain-Modulate Whole Cortical Columns According to an Animal's Behavioral State', *Neuron*, 109.13 (2021), pp. 2150-2164.e5, doi:10.1016/j.neuron.2021.05.001.

[141] Hansruedi Mathys and others, 'Single-Cell Transcriptomic Analysis of Alzheimer's Disease', *Nature*, 570.7761 (2019), pp. 332–37, doi:10.1038/s41586-019-1195-2.

[142] Mary H. Wertz and others, 'Genome-Wide in Vivo CNS Screening Identifies Genes That Modify CNS Neuronal Survival and mHTT Toxicity', *Neuron*, 106.1 (2020), pp. 76-89.e8, doi:10.1016/j.neuron.2020.01.004.

[143] Dennis Feigenbutz, 'Temporally resolved single-nucleus RNA-sequencing profiling of the cortex reveals mechanisms of neuronal vulnerability in Huntington's disease' (Ludwig-Maximilians-Universität München).

[144] Anthony Holtmaat and others, 'Long-Term, High-Resolution Imaging in the Mouse Neocortex through a Chronic Cranial Window', *Nature Protocols*, 4.8 (2009), pp. 1128–44, doi:10.1038/nprot.2009.89.

[145] Richard A Warren and others, 'A Rapid Whisker-Based Decision Underlying Skilled Locomotion in Mice', ed. by Jesse H Goldberg, Ronald L Calabrese, and Jesse H Goldberg, *eLife*, 10 (2021), p. e63596, doi:10.7554/eLife.63596.

[146] Marius Pachitariu and others, 'Suite2p: Beyond 10,000 Neurons with Standard Two-Photon Microscop', 2016, doi:10.1101/061507.

[147] Carsen Stringer and others, 'Cellpose: A Generalist Algorithm for Cellular Segmentation', *Nature Methods*, 18.1 (2021), pp. 100–06, doi:10.1038/s41592-020-01018-x.

[148] Alexander Mathis and others, 'DeepLabCut: Markerless Pose Estimation of User-Defined Body Parts with Deep Learning', *Nature Neuroscience*, 21.9 (2018), pp. 1281–89, doi:10.1038/s41593-018-0209-y.

[149] Andrew J. Peters, Simon X. Chen, and Takaki Komiyama, 'Emergence of Reproducible Spatiotemporal Activity during Motor Learning', *Nature*, 510.7504 (2014), pp. 263–67, doi:10.1038/nature13235.

[150] Bernardo Rudy and others, 'Three Groups of Interneurons Account for Nearly 100% of Neocortical GABAergic Neurons', *Developmental Neurobiology*, 71.1 (2011), pp. 45–61, doi:10.1002/dneu.20853.

[151] Hanna Yousuf and others, 'Modulation of Intrinsic Excitability as a Function of Learning within the Fear Conditioning Circuit', *Neurobiology of Learning and Memory*, 167 (2020), p. 107132, doi:10.1016/j.nlm.2019.107132.

[152] Helen Motanis, Mouna Maroun, and Edi Barkai, 'Learning-Induced Bidirectional Plasticity of Intrinsic Neuronal Excitability Reflects the Valence of the Outcome', *Cerebral Cortex*, 24.4 (2014), pp. 1075–87, doi:10.1093/cercor/bhs394.

[153] Liron Sheintuch and others, 'Tracking the Same Neurons across Multiple Days in Ca2+ Imaging Data', *Cell Reports*, 21.4 (2017), pp. 1102–15, doi:10.1016/j.celrep.2017.10.013.

[154] Arpiar Saunders, Caroline Johnson, and Bernardo Sabatini, 'Novel Recombinant Adeno-Associated Viruses for Cre Activated and Inactivated Transgene Expression in Neurons', *Frontiers in Neural Circuits*, 6 (2012), doi:10.3389/fncir.2012.00047.

[155] Mathew D. Edwards and others, 'Combined Transcriptomic, Connectivity, and Activity Profiling of the Medial Amygdala Using Highly Amplified Multiplexed in Situ Hybridization (hamFISH)' (bioRxiv, 15 September 2024), p. 2024.09.14.613026, doi:10.1101/2024.09.14.613026.

[156] Hansruedi Mathys and others, 'Single-Cell Atlas Reveals Correlates of High Cognitive Function, Dementia, and Resilience to Alzheimer's Disease Pathology', *Cell*, 186.20 (2023), pp. 4365-4385.e27, doi:10.1016/j.cell.2023.08.039.